METHODOLOGY FOR APPROXIMATING MATERIAL LOSS ON STRUCTURAL PLATING SUBJECTED TO DISSIMILAR MARINE ENVIRONMENTS

by Robert A. Ernsting, P.E.

B.S. in Civil Engineering, August 1982, Trine University (formally Tri-State University)
M.S. in Engineering Management, December 1992, Old Dominion University

A Dissertation submitted to

the Faculty of
The School of Engineering and Applied Science
of The George Washington University
in partial satisfaction of the requirements
for the degree of Doctor of Philosophy

May 17, 2009

Dissertation directed by

Thomas A. Mazzuchi
Professor of Operations Research and of Engineering Management
and
Shahram Sarkani
Professor of Engineering Management and Systems Engineering

The School of Engineering and Applied Science of The George Washington University certifies that Robert Alan Ernsting has passed the Final Examination for the degree of Doctor of Philosophy as of March 6, 2009. This is the final and approved form of the dissertation.

METHODOLOGY FOR APPROXIMATING MATERIAL LOSS ON STRUCTURAL PLATING SUBJECTED TO DISSIMILAR MARINE ENVIRONMENTS

Robert A. Ernsting, P.E.

Dissertation Research Committee:

Thomas Andrew Mazzuchi, Professor of Operations Research and of Engineering Management, Dissertation Co-Director

Shahram Sarkani, Professor of Engineering Management and Systems Engineering, Dissertation Co-Director

Edward Lile Murphree, Jr., Professor of Engineering Management and Systems Engineering, Committee Chair

Frank Allario, Professorial Lecturer in Engineering, Committee Member

Harvey Paul Hack, Senior Advisory Engineer, Northrop Grumman Undersea Systems, Committee Member

Copyright © 2009 by Robert A. Ernsting

All rights reserved

Dedication

This work is a dedication to my beloved wife Judi who provided the much treasured love and support throughout this three-year research. She stood beside me throughout the countless long nights, weekend sacrifices and household neglect in pursuit of this topic. Now that this phase of the research is complete, the chapters written and the ink has dried, she provides the inspiration for my next endeavor and hints that the research involves applying coating protection systems to well neglected household fixtures…

Acknowledgment

Several colleagues, co-workers and advisors assisted in this research effort and are worthy of recognition. Their steadfast support and objectivity kept the author focused, true and on track throughout this endeavor.

The author would like to acknowledge David B. McKercher, P.E., Robert E. Fallon, P.E., and Mr. James L. Kelly, P.E. of Northrop Grumman Shipbuilding-Newport News for providing the invaluable dry dock caisson gate and environmental data needed for this research.

Thanks also to doctoral advisors Harvey P. Hack, Ph.D, P.E., Northrop Grumman Undersea Systems and Frank Allario, Ph.D, The George Washington University, for providing much needed direction and periodic, in-depth peer reviews. The inspiration of this research came from Robert E. Melchers, Ph.D, The University of Newcastle who early on provided clear direction and encouragement for this unexplored topic.

Thanks to the peers and co-workers that took time out of their busy schedules to assist in the field collecting data, reviewing calculations and providing much needed candid comments on this work. Namely, Don Lawson, Rocco Mannino and Ryan Van Booven of Northrop Grumman Shipbuilding-Newport News; Jim Armacost, P.E., John Watts, P.E., Rusty Sandidge, Rick Godwin of Whitman Requardt and Associates and Chip Conrad, P.E. of Collins Engineering.

In memory of
Jan M. van Noortwijk, Ph.D
1961-2008

Abstract

Methodology for Approximating Material Loss on Structural Plating Subjected To Dissimilar Marine Environments

Non destructive measurement technologies such ultrasonic pulse echo are typically employed to measure remaining shell plating thickness for determining remaining life on marine structures. However, the technology provides *total* material loss across the shell plate and cannot distinguish how much material loss occurs on each plate side. By understanding material loss contribution on each plate side, engineers and maintenance personnel can have a better understanding of the environments influencing material loss, optimally plan, and schedule maintenance activities. This need is evermore important today as the U.S. proceeds to address its aging infrastructure problems.

This research defines and tests a new maintenance inspection methodology called *relative material loss* (RML) used for distinguishing the material loss contribution on each shell plate side separating dissimilar marine environments. The RML methodology leverages actual "at sea" environmental and operational conditions and the relationships between to solve for material loss contribution. In much the same fashion as a structural engineer isolate joints on a truss and solve free body diagram equations to determine member forces, *relative loss equations* are defined across various environmental boundaries (such as shell plating) and solved simultaneously to suggest solutions.

To demonstrate and test the RML theory, a case study is presented using a sixty five year old "at-sea" structure; a dry dock caisson gate. Both qualitative and quantitative techniques are used to valid the model. Shell plate material loss contribution profiles are defined using statistical and regression techniques and correlated to profiles of

environmental factors known to influence marine corrosion. Spin off discoveries and recommendations for future research are included.

Table of Contents

Dedication ..... **iv**

Acknowledgment ..... **v**

Abstract ..... **vi**

Table of Contents ..... **viii**

List of Figures ..... **xii**

List of Tables ..... **xiv**

List of Symbols ..... **xv**

List of Acronyms ..... **xvii**

Glossary of Terms ..... **xviii**

Chapter 1 - Introduction **1**

1.1 Background 1

1.2 Statement of the Problem 2

1.3 Significance of the Research 2

1.4 Research Outline 3

Chapter 2 - Literature Review **5**

2.1 Condition Based Maintenance 5

2.2 Life Cycle Cost Models 6

2.3 Marine Corrosion – Early Research 7

2.4 Linear and Non-Linear Corrosion Models 8

2.5 Multi-Phase Phenomenological Corrosion Model 9

2.6 Corrosion Models that Include Coating Protection System 11

2.6.1 Model Limitations 14

2.6.2 Gradual CPS Degradation Model 15
2.6.3 Other Corrosion and CPS Research 17
2.7 Environmental Factors - Seawater Immersion 18
2.8 Environmental Factors – Ballast Tank 19
Chapter 3 - Relative Material Loss Theory 20
3.1 Material Loss Function 21
3.1.1 Bias function 21
3.1.2 Zero mean uncertainty function (precision error) 23
3.2 Relative Material Loss 23
3.2.1 Single plate, dissimilar environments 24
3.2.2 Two Plates Separating Three Dissimilar Environments 26
3.3 Assumptions 27
Chapter 4 - Experiment 30
4.1 Research Objective and Questions 30
4.2 Dry Dock Caisson Gate 31
4.3 Caisson Gate "D" 33
4.4 Main Ballast Tank Marine Environments 34
4.5 Shell Plating Thickness Measurements 36
4.6 Water Quality Samples 38
4.7 Supporting Questions 38
4.7.1 Environmental Dissimilarity 39
4.7.2 Environmental Stratification 40
4.7.3 Test for Normality and Outliers 41

4.8 Robust Locally Weighted Regression (LOWESS) 44
4.9 Polynomial Regression Models (Curve Fitting) 45
4.10 Negative Wastage Measurements 48
4.11 Relative Loss Equations 49
4.12 Gate Rotation Parameter, *n* 50
4.13 Relative Loss Variables, R_{em} 51
4.14 Relative Material Loss Contributions, *c(t)* 52
Chapter 5 - Results 56
5.1 RML Profiles 56
5.2 River Side RML Profile (Side "A") 57
5.3 Model Validation 59
5.3.1 Side "A", Shell Plating Total Loss Validation 60
5.3.2 Side "A", Shell Plating River Loss Contribution Validation 62
5.3.3 Shell Plating Ballast Tank Loss Contribution Validation 63
5.3.3.1 Ballast Tank Atmospheric 64
5.3.3.2 Ballast Tank Water 65
5.3.3.3 Ballast Tank Concrete 66
5.4 Atmospheric Side RML Profile (Side "B") 67
Chapter 6 - Conclusion 69
6.1 Future Research and Spinoffs 70
6.1.1 Negative "Wastage" 70
6.1.2 Diminution of Precision Error 71
6.1.3 Bootstrap Inflections for Detecting Anomalies 71

References **72**

Appendix A – Ultrasonic Test Procedures and Device Specifications **79**

Appendix B – Water Quality Measuring Device Specifications and Calibration **81**

Appendix C – Water Temperature and Dissolved Oxygen Comparisons **83**

Appendix D - Lateral Homogeneity Test for Sides "A" and "B **84**

Appendix E - Longitudinal Heterogeneity Test for Sides "A" and "B" **86**

Appendix F – LOWESS and Polynomial Regression Models **88**

Appendix G – "Negative" Wastage Distributions of Four Caisson Gates **98**

List of Figures

Figure 1. Basic Condition-Based Maintenance Model 5

Figure 2. Melchers Multi-Phase Phenomenological Model 10

Figure 3. Guedes Soares/Garbatov 3-Phase Corrosion Model 12

Figure 4. Paik and Thayamballi 3-Phase Corrosion Model 13

Figure 5. Qin & Cui 3-Phase Corrosion Model 16

Figure 6. Relationship between bias and precision error 22

Figure 7. Single plate separating two dissimilar environments 24

Figure 8. Two plates separating three dissimilar environments 26

Figure 9. Dry Dock Caisson Gate "D" and Section View 31

Figure 10. Caisson Gate Ballast Tanks 32

Figure 11. Caisson Gate Marine Environments 35

Figure 12. UT Measurement Locations and Nomenclature 37

Figure 13. Normal Probability Plots for D-BASP & D-BBSP 43

Figure 14. Polynomial Regression Models - Sides "A" and "B" 47

Figure 15. Relative Loss Equations Across Shell Plating on Caisson Gate "D" 49

Figure 16. Caisson Gate "D", Side "A", Total Shell Plating Material Loss 56

Figure 17. Caisson Gate "D", Side "A", River Side Material Loss Contribution 58

Figure 18. Correlations of Temperature and Dissolved Oxygen to Total Shell Plating Loss 60

Figure 19. Correlations of Temperature and Dissolved Oxygen to River Side Contribution 62

Figure 20. Caisson Gate "D", Side "A", Ballast Tank Side Material Loss Contribution 64
Figure 21. Correlations of Temperature and Dissolved Oxygen to Ballast Tank Contribution 66
Figure 22. Caisson Gate "D", Side "B", Total Shell Plating Material Loss.....67
Figure 23. Caisson Gate "D", Side "B", Marine Atmospheric Side Material Loss Contribution 68

List of Tables

Table 1. Environmental Factors Influencing Marine Immersion Corrosion.....18

Table 2. Anderson-Darling Normality and Grubb's Test for Outliers 42

Table 3. Step, Fit and Maximum Anderson-Darling p-values on the LOWESS Residuals 44

Table 4. Polynomial Regression Models - R-squared and p-values 46

Table 5. Comparisons of shell plating negative wastage measurements 48

Table 6. Relative Loss Variables, Rem (at frame location: x=10).....53

Table 7. RML Contributions, c(t) (at frame location: x=10) 54

Table 8. Environmental Profiles (Dissolved Oxygen & Temperature) 59

List of Symbols

A^2	Anderson-Darling test statistic
A^{2*}	Anderson-Darling test statistic (adjusted)
A	non singular, coefficient matrix
adj. R^2	regression coefficient (adjusted)
b	bias
b(t)	bias function (as a function of time)
c_a, c_s	intercepts (multi-phase phenomenological corrosion model)
c(t)	material loss (as a function of time)
C_1	annual corrosion rate (Paik and Thayamballi model)
C_2	structural dynamics and water velocity environmental coefficient (Paik and Thayamballi model)
d	corrosion loss depth
d(t)	corrosion loss depth as a function of time
d_o	original plate thickness
E_n	caisson gate marine environments
E	vector of environmental factors that influence material loss
f-value	Fisher distribution probability
fn(t)	material loss function
H_0	null hypothesis
H_1	alternate hypothesis
mm	millimeters
n	gate rotation parameter (%)
p-value	probability (for hypothesizes testing)
P	vector of corrosion protection system factors that inhibit material loss
r-value	Pearson product-moment correlation coefficient
R^2	regression coefficient
R_{em}	relative loss contribution influenced by environment *e*, at level *m*
R	column vector of unknown variables in terms of relative loss R_{em}
r_o, r_a, r_s	corrosion rates (multi-phase phenomenological corrosion model)
s	failure level (condition based maintenance)
t	time

t_n	time interval (condition based maintenance)
t-value	Student t distribution probability
T_c	time at which coating begins to loss its effectiveness (Paik and Thayamballi model)
T_t	time at which coating loss all effectiveness (Paik and Thayamballi model)
T_{st}	time at which pitting starts (Qin & Cui model)
T_A	time at which corrosion rate begins to decelerate (Qin & Cui model)
W	wastage
$W_{D\text{-}nmSP}$	total wastage measured on side *n*, level *m*
$\mathbf{W}$	column vector of known total plate thickness loss (wastage) measurements
α	significance level (type I error)
ε	error
$\varepsilon(t)$	zero mean uncertainty function (or precision error)
σ	standard deviation
ρ	preventative maintenance level (condition based maintenance)
τ_c	time period of effective CPS (Guedes Soares and Garbatov model)
$\tau_{t,}$	time period after corrosion initiates due to ineffective CPS (Guedes Soares and Garbatov model)
μ	mean
η, β	Wiebull parameters (Qin & Cui model)

List of Acronyms

AD	Anderson-Darling
ANOVA	Analysis of variance
ASCE	American Society of Civil Engineers
ASTM	American Society for Testing and Materials
CBM	condition based maintenance
CPS	coating protection systems
CG	caisson gate
CI	confidence interval
DO	dissolved oxygen
LOWESS	Locally Weighted Estimated Scatter Smoother
MIL-STD	military standard
NRL	Naval Research Laboratory
RL	relative loss
RML	relative material loss
SSC	Ship Structure Committee
SSPC	Steel Structures Painting Council
T	temperature
TDM	time-directed maintenance
TOW	time of wetness
U.S.	United States

Glossary of Terms

Relative Material Loss – A maintenance inspection methodology for approximating material loss contribution on each side of structural shell plating subjected to dissimilar marine environments.

Relative Loss Equations - Mathematical relationships or equations defined across various environmental boundaries (such as shell plating) and solved simultaneously to suggest solutions.

Material Loss Contribution – The amount of material loss on a structural member that is attributable to the environment from which it exists.

Laterally homogeneous – Environmental parameters are equivalent laterally on either side of a point within an environment.

Longitudinally heterogeneous - Environmental parameters are not equivalent longitudinally above or below a point within an environment.

Chapter 1 - Introduction

1.1 Background

The August 2007 collapse of the I35W Bridge in Minneapolis killed 13 and injured nearly 100 rush-hour motorists. This catastrophe has renewed public concern over the condition of the U.S. aging infrastructure. In 2009, the American Society of Civil Engineers (ASCE) published a report that estimates $2.2 trillion over five years is needed to repair the deteriorating U.S. infrastructure [1]. This figure is up from $1.6 trillion in the 2005 ASCE report. Compounding this problem, construction and repair costs continue to escalate [5] and a shortage of engineering expertise needed to address these problems is predicted [15].

After a series of maritime accidents starting with the *Exxon-Valdez* accident in 1989, the *Erika* (1999) sinking off the French Brittany coast and the *Prestige* (2003) sinking off the Spanish Galician coast, a high demand for more in depth research ensued [67, 81]. The maritime industry needed a better understanding of predicting marine corrosion on hull structure of tankers and cargo vessels under operational and “at sea” conditions and a maritime reliability and maintainability paradigm shift was needed.

Adding to the risk management issues with these aging infrastructures, economic and political pressures in the private and public sectors are placing new demands to extend service lives on aging facilities. The service lives of U.S. infrastructure systems are being pressed to, and more frequently expected to perform beyond, original design lives [48]. As available capital for replacement facilities dwindle, service life extensions are becoming more commonplace. These trends are placing new challenges on facilities engineers and managers to do more with less and are resulting in a paradigmatic shift

towards exploration of new and innovative maintenance inspection methodologies [25, 48].

In response to this new demand, this research sets the foundation for a new maintenance inspection theory called relative material loss (RML).

1.2 Statement of the Problem

Two-sided corrosion occurs when corrosion initiates on both sides of a metal plate. The solution to determine the material loss contribution on each plate side is straightforward when the corrosion environment is homogeneous and equivalent on both plate sides. It involves is a simple two-sided corrosion calculation. However, when the environments on each plate sides are dissimilar, determining the wastage on each plate side is not so elementary.

Current ultrasonic testing methods for measuring plate thickness wastage can only determine *total* material loss across hull shell plating and cannot distinguish the amount of material loss contribution on each shell plate side. To solve this problem, this research proposes a new maintenance inspection methodology called *relative material loss* (RML). The methodology, when applied to "at-sea" structures, approximates the material loss contribution on each shell plate side separating dissimilar marine environments.

1.3 Significance of the Research

The innovation from this research provides a (1) new paradigm from which marine corrosion researchers can apply their corrosion models directly using actual "at-sea" conditions as well as a (2) new maintenance inspection method that can better approximate marine material loss directly from structural shell plating thickness

measurements taken from “at-sea” marine structures. The new methodology takes a deterministic approach by including actual operational and environmental conditions of the sea structure into the RML model.

The new tool gives material science researchers and maintenance engineers the ability to study operational and environmental effects on shell plating more directly and definitively than current methods. Better understanding of operational and environmental conditions reduces modeling variability and improves predictability. The knowledge from the research has the potential to extend structural performance and optimize maintenance costs for “at-sea” structures in the maritime shipping (commercial and naval) and offshore oil industries as well as benefit shipyards (commercial and naval), ports, harbors and various waterfront communities.

1.4 Research Outline

A 65-year-old dry dock caisson gate (CG) provides the research platform to test the RML theory. Mathematical models in the form of polynomial regression models describe shell plating material loss across various caisson gate levels. Using the polynomial regression models, relative loss (RL) equations describe material loss contributions taking into account the CG operational and environmental relationships at each CG frame location.

The material loss contribution on each plate side is calculated and profiles created at each CG frame location. The mean value of the profiles provides an approximation of the material loss contribution on each plate side. The profiles, collectively, provide an approximate bootstrap [3] representation of the confidence interval. The profiles are both qualitatively and quantitatively compared to environmental factors known to influence

corrosion and strengths of correlations determined to provide RML model validation [53].

Chapter 2 sets the stage for this research through a literature review of how condition-based maintenance differs from traditional time-directed strategies. Ship reliability and life expectancy models in the maritime industry that provide important optimization of maintenance policies are in high demand. Past and recent marine corrosion research and several popular probabilistic and parametric-based corrosion loss models provide the foundation of for the relative material loss (RML) research. Chapter 3 develops the RML theory from a material loss function found in the literature as the base equation. A sequential storyboard with mathematical theory provides backup. In Chapter 4, a unique "at-sea" marine structure, the dry dock caisson gate, provides a unique corrosion research laboratory and case study for RML testing and model validation. Chapter 5 provides research results, model validation and test significance. Chapter 6 concludes with the research findings, spinoff discoveries and recommendations for future research. The appendices provide supporting information on the processed data and detailed background on data collection methodologies.

Chapter 2 - Literature Review

2.1 Condition Based Maintenance

Two main categories of preventative maintenance exist: time-directed and condition-based maintenance. Traditionally, time-directed maintenance (TDM) has been the norm where pre-designed plans initiate maintenance activities on facilities on a periodic basis. TDM requires securing the system at regular intervals to perform intrusive and often-costly component replacement [80]. The periodicities are somewhat subjective and based on failure history, experience, judgment, or vendor recommendation.

Recently, condition-based maintenance (CBM) has gained recognition and wide acceptance in industry as an optimal maintenance strategy to TDM [80], [12]. The basic CBM model is most commonly a reliability index model (Figure 1).

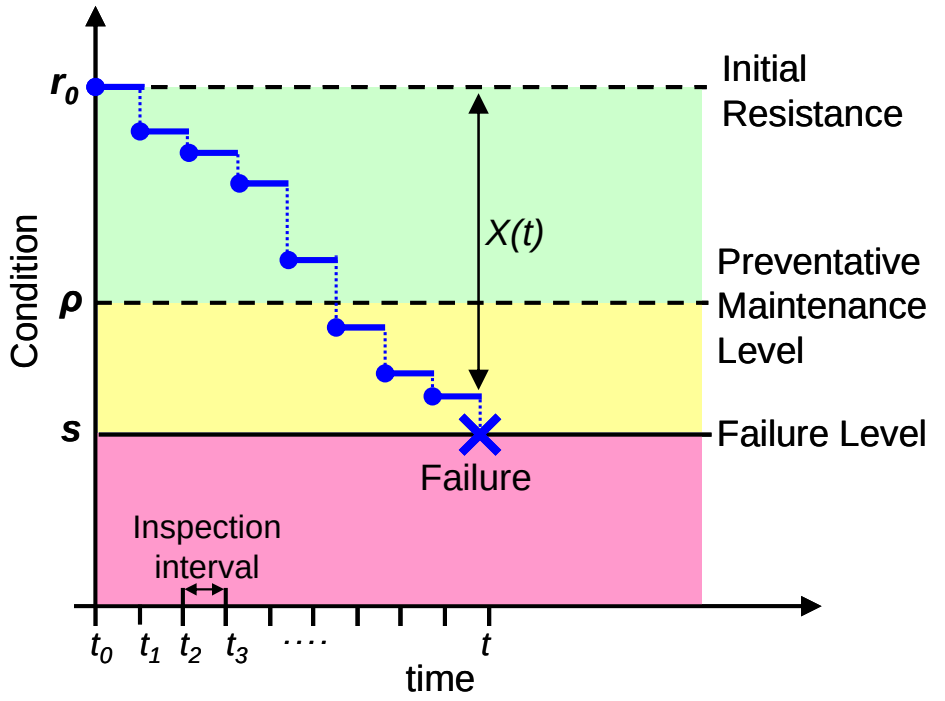

Figure 1. Basic Condition-Based Maintenance Model

A preventative maintenance level, ρ, is set and based on an acceptable risk of failure for the system or component [25]. Over time, t, the system or component will deteriorate (or wear) and reliability will decrease and approach the preventative maintenance level, ρ. At level ρ, an action event triggers planned maintenance well in advance of the failure level, s. Similar to TDM, the inspection of the system is performed at fixed time intervals, t_n, however, the inspections are typically less intrusive and therefore, less costly and disruptive to production.

2.2 Life Cycle Cost Models

Between 1970 and 1980, ship repair and construction costs quadrupled and the Ship Structure Committee (SSC) commissioned a study to determine the optimum corrosion control system on typical cargo ship ballast tanks under various coating systems, operating and environmental conditions [35]. The study emphasized the importance of understanding hull and ballast tank environmental and operational conditions to predict structural performance. It concluded that, due to the decade's sudden rise in cost of steel, planned steel replacement strategies of hull plating were no longer "status quo". A paradigm shift by ship designers to incorporate more optimal coating protection and cathodic protection systems into the ship designs was paramount to maintain competitiveness in the U.S. shipbuilding industry.

More recent ship reliability and life expectancy models combine corrosion mechanisms with various modes of hull loading conditions from a structural limit state perspective [10, 20, 64]. The key to designing optimal maintenance strategies in concert with coating protection and cathodic protection systems is improving the understanding

of shell plating material loss as a function of its environmental and operational conditions.

As illustrated by Wang, Spencer and Sun [82], corrosion wastage exhibits a high level of variability. Improving model predictability by reducing variability is the ultimate objective of the marine corrosion research community. Typically, researchers use non-destructive techniques such as ultrasonic echo pulse for measuring the remaining plate thickness. However, a lack of framework for properly analyzing the data in the industry exists [51]. Through the development of new maintenance inspection methodologies, a new framework for accounting for environmental and operational influences and potentially reducing variability provides future promise.

2.3 Marine Corrosion – Early Research

Some of the first in-depth marine corrosion research studies occurred after World War II when engineers designing the second phase of the sea-level Panama Canal tidal locks required accurate corrosion rate data for various canal lock materials under consideration. Funded by the Naval Research Laboratory (NRL), Washington, D.C. circa 1958, a 16 year corrosion research project was conducted and results published in 1976 [76]. The research exposed more than 13,000 individual samples of 52 different metal alloys to five different marine environments (seawater immersion, seawater mean tide, fresh water immersion, marine atmospheric, inland atmospheric) resulting in 168,000 data measurements taken over a 16-year span. The only corrosion mechanisms considered in the research were localized pitting and general surface corrosion. The study produced a series of corrosion-vs.-time curves based on sample mean values describing general corrosion and pitting penetration with two significant findings:

1. Marine immersion corrosion occurs non-linearly over time
2. Environmental conditions and material composition are important influential factors.

The study was conducted using exposed (uncoated) steel test coupons and did not consider "at-sea" conditions such as coating protection systems (CPS), cathodic protection or any special operational conditions. In addition, the second statistical moment (variability) was lacking.

2.4 Linear and Non-Linear Corrosion Models

Using results from the NRL research, Southwell, Bultman and Hummer [77] developed linear and bilinear corrosion prediction models. Since the predicted corrosion loss over-estimates during the early stages of marine exposure, these models are conservative and considered sufficient for structural design purposes, but not accurate for maintenance prediction modeling. Melchers [47] would later extend the Southwell, Bultman and Hummer linear models [77] by including the second statistical moment and fitting a non-linear power model over the curves.

- Melchers extended Southwell *et al*. Linear Model:

$$\begin{aligned} \mu_d(t) &= 0.076 + 0.038t \\ \sigma_d(t) &= 0.051 + 0.025t \end{aligned} \qquad \textit{(2-1)}$$

- Melchers extended Southwell *et al*. Bi-Linear Model:

$$\begin{aligned} \mu_d(t) &= \begin{cases} 0.09t, & 0 < t < 1.46 \text{ years} \\ 0.076 + 0.038t, & 1.46 < t < 16 \text{ years} \end{cases} \\ \sigma_d(t) &= \begin{cases} 0.062t, & 0 < t < 1.46 \text{ years} \\ 0.035 + 0.017t, & 1.46 < t < 16 \text{ years} \end{cases} \end{aligned} \qquad \textit{(2-2)}$$

- Melchers-Southwell Non-Linear Model:

$$\mu_d(t) = 0.084t^{0.823}$$
$$\sigma_d(t) = 0.056t^{0.823} \qquad \textit{(2-3)}$$

Where $\mu(t)$ is the mean and $\sigma(t)$ the standard deviation of the thickness of the corrosion wastage from a probabilistic standpoint. Melchers also suggested a tri-linear and another non-linear power model [46].

- Melchers Tri-Linear Model:

$$d(t) = \begin{cases} 0.170t, & 0 \le t < 1 \text{ years} \\ 0.152 + 0.0186t, & 1 \le t < 8 \text{ years} \\ -0.364 + .083t, & 8 \le t < 16 \text{ years} \end{cases} \qquad \textit{(2-4)}$$

- Melchers Non-Linear Power Model:

$$d(t) = 0.1207t^{0.6257} \qquad \textit{(2-5)}$$

Where $d(t)$ is the depth of corrosion loss at time, t from a deterministic standpoint.

In 1983, a five-year test program was undertaken to assess the relative corrosiveness of seawater at 14 test sites world-wide [68]. The findings indicate that while seawater environments are ubiquitous, and similar in terms of chloride content and pH, corrosiveness is site-specific, and influenced by other factors such as temperature, dissolved oxygen, flow, degree of fouling, bacterial activity and pollution [47].

2.5 Multi-Phase Phenomenological Corrosion Model

In 1995, R. E. Melchers [45] published a concept for a corrosion prediction model (the multi-phase phenomenological corrosion model) that describes marine corrosion in multiple phases (Figure 2).

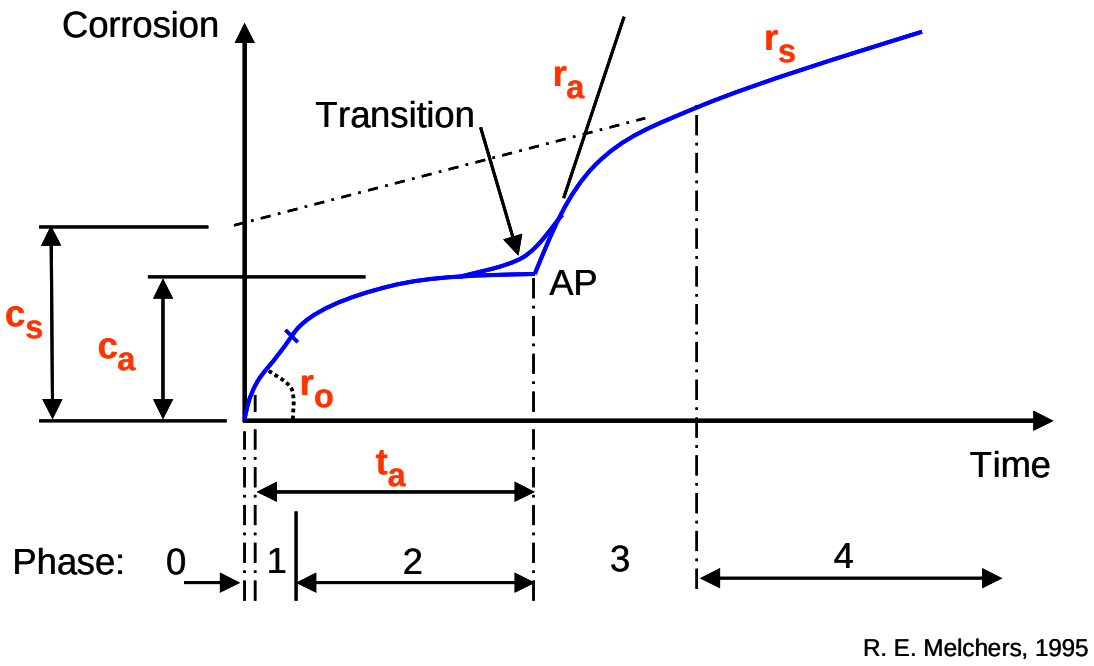

Figure 2. Melchers Multi-Phase Phenomenological Model

The model shows the progression of corrosion verses time. Immersion corrosion loss is expressed as a function of exposure time, *t*. Phases 0-2 are aerobic corrosion (oxidation) and Phases 3 and 4 are anaerobic and controlled by anaerobic microbial conditions. Rates r_o, r_a, and r_s define, respectively, initial corrosion rate due to oxidation, initial corrosion rate for corrosion influenced by bacteria, and long-term rate for bacterial influenced corrosion. Intercepts c_a and c_s are defined as shown. t_a defines the theoretical time to changeover from oxidation to microbiologically influenced corrosion.

A significant finding is environmental and material influences change dramatically when bacterial action on the corrosion product is present. With its six parameters, the Melchers phenomenological corrosion model provides flexibility to customize the model for various environmental conditions. Through a series of separate research initiatives,

Melchers developed approximations of these parameters under various environmental conditions [52, 56, 60]

Rather than measuring material loss of actual "at-sea" steel structures, Melchers exposed uncoated steel test coupons to various "at-sea" environments to develop the multi-phase phenomenological corrosion model. The model does not account for any site-specific conditions such as cathodic effects due to stray electrical currents or coating protection systems. However, the Melchers model is based on a material loss function consisting of a mean valued function $fn(t,\mathbf{E})$ defined as:

$$c(t,\mathbf{E}) = b(t,\mathbf{E}) \cdot fn(t,\mathbf{E}) + \varepsilon(t,\mathbf{E}) \qquad (2\text{-}6)$$

where $c(t,\mathbf{E})$ is material loss, $b(t,\mathbf{E})$ is a bias function, $\varepsilon(t,\mathbf{E})$ is a zero mean uncertainty function (or precision error) about the mean value function. **E** is a vector of environmental factors that influence material loss and t is the time of exposure to the environment [50, 52, 57, 60]. This material loss function provides the foundation for the relative material loss theory developed later in Chapter 3.

2.6 Corrosion Models that Include Coating Protection System

After a surge in corrosion research caused by several ship catastrophes between 1998 and 2003 (Section 1.1), it became evident that better understanding of coating protection systems (CPS), environmental and operational conditions is important for better approximating remaining structural life of "at-sea" structures. In response, corrosion researchers incorporated CPS life as a probabilistic function to the front end of the corrosion models and used actual plate thickness measurements from cargo and bulk container ships to validate the models [26, 62, 79, 85, 86].

Guedes Soares and Garbatov [32] account for CPS in a corrosion model that describes immersion corrosion progression as a three phase process (Figure 3).

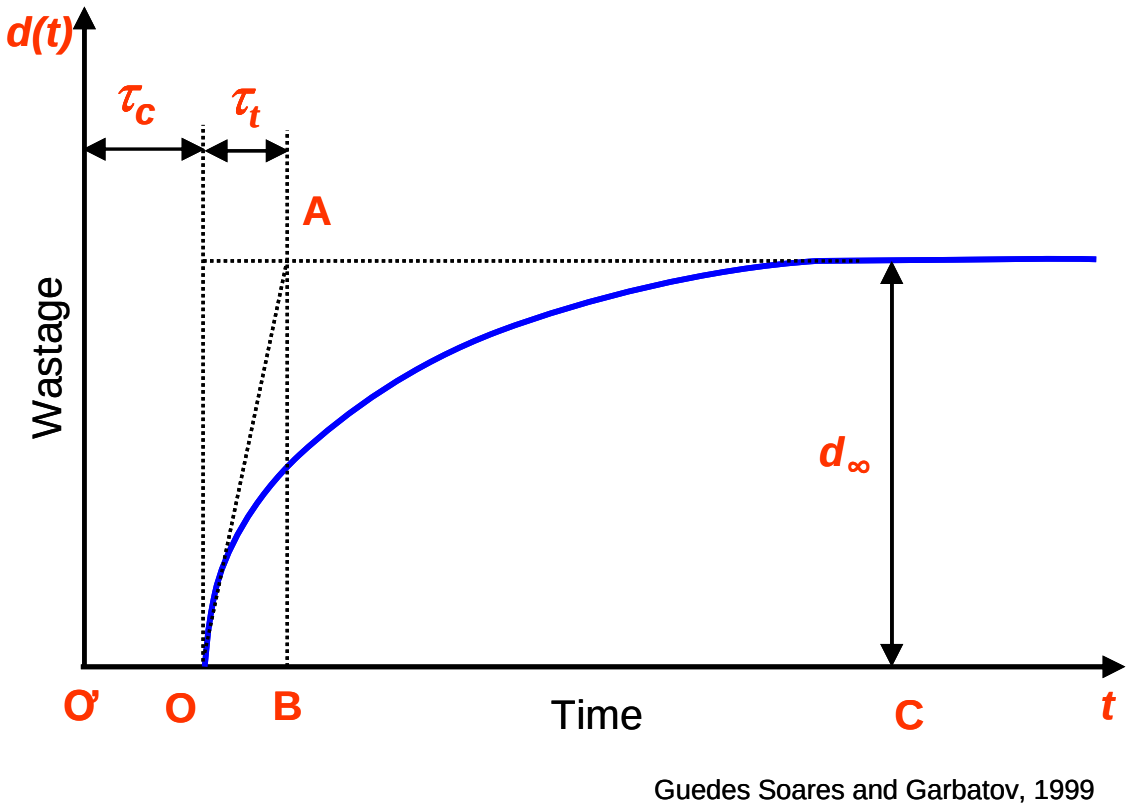

Figure 3. Guedes Soares/Garbatov 3-Phase Corrosion Model

The first phase occurs when the CPS is effective and no corrosion occurs. Statistics show that the time period without corrosion, τ_c, varies from 1.5 to 5.5 year [22] and can be probabilistically modeled. At some point, *o*, the CPS becomes ineffective and corrosion initiates (second phase). This period, τ_t, may last up to 4 or 5 years and is dependant on many environmental and operational factors inherent with the CPS. At some point B, corrosion products build up and prevent oxygen from reaching the metal surface, thus reducing the oxidation rate. As a result, corrosion enters the third phase, the

corrosion rate decelerates and the thickness of corrosion wastage becomes constant, d_∞, as it approaches point C. Three parameters τ_c, τ_t, and d_∞ are used to describe the corrosion process.

$$d(t) = \begin{cases} 0, & t \le \tau_c \\ d_\infty (1 - e^{-(t-\tau_c)/\tau_t}), & t > \tau_c \end{cases} \qquad (2\text{-}7)$$

The Paik and Thayamballi [64] three-phase model accounts for (1) durability of coating, (2) transition, and (3) progress of corrosion (Figure 4).

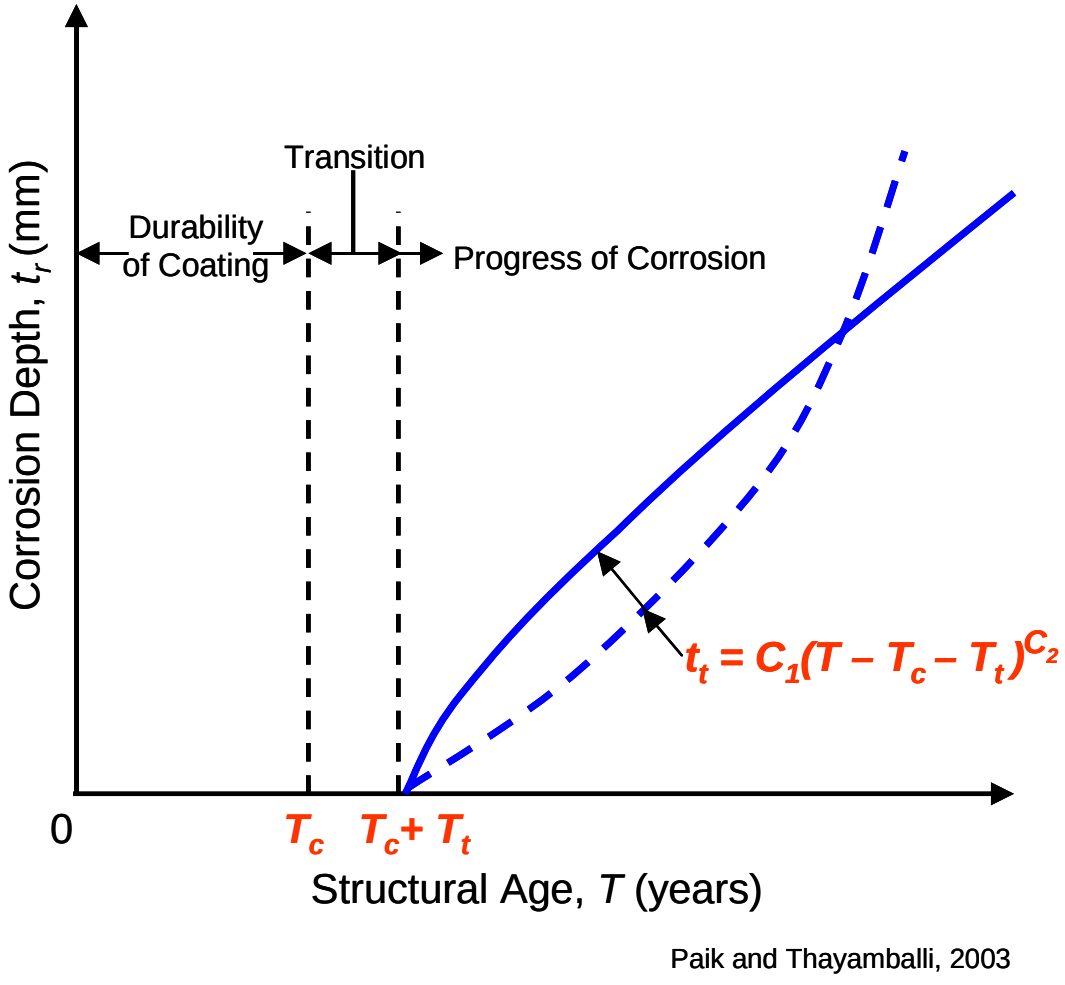

Figure 4. Paik and Thayamballi 3-Phase Corrosion Model

Similar to the Guedes Soares and Garbatov model [32], the first phase accounts for durability of the coating to some point in time, T_c. The durability of the coating models as a log-normally distributed random variable. The mean coating life is defined as being between 5 and 10 years [43] with 5 years considered undesirable and 10 years more than desirable. The transition period is the duration from the time of the effective loss of the coating, T_c to the time of corrosion initiation, T_t. The model is an exponentially distributed random variable. The progress of corrosion is modeled as a power function with coefficient C_1 indicative of the annual corrosion rate and C_2 being an environmental coefficient to account for structural dynamics and water velocity. For static structures, the corrosion curve is slightly convex (solid line) and is similar to other power models previously discussed. For dynamically loaded structures, such as ships at sea subject to dynamic forces due to wave action, the concave (dotted) line is more appropriate. Paik and Thayamballi used this data to produce charts that indicate *total* corrosion rates in terms of mean and coefficient of variance for steel plates separating various ballast tank conditions for 5, 7.5 and 10-year average coating lives.

Other researchers using the Paik and Thayamballi data produced a time-dependant corrosion depth model for statistically determining corrosion in seawater ballast tanks. This research recognizes that seawater ballast tank corrosion data exhibits high variability and proposes a methodology that approximates corrosion depth variability at any point of time [61].

2.6.1 Model Limitations

The Southwell *et al.* [77] and Melchers [47] models were developed using material thickness loss over time on uncoated (exposed) steel test coupons in actual marine

environments. As a result, these models are not efficient in predicting remaining material life extension due to an effective CPS or cathodic protection system.

The Guedes Soares and Garbatov [32] and Paik and Thayamballi [64] models where developed from actual plate thickness readings from ship hull structures and do attempt to account for the existence of a CPS. However, these models assume initiation of corrosion is instantaneous and occurs at some point in time and only upon the total loss of CPS effectiveness. The assumption ignores any interaction between the CPS and its marine environment. In reality, degradation of the CPS is gradual and pitting is likely to occur somewhat earlier than the initiation of corrosion [71].

None of the models found have the capability of differentiating the degree of material loss contribution on each plate side subjected to two dissimilar environments.

2.6.2 Gradual CPS Degradation Model

Qin & Cui [71] introduced a three phase model where gradual degradation of CPS is considered and influenced by environmental factors. Like the previous models, in the first phase, the CPS is effective and no corrosion exists (Figure 5).

At some point T_{st}, corrosion will start as pitting and eventually accelerate to general corrosion, as the effectiveness of the coating is lost in its entirety. At some inflection point, T_A, the corrosion rate will begin to decelerate due to the increasing thickness of the products from corrosion and microbial biomass. Eventually, similar to the Guedes Soares and Garbatov model [33], a constant rate is reached at d_∞. The corrosion model follows a Wiebull function with four parameters: d_∞, T_{st}, η, and β .

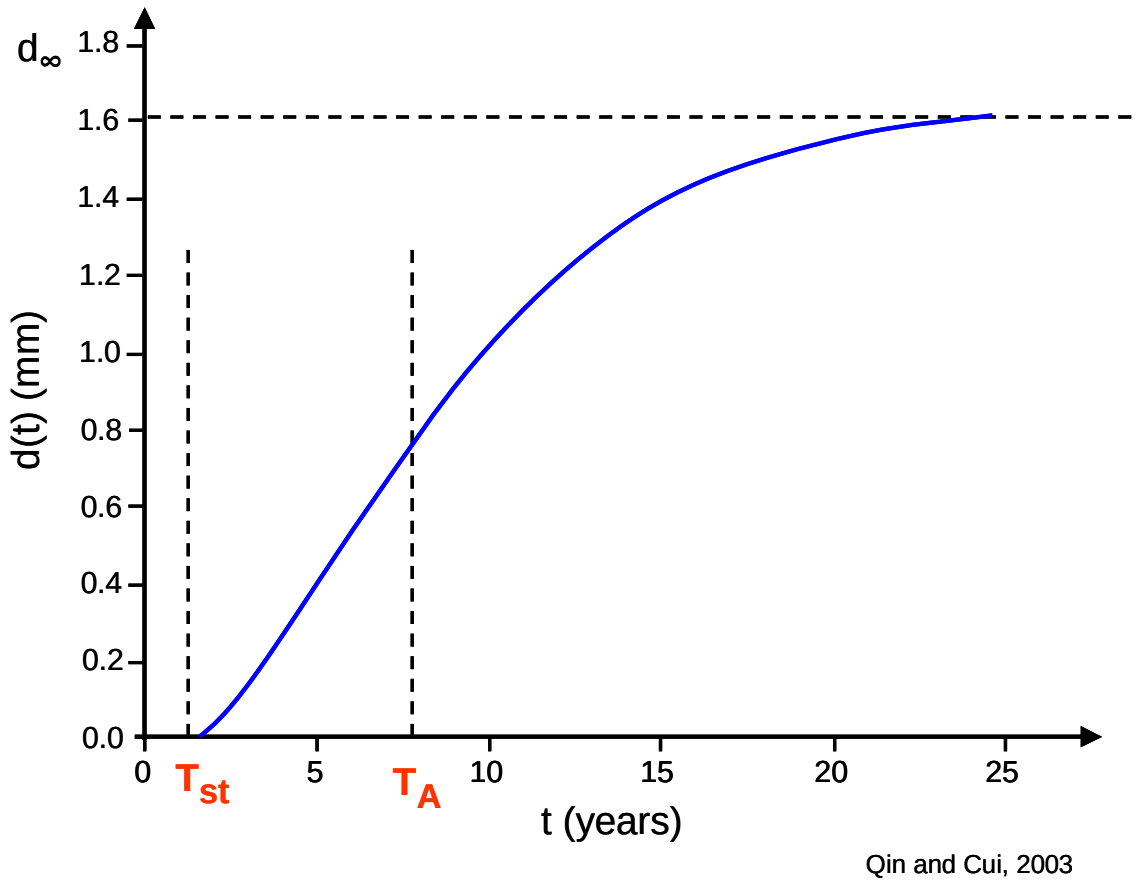

Figure 5. Qin & Cui 3-Phase Corrosion Model

$$d(t) = \begin{cases} 0, & 0 \le t \le T_{st} \\ d_{\infty}\left\{1 - \exp\left[-\left(\frac{t - T_{st}}{\eta}\right)^{\beta}\right]\right\}, & T_{st} \le t \le T_L \end{cases} \qquad (2\text{-}8)$$

The Qin & Cui [71] model is flexible such that by using certain parameters, the model can approximate the Guedes Soares and Garbatov model [33], Paik and Thayamballi [64] and Melchers [47] models.

2.6.3 Other Corrosion and CPS Research

More recent corrosion studies include Wang, Spencer and Sun [82] who created and published a database of corrosion wastage of over 110,000 thickness measurements collected from 140 tankers. This database is larger than most other corrosion databases in the public domain. The data confirms that marine corrosion wastage exhibits a high level of variability.

Gudze and Melchers [31] applied condition-based maintenance (CBM) techniques by further refining the Melchers multi-phase phenomenological corrosion model and taking into account operational environments of the vessel. Operational parameters such as seawater surface temperature based on specific travel route and varying water levels in the ballast tank are inherent with this particular study. Using simulation, the authors compared a time-directed maintenance policy with condition-based maintenance. The results provide evidence that adopting a condition-based maintenance strategy over a time-directed policy can result in a cost savings of as much as 32%. Again, uncoated test coupons suspended in the ballast tank environments provide the wastage data for model development with no means to distinguish material loss on each plate side.

In an effort to quantify coating life using expert judgment, Melchers and Jiang [58] conducted qualitative surveys using experts from vessel owners, coating contractors and suppliers, and an independent expert to determine the expected durability of epoxy coatings in water ballast tanks. The study concluded coating life, described as percentage area breakdown, approximates a normal distribution. Due to the sample size being relatively small (five experts), the ability to draw conclusions from the results is arguable.

2.7 Environmental Factors - Seawater Immersion

Melchers through a series of research initiatives [45, 49, 57] published a list of environmental factors that influence marine immersion corrosion on carbon steel with their relative importance (Table 1).

Table 1. Environmental Factors Influencing Marine Immersion Corrosion

Factor	Importance
Bacteria	Very important, long-term
Biomass	Likely of low importance
Oxygen supply	Very important, shorter term
Carbon dioxide	Little importance
Salinity	Not important by itself
pH	Important
Carbonate solubility	Not very important
Pollutants	Importance varies
Temperature	Very important
Pressure	Not important
Suspended solids	Not important
Wave action	Important
Water velocity	Important

Source: R. E. Melchers, 2006

Compared to the other factors, oxygen supply (or dissolved oxygen content) and temperature are very important influences over short-term exposure to marine immersive environment. For low velocity, shallow and unpolluted waters, these environmental factors can be reduced to average seawater temperature with minimal error [60]. Dissolved oxygen content and temperature will later provide the basis for model validation for the relative material loss experiment.

2.8 Environmental Factors – Ballast Tank

Important factors that influence corrosion rate in crude and product tanker ballast tanks include tank humidity, tank temperature, ballast type, ballast age, tank location and corrosion protection [69]. Research shows that corrosion rates vary significantly in general in different tank elevations within the ballast tank (i.e. upper, middle and lower levels) [11].

Using the Paik & Thayamballi model (Figure 4) and a somewhat sophisticated method, Paik, Lee, Hwang, and Park [65] approach relative material loss methodology by publishing average corrosion rate charts for numerous steel members and shell plating using 110,000 wastage measurements taken from 140 cargo and oil tankers. Paik, Lee, Hwang, and Park identified 34 structural member groups on a typical single hull cargo ship based on structural type, location and the adjacent marine environments.

For example, "A/B-V" = Air/Ballast Water-Vertical Shell Plate and "B/S-V" = Ballast Water/Seawater-Vertical Shell Plate. For each of the member groups, a mean corrosion rate (50%) and a severe corrosion rate (95% and above) is calculated for coating lives 5, 7.5 and 10 years. However, the methodology takes a holistic approach and does not differentiate the degree of material loss contribution on each plate side caused by each of the dissimilar environments.

Chapter 3 - Relative Material Loss Theory

Current marine corrosion research focuses on the development of probabilistic models that predict structural member thinning from a risk management and reliability perspective [28, 33, 67]. These models provide maintenance engineers with valuable tools for predicting structural failure from an ultimate limit state perspective [63]. However, the models predict material thinning from a holistic perspective and offer no means for determining material loss contribution on a particular side of the plate. Paik, Lee, Hwang, and Park [66] approached this concept by publishing charts that indicate *total* corrosion loss rates in terms of mean and coefficient of variance for steel shell plating separating various cargo tanker ballast tank environments.

Relative material loss (RML) theory leverages actual "at sea" environmental and operational conditions and the relationships between them to solve for material loss contribution of each plate side of shell plating separating two dissimilar corrosion environments. In much the same fashion as a structural engineer isolates joints on a truss and solves free body diagram equations to determine member forces [72], relative loss (RL) equations are defined across various environmental boundaries (i.e. shell plating) and solved simultaneously to suggest solutions (or material loss contributions). Implementation of RML provides the following benefits:

1. Estimating material loss contribution on each plate side provides a new tool for refining structural overhaul schedules and optimizing lifecycle performance [25].
2. RML theory provides corrosion researchers a new framework for studying the effects of environmental and operational influences on steel shell plating. The

probabilistic models found in literature can be adapted to use RML to better approximate corrosion loss of "at-sea" structures [67].

3.1 Material Loss Function

Corrosion loss of uncoated steel plate due to exposure to seawater is difficult to model due to inherit high variability in the corrosion loss data [42, 75]. Therefore, it is appropriate to represent corrosion or material loss from a probabilistic standpoint using parametric random variables. A material loss function consisting of a mean-valued function $fn(t,\mathbf{E})$ is defined:

$$c(t,\mathbf{E}) = b(t,\mathbf{E}) \cdot fn(t,\mathbf{E}) + \varepsilon(t,\mathbf{E}) \qquad (3\text{-}1)$$

where $c(t,\mathbf{E})$ is material loss, $b(t,\mathbf{E})$ is a bias function, $\varepsilon(t,\mathbf{E})$ is a zero mean uncertainty function (or precision error) about the mean value function. **E** is a vector of environmental factors that influence material loss and t is the time of exposure to the environment [50, 52, 57, 60].

For in-service or "at-sea" marine structures, corrosion protection systems such as coatings and cathodic protection are used to inhibit corrosion and extend structure service life [52, 70]. A parametric vector **P** is added to account for the effectiveness of the corrosion protection system (CPS) [71]. Accounting for CPS, the definition of the material loss function for "at-sea" structures becomes:

$$c(t,\mathbf{P},\mathbf{E}) = b(t,\mathbf{P},\mathbf{E}) \cdot fn(t,\mathbf{P},\mathbf{E}) + \varepsilon(t,\mathbf{P},\mathbf{E}) \qquad (3\text{-}2)$$

3.1.1 Bias function

Bias error is a shift of the measured mean from the true value (Figure 6). Bias error remains the same regardless of the size of the sample.

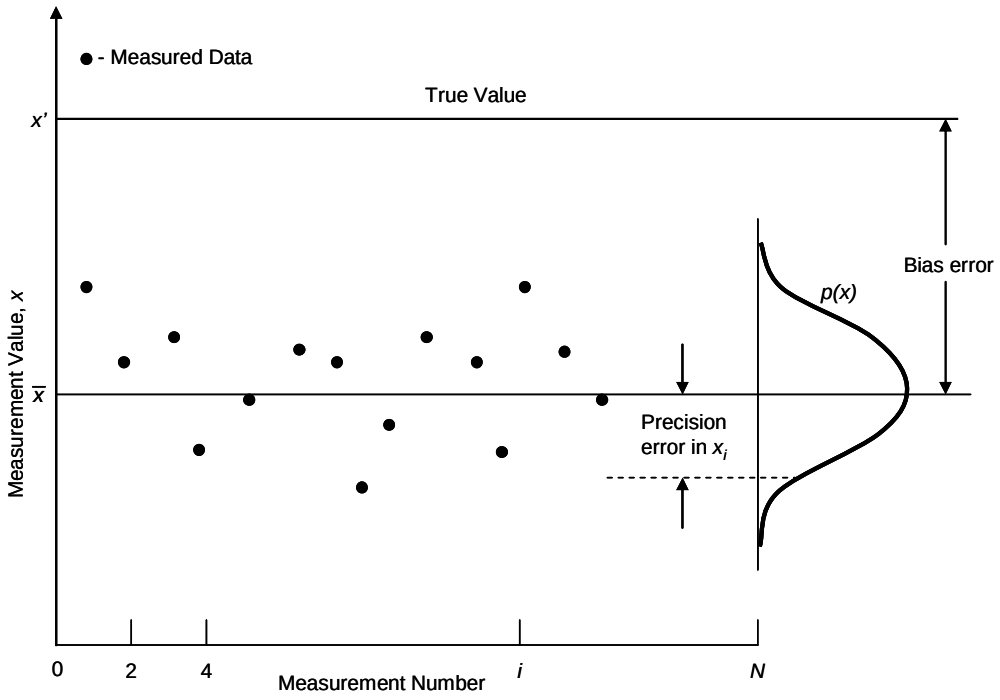

Figure 6. Relationship between bias and precision error

For example, an out of tolerance ultrasonic test device will introduce bias into the data and shift the mean from the true value. The bias function[1] *b(t)* in the material loss function is a calibration mechanism used to correct for irregularities in instrumentation and/or sampling technique [24, 70, 74]. Material loss function model calibration is performed by comparing the mean values of the material loss *c(t)* from field collected data with the predictions of the mean value model *fn(t).* Under careful experimental control and the use of sound sampling methodologies, *fn(t)* is assumed to exactly represent *c(t)* and bias is defined as unity [52]. Under this condition, the material loss function is simplified:

$$c(t) = fn(t) + \varepsilon(t) \qquad (3\text{-}3)$$

[1] Vector parameters P and E are omitted for clarity purposes.

3.1.2 Zero mean uncertainty function (precision error)

Random error occurs either by nature, process or procedure and represents data variability [24, 70, 74]. For example, a surveyor measuring plate thickness introduces a certain degree of precision error into the data based on the surveyor's experience, fatigue (mental and physical condition), motivation and training. An inexperienced surveyor is likely to introduce more precision error than an experienced surveyor, resulting in higher variability in the data [11].

The zero mean uncertainty function $\varepsilon(t)$ in the material loss function represents variability in $c(t)$ that occurs as a result of individual measurements that fall on either side of the mean value. $\varepsilon(t)$ is approximately normal with a zero mean and standard deviation, σ [52, 70].

$$\varepsilon(t) \approx N(0, \sigma) \qquad (3\text{-}4)$$

Increasing sample size reduces variability. Although complete elimination of variability is theoretically impossible, the RML theory suggests a dramatic reduction in zero mean uncertainty is possible. Using a storyboard approach, development of the RML theory continues.

3.2 Relative Material Loss

A single steel plate is fully immersed in a homogeneous marine environment. Since a homogeneous environment exists wholly around the plate, it is reasonable to assume that the rate of material loss over time is equivalent on both sides of the steel plate. The material loss contribution per side at any given time t is easily calculated by simply dividing the total measured plate material loss by two [52]. However, the determination of material loss contribution on each plate side is more complex when a single steel plate

provides a boundary between two or more dissimilar environments. The next section explores this phenomenon.

3.2.1 Single plate, dissimilar environments

A single Steel Plate A (Figure 7) with original plate thickness d_{oA} creates a boundary between two dissimilar marine environments $\mathbf{E}_1$ and $\mathbf{E}_2$, where $\mathbf{E}_1 \neq \mathbf{E}_2$. Environments $\mathbf{E}_1$ and $\mathbf{E}_2$ contribute to material loss $c_1(t)$ and $c_2(t)$, respectively, such that over time t, $c_1(t) \neq c_2(t)$. Corrosion protection systems such as coatings and cathodic protection $\mathbf{P}_1$ and $\mathbf{P}_2$ postpone the effects of material loss $c_1(t)$ and $c_2(t)$, respectively. Through ultrasonic or caliper measurement, a thickness reading of Steel Plate A at time t is taken to determine remaining plate thickness $d(t)_A$.

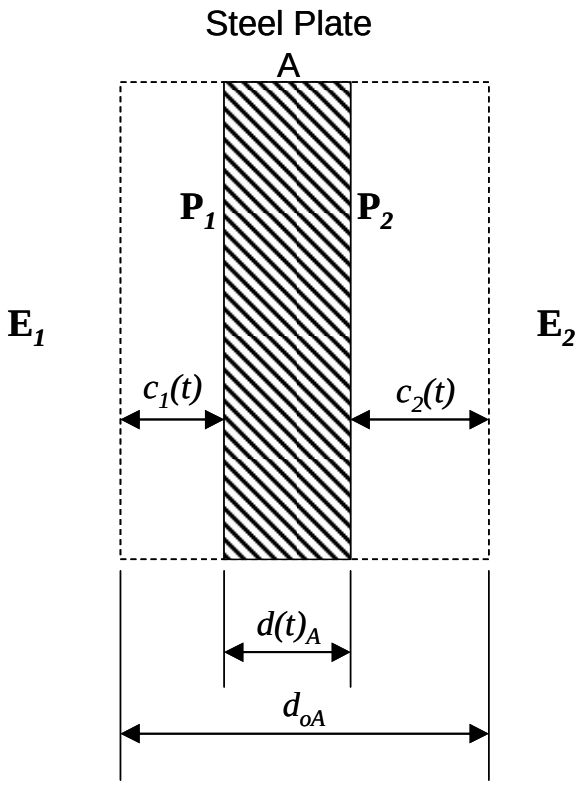

Figure 7. Single plate separating two dissimilar environments

The definition of total corrosion loss (or wastage) W_A across Steel Plate A is:

$$W_A(t) = c_1(t) + c_2(t) \tag{3-5}$$

Note: Parameter vectors **E** and **P** are omitted for clarity purposes and later added back at the end of this section. Applying the material loss function to Eq. (3-5), the bias function $b_A(t)$ and zero mean uncertainty function $\varepsilon_A(t)$ are added:

$$W_A(t) = b_A(t) \cdot \left[c_1(t) + c_2(t)\right] + \varepsilon_A(t) \tag{3-6}$$

The bias and zero mean error terms are represented holistically due to the *single* measurement W_A across Steel Plate A.

Solving for $c_1(t)$, the relative loss (RL) equation in terms $c_2(t)$ is defined as:

$$c_1(t) = \frac{W_A(t)}{b_A(t)} - c_2(t) - \frac{\varepsilon_A(t)}{b_A(t)} \tag{3-7}$$

Under careful experimental control and the use of sound sampling methodologies, bias is assumed to be unity; the RL equation reduces to:

$$c_1(t) = W_A(t) - c_2(t) - \varepsilon_A(t) \tag{3-8}$$

Where $c_1(t)$ is the material loss contribution of Steel Plate A, side 1 in terms $c_2(t)$. The parametric vectors **P** and **E** omitted earlier for clarity reasons are added back:

$$c_1(t, \mathbf{P}_1, \mathbf{E}_1) = W_A(t) - c_2(t, \mathbf{P}_2, \mathbf{E}_2) - \varepsilon_A(t) \tag{3-9}$$

$W_A(t)$ is obtained from direct field measurement (i.e. ultrasonic measuring device). However, the solution remains indeterminate. Since $c_2(t)$ is unknown, it must be determined either by assumption or modeled probabilistically. Note that the scalar value of the error term $\varepsilon(t)$ did not change. The importance of error reduction becomes apparent in the next section as a third environment and a second RL equation is considered.

3.2.2 Two Plates Separating Three Dissimilar Environments

A second steel plate (Figure 8) with original plate thickness d_{oB} shares environment $\mathbf{E}_2$ and provides a boundary between a third dissimilar marine environment, $\mathbf{E}_3$, where $\mathbf{E}_1 \neq \mathbf{E}_2 \neq \mathbf{E}_3$. Since the environments are assumed to be homogeneous, $c_2(t)_{PLATE\ A} = c_2(t)_{PLATE\ B}$.

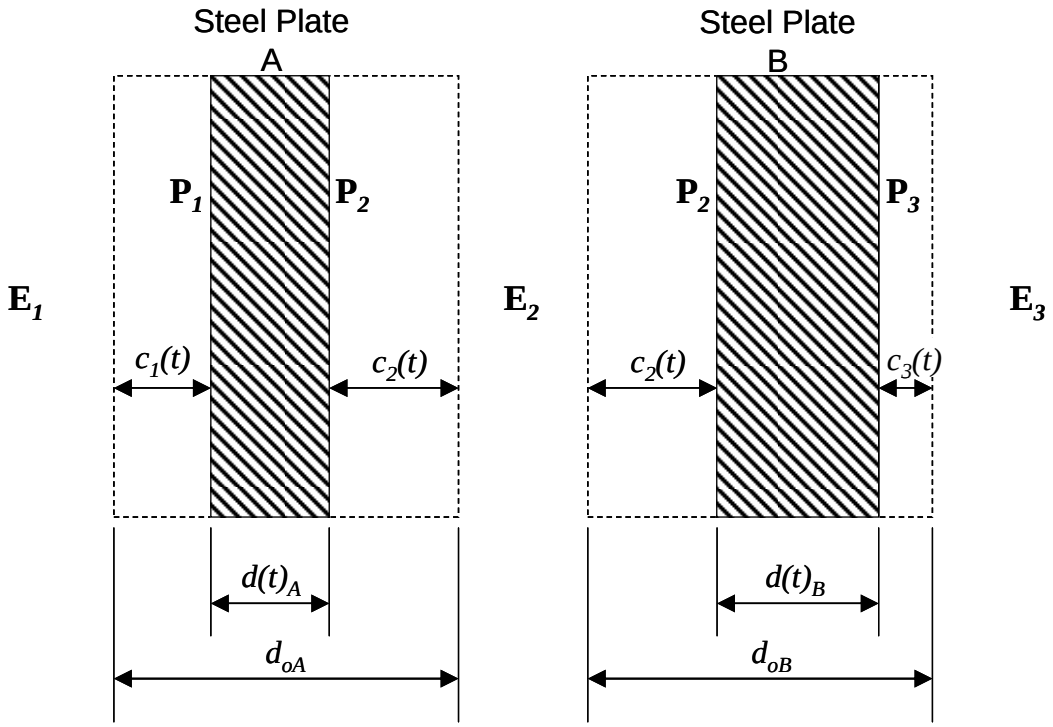

Figure 8. Two plates separating three dissimilar environments

The definition of total corrosion loss of the steel plate, W_B across steel plate B is:

$$W_B(t) = c_2(t) + c_3(t) \qquad (3\text{-}10)$$

The bias function $b_B(t)$ and zero mean uncertainty function $\varepsilon_B(t)$ are added:

$$W_B(t) = b_B(t) \cdot \left[c_2(t) + c_3(t)\right] + \varepsilon_B(t) \qquad (3\text{-}11)$$

Solving for $c_2(t)$, a second RL equation is defined:

$$b_B(t) \cdot c_2(t) = W_B(t) - b_B(t) \cdot c_3(t) - \varepsilon_B(t) \qquad (3\text{-}12)$$

Combining the two RL equations (3-8) and (3-12) and solving simultaneously, the RL equation in terms of $c_1(t)$ is defined as a function of $c_3(t)$:

$$c_1(t) = c_3(t) + \left[\frac{W_A(t) - \varepsilon_A(t)}{b_A(t)}\right] - \left[\frac{W_B(t) - \varepsilon_B(t)}{b_B(t)}\right] \qquad (3\text{-}13)$$

Rewriting the RL equation to isolate the two error terms:

$$c_1(t) = c_3(t) + \frac{W_A(t)}{b_A(t)} - \frac{W_B(t)}{b_B(t)} + \frac{\varepsilon_B(t)}{b_B(t)} - \frac{\varepsilon_A(t)}{b_A(t)} \qquad (3\text{-}14)$$

Under careful experimental control and the use of sound sampling methodologies, bias is assumed to be unity; the RL equation reduces to:

$$c_1(t) = c_3(t) + W_A(t) - W_B(t) + \varepsilon_B(t) - \varepsilon_A(t) \qquad (3\text{-}15)$$

Note that under conditions where $\varepsilon_A(t) \approx \varepsilon_B(t)$, the error term in Eq. (3-15) approaches zero. Under this condition, it is assumed the error term approaches negligibility (or "zero error"). The parametric vectors **P** and **E** omitted earlier for clarity reasons are added back. A "zero error" RL equation $c_1(t)$ as a function of $c_3(t)$, $W_A(t)$ and $W_B(t)$ is defined:

$$c_1(t, \mathbf{P}_1, \mathbf{E}_1) = c_3(t, \mathbf{P}_3, \mathbf{E}_3) + W_A(t) - W_B(t) \qquad (3\text{-}16)$$

3.3 Assumptions

Under "zero error" conditions, the following assumptions are made:

1. The marine immersion environments are stratified such that conditions that cause material loss are laterally homogeneous and longitudinally heterogeneous. Studies have shown that water depth is an important influential factor [56, 61].
2. Workmanship for surface preparation and application of the coating protection system is assumed consistent and equivalent on all sides of the plates. This

assumption is reasonable for work crews that typically work to an industry standard such as the Steel Structures Painting Council (SSPC) [40].

3. The material thinning due to grit blast or water blasting is assumed to be consistent and equal on all sides of the plates [25].
4. The durability and coating life of the coating protection system is assumed to be the same on all sides of the plates [58].
5. Where cathodic activity exists, the electrical current flow through the electrolyte (i.e. seawater) is assumed equal on both sides of the immersed plate. Therefore, if cathodic protection exists, the resistance to corrosion by cathodic protection is assumed equal.
6. Inspector's qualifications and equipment calibration is assumed to be of high quality and data sampling conducted in a controlled manner.

The "zero error" assumptions made above simplify the solution for the variability due to these elements exists on both sides of the plates and are assumed equal. Since RML is based on two-sided corrosion, these errors mathematically drop out when introduced into the RL equations. The resulting difference (or relative material loss) between the two sides of a boundary plate represent wastage influenced by known environmental and operational parameters.

If $c_3(t)$ in Eq. (3-16) is not known or cannot be reasonably assumed, additional RL equations can be defined to provide a more deterministic solution. For example, a third relationship between vertical shell plate stiffeners that exists in $\mathbf{E}_2$ and adjacent to Shell Plates A and B can be established and RL equations defined and solved for $c_2(t)$. The more RL equations that are introduced, the more the solution becomes potentially

constrained. By using RL equations to define upper and lower bounds, linear programming techniques can be employed to solve the more complex RML problems [83]. To constrain the research, the experiment is conducted on a structure that lends itself to a reasonable assumption of $c_3(t)$.

Chapter 4 - Experiment

4.1 Research Objective and Questions

The main research objective is to answer the following:

Q: Is the relative material loss (RML) theory valid?

This question is tested through experimentation using actual material loss data obtained from an "at-sea" structure: a dry dock caisson gate. The following main research hypothesis is tested:

H_0: Using relative loss (RL) equations to describe material loss across steel shell plating exposed to dissimilar environments, an effective solution is possible that approximates material loss contribution on each plate side.

H_1: An effective solution is not found.

Effectiveness will be determined both qualitatively and quantitatively. Qualitative effectiveness will be determined by visually comparing the material loss contribution profiles with profiles of environmental factors that are known to influence marine corrosion found in the literature. To approximate effectiveness quantitatively, the profiles are simplified to linear relationships and a correlation made using Pearson's product moment correlation [18, 73]. The correlation will determine how well material loss of the isolated side correlates with environmental factors that are known to cause marine corrosion found in the literature. A significant level of $\alpha = 0.05$ will be used to test for effectiveness.

4.2 Dry Dock Caisson Gate

A dry dock caisson gate is a floatable steel vessel positioned and submerged on the sill of the open end of a dry dock to serve as a barrier between the free water and the dry dock interior (Figure 9).

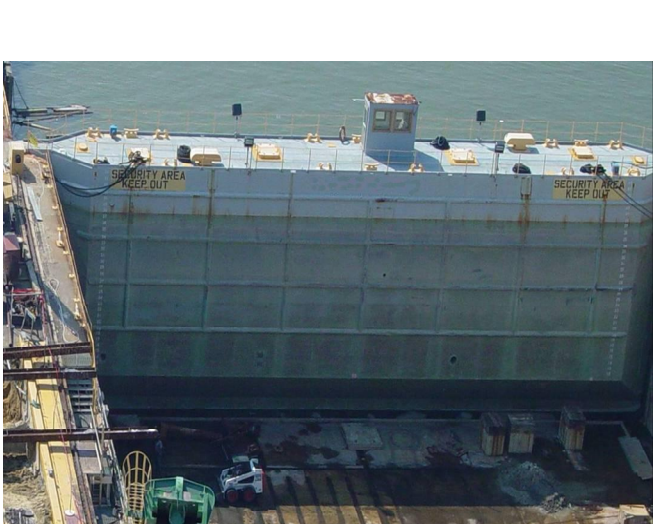

Courtesy: Northrop Grumman Shipbuilding

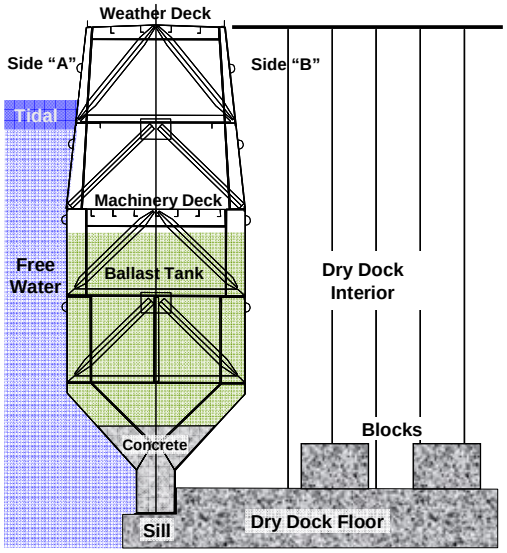

Figure 9. Dry Dock Caisson Gate "D" and Section View

Once the dry dock caisson gate is in place and the ship aligned over prearranged blocks, the dry dock is dewatered and the ship is safely lowered onto the blocks. As the water level of the dry dock lowers, hydrostatic forces from the free water side of the gate increase and cause a natural water seal, forcing the caisson gate rubber seal to press into the concrete abutments around the bottom and two sides of the gate. Upon completion of dry dock dewatering and the ship safely seated on the blocks, ship maintenance and repair operations can safely be conducted on the ship hull, waterborne structures, and mechanical systems otherwise exposed to the sea [37].

A caisson gate is designed and constructed for a specific dry dock and its dimensions will vary in accordance with the particular dry dock it services. Similar to ship hull structures, caisson gates are made of mild carbon steel plates, shapes and stiffeners. A typical caisson gate contains four tank compartments - one main ballast tank for buoyancy control, two trim tanks on each end for leveling and one concrete "tank" to maintain negative buoyancy when seated on the dry dock sill (Figure 10).

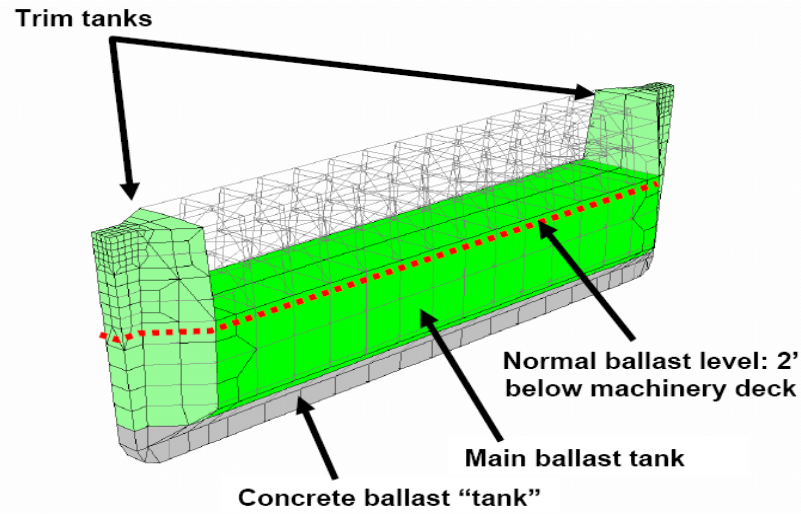

Courtesy: Northrop Grumman Shipbuilding

Figure 10. Caisson Gate Ballast Tanks

Employment of cathodic protection in the form of zinc anodes is typical in areas susceptible to high corrosion rates to attempt to abate the rate of corrosion [35, 40]. Unlike the dynamic loading of ship hull structures at sea, caisson gate loading conditions are static in nature. Hence, caisson gate structural plating, framing and coating protection system are not typically subjected to cyclical fatigue stress and wear as is usual with "at sea" ship hull structures [33, 67].

4.3 Caisson Gate "D"

The material loss data obtained for this research is from 2005 maintenance records from a dry dock caisson gate located along the James River in the Tidewater Virginia area. The owner requires anonymity for the caisson gate so the structure is designated as caisson gate “D” herein.

Caisson gate “D” was originally constructed in 1940-1941 and is 138’-0” in length, 45’-0” in depth and 18’-0” in breadth. The dry weight displacement including the concrete ballast is 545 long tons. The gate is symmetric about its longitudinal centerline as well as the transverse plane amidships. The gate is rotatable and at the time of data collection, the forward end of the gate was orientated towards the north side of the dock; the port, or side “A”, faced the river and the starboard, or side “B”, side faced the dry dock (Figure 9). The weather deck and machinery deck are watertight and access is through two (2) watertight hatches. There is permanent concrete ballast the length of the gate up to approximately 8’ above baseline. It is sloped towards the gate’s longitudinal center as well as forward and aft towards the two ballast pump sumps, near forward and aft [23].

The main ballast tank is beneath the machinery deck, above the concrete ballast and between the watertight bulkheads (Figure 9). While the gate is seated and the dock is dry, the main ballast and trim tanks are flooded to about 2’ beneath the machinery deck, (Figure 10). The gate has a rubber seal on the side shell about 8” from the lower and outboard edges of the seat section.

The owner uses a reference plane when referring to the height of the water inside and outside of all of its caisson gates. This water level, "elevation 101.19' ", is at the height of the mean high water[2]. Elevation 100' is at 37'-0" above the gate baseline.

Caisson gate "D" was chosen for the research for the following reasons:

1. The marine environments are conducive for allowing a reasonable assumption of $c_3(t)$, thus simplifying the experiment, see Eq. (3-16).
2. At the time of data collection, the age of the caisson gate was 65 years old. The advanced age of the structure provides a "ripe" marine environment for studying material loss on "at-sea" structures due to mature data variability [14].
3. The caisson gate marine environments are static and docile, thus structural plating, framing and coating protection system are not subject to cyclical fatigue stress and wear. Therefore, eliminating dynamic loading as an environmental consideration.
4. The data collection process was performed by experienced marine surveyors, supporting the reasonable assumption that the inspector's qualifications and equipment calibration is of high quality and the data sampling was conducted in a controlled manner.

4.4 Main Ballast Tank Marine Environments

The scope of the research is constrained to the main ballast tank shell plating and excludes the two trim tanks fore and aft (Figure 10). Caisson gate "D" main ballast tank shell plating is exposed to five marine environments (Figure 11): ballast tank atmospheric

[2] Mean high water (MHW) was originally defined at 100.00 when the shipyard was founded in early 1900s to maintain positive dock floor elevations. Over time, the shipyards MHW has been recalibrated to keep up with rising sea level trends [13].

(E_1), marine atmospheric (E_2), ballast tank immersed (E_3), river water (E_4), and concrete ballast (E_5).

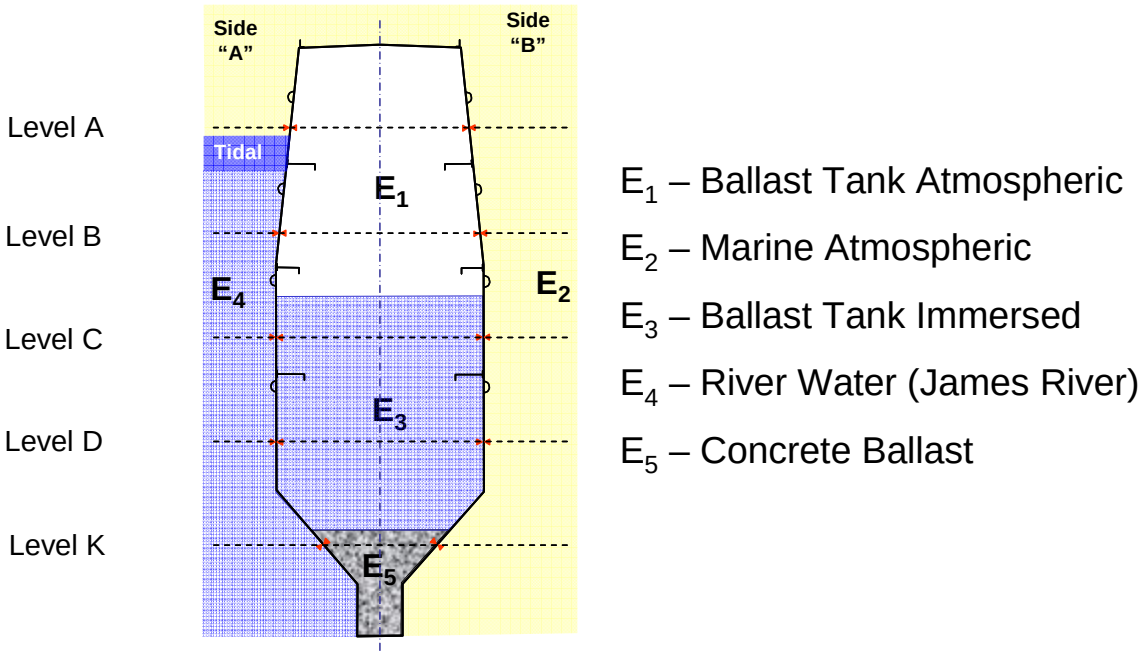

Figure 11. Caisson Gate Marine Environments

Time of wetness, salt disposition and temperature are factors influencing material loss of shell plating inside the ballast tank atmosphere, E_1. A thin layer of moisture due to high humidity within the enclosed tank environment yields partial anodic and partial cathodic reactions, resulting in expected lower corrosion rates compared to the immersed water environments [27, 61, 78]. For the marine atmosphere, E_2, periods of wetness and temperature are further reduced, causing an anticipated further corrosion rate reduction of the exterior shell plating. Due to assumed sound maintenance practices on the E_1 and E_2 exposed surfaces (e.g. ease of access for maintenance inspections, painting and paint longevity), material loss in these areas is expected to be minimal or even negligible.

Average mean ballast tank water temperatures are expected to exceed river water temperatures due to solar heating of the caisson gate structure [78]. With stagnate water and elevated water temperatures inside the ballast tank, microbial and organic plant life inside the ballast tank are expected to exceed typical river levels. The expectation is a lower dissolved oxygen content in the ballast water than the river water [54].

The river water environment, E_4, is classified by the Commonwealth of Virginia as a *Class II: estuarine water* (tidal water-coastal zone to fall line). Meaning, the river water in the vicinity of the caisson gate is tidally influenced with semidiurnal tides and contains brackish water [44].

The concrete ballast environment, E_5, is dependant on the condition of the 65 year old concrete. Sea water attack on immersed concrete can cause the ingress of chemical constituents from sea water on the cement hydration products (paste matrix), ultimately allowing salts to leach into the concrete structure and reach the interior shell plating over time [36]. Since the interior shell plating is non accessible and the interior steel surface has achieved a service life of 65 years without maintenance, pitting corrosion due to anaerobic conditions is plausible [55, 59].

4.5 Shell Plating Thickness Measurements

The requirements for structural inspection of caisson gate "D" is governed by MIL-STD-1625C [7, 8]. MIL-STD-1625C requires thickness measurements of the caisson gate shell plating on an 8' x 8' grid pattern (Figure 12). The sample sets are grouped according to caisson gate level (A, B, C, D and K[3]), each containing 14 samples. The

[3] Keel level

measurements are taken from forward to aft, every third frame starting at frame number 2 and ending at frame number 41. Five sample sets are collected from each side (Side "A" and Side "B") for a total of ten sample sets. The naming convention as shown in Figure 12 is adopted. The owner's elevation datum is used where mean high water is equal to 101.19. It is important to note that the Level A samples for Side "A" and Side "B" (D-AASP and D-BASP) are taken at elevation 101.3 and, therefore, are considered in marine atmospheric environment and not in the river or tidal zones. No measurements are taken in the tidal/splash zone.

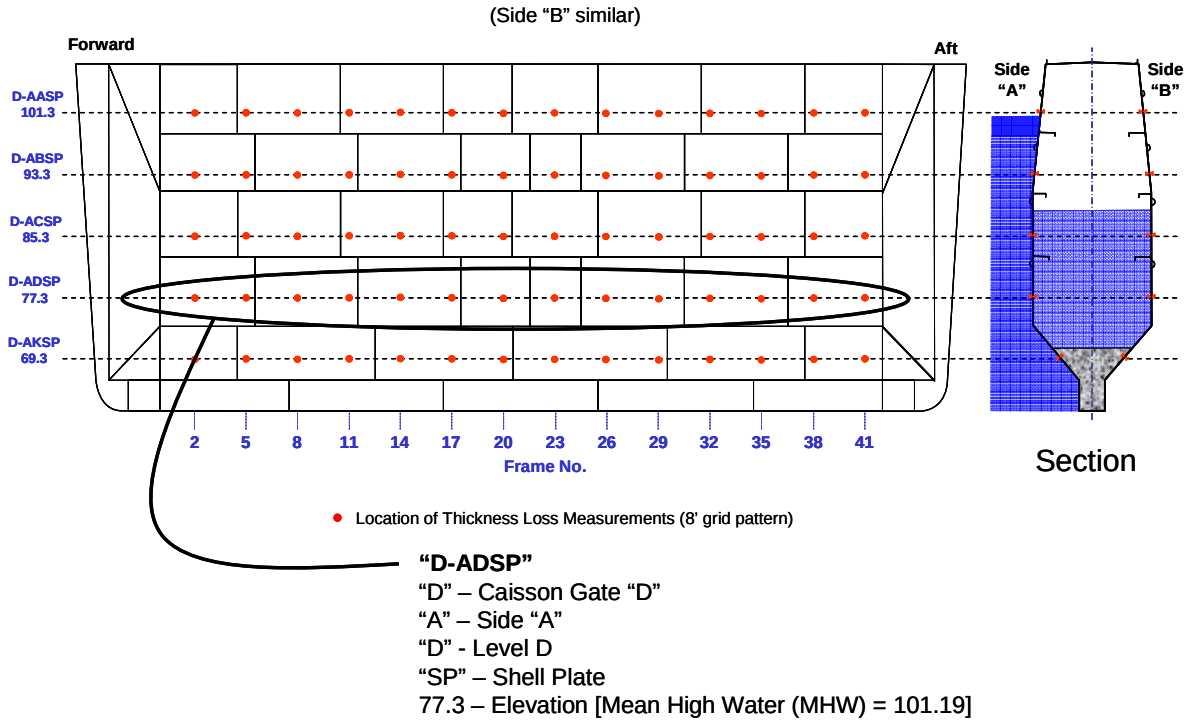

Figure 12. UT Measurement Locations and Nomenclature

Typical sampling techniques often used for inspection of underwater structures include "systematic", "pure random" and "cluster" sampling [13, 39]. The MIL-STD-1625C

sampling strategy approaches "systematic" sampling, where samples are taken on a set spacing [8]. In this case, the spacing is every third frame (or approximately 8'). The marine surveyor's methodology and equipment specifications are of high quality and data sampling conducted in a controlled manner. See Appendix A for further details.

4.6 Water Quality Samples

Water quality parameters will be used for model validation. On July 16, 2008, water quality parameters temperature and dissolved oxygen were measured inside the caisson gate main ballast tank and immediately outboard of the caisson gate (river water). A digital water quality multi-meter[4] was lowered and readings recorded at water depths 2', 5', 10', and just above the top of concrete in the ballast tank (17.9'). Outboard the caisson gate, the device was lowered and readings recorded at 2', 5', 10', 20 and 30' from top of river water. See Appendix B for further details regarding the device specifications and calibration data.

4.7 Supporting Questions

To support the main research objective in Section 4.1, the following three supporting questions concerning the marine environments and material loss data are answered. The first test is to determine if the marine immersion environments (E_3 and E_4) separated by shell plating are in fact dissimilar.

[4] Yellow Springs Instruments, Inc. model no. YSI 600 XL

4.7.1 Environmental Dissimilarity

Q1: Are the marine immersion environments separated by the shell plating dissimilar?

To answer this question, a paired t-test [19] is performed on the environmental factors known to cause marine corrosion found in literature between the river and ballast tank waters. It is known that temperature and dissolved oxygen are important environmental factors that influence corrosion (Table 1) [34, 49, 67]. To test for environmental dissimilarity, water temperature (T) and dissolved oxygen (DO) content will be tested at various depths inside the caisson gate ballast tank and immediately outside along the river side of gate. For the temperature paired t-test, the following hypothesis is tested using a significance level of $\alpha = 0.05$ and confidence interval = 95%:

$H1.1_0$: $\mu_{Temp\ River\ Water} - \mu_{Temp\ Ballast\ Water} = 0$
$H1.1_1$: $\mu_{Temp\ River\ Water} - \mu_{Temp\ Ballast\ Water} \neq 0$

The paired t-test results in a T-value = -9.91 and p-value < 0.001. Meaning, there is strong evidence that the mean water temperatures are significantly different. See Appendix C for more information on the water temperature paired t-test and the associated 95% confidence intervals.

Next, a paired t-test is performed between the ballast tank and river water dissolved oxygen content at various elevations and the following hypothesis is tested using a significance level of $\alpha = 0.05$ and confidence interval = 95%:

$H1.2_0$: $\mu_{DO\ River\ Water} - \mu_{DO\ Ballast\ Water} = 0$
$H1.2_1$: $\mu_{DO\ River\ Water} - \mu_{DO\ Ballast\ Water} \neq 0$

The paired t-test results in a T-value = 2.39 and p-value = 0.029. Meaning, there is evidence that the mean dissolved oxygen contents are significantly different. See

Appendix C for more information on the dissolved oxygen content paired t-test and the associated 95% confidence intervals.

Since neither of the confidence intervals in both tests contains zero and the p-values are less than 0.05, it is concluded that there is significant evidence that the environmental factors temperature and dissolved oxygen content between the ballast tank and river water environments are in fact dissimilar. A similar conclusion is deduced qualitatively by simple inspection of the figures in the appendices as well.

4.7.2 Environmental Stratification

The marine immersion environments are stratified such that conditions that cause material loss are laterally homogeneous and longitudinally heterogeneous. The following question is addressed.

Q2: Are the immersed marine environments laterally homogeneous and longitudinally heterogeneous?

To answer this question, the caisson gate material loss samples are grouped into two halves: forward end to mid-gate and aft end to mid-gate. A one-way analysis of variance (ANOVA) of the two sample means is conducted [2, 18]. The following hypothesis is tested using a significance level of $\alpha = 0.05$:

$H2.1_0$: $\mu_{Aft\ Half} = \mu_{Forward\ Half}$
$H2.1_1$: $\mu_{Aft\ Half} \neq \mu_{Forward\ Half}$

For the environments to be laterally homogeneous, the null hypothesis must fail to reject. The one-way analysis of variance results for Sides “A” and “B” are summarized below:

Side “A”	F-value = 0.66	p-value = 0.421
Side “B”	F-value = 1.84	p-value = 0.180

For both sides, since both p-values > 0.05, there is not enough evidence to reject the null hypothesis. Therefore, both null hypotheses fail to reject and the conclusion is marine immersion environments for Sides "A" and "B" are laterally homogeneous. See Appendix D for the one-way analysis of variance and box plots.

To test for longitudinally heterogeneity, ANOVA is performed on the material loss at each caisson gate level. The following hypothesis is tested:

$H2.2_0$: The means at each level are equal: $\mu_{Loss\ Level} = \mu_{Loss\ Other\ Levels}$
$H2.2_1$: At least one mean is significantly different: $\mu_{Loss\ Level} \neq \mu_{Loss\ Other\ Levels}$

For the environments to be longitudinally heterogeneous, at least one level will be significantly different, causing the null hypothesis to reject. The one-way analysis of variance results for Sides "A" and "B" are summarized below:

Side "A"	F-value = 24.69	p-value < 0.001
Side "B"	F-value = 11.34	p-value < 0.001

For both sides, since both p-values are significantly less than 0.05, at least one level on each side is different, providing evidence to reject the null hypothesis. Therefore, both null hypotheses are rejected and it is concluded that the marine immersion environments for Sides "A" and "B" are longitudinally heterogeneous. See Appendix E for the one-way analysis of variance and box plots. A similar conclusion is deduced qualitatively by simple inspection of the box plots in the appendices as well.

4.7.3 Test for Normality and Outliers

Once laterally homogeneity and longitudinally heterogeneity has been established, the sample sets as defined in Section by 4.5 are tested for normality and outliers [2]. Establishing normality is fundamentally important for the subsequent sections on

polynomial regression assume normality. The following question is addressed in this section:

Q3: Are the sample sets normally distributed?

Using $\alpha = 0.05$ ($A^{2*} = 0.752$) as a two-tailed test statistic, each of the ten sample sets are tested for normality using the Anderson-Darling normality test [9] and outliers using Extreme Studentized Deviate test (Grubbs' Test) [29, 30]. No outliers were detected. A summary of the results is presented in Table 2.

Table 2. Anderson-Darling Normality and Grubb's Test for Outliers

Sample Set	A^2	A^{2*}	P-value	Outliers (Grubbs)
D-AASP	0.300	0.319	0.535	None detected
D-ABSP	0.265	0.283	0.636	None detected
D-ACSP	0.360	0.383	0.396	None detected
D-ADSP	0.395	0.421	0.324	None detected
D-AKSP	0.371	0.395	0.373	None detected
D-BASP	0.709	0.755	0.050	None detected
D-BBSP	0.914	0.974	0.014	None detected
D-BCSP	0.526	0.560	0.147	None detected
D-BDSP	0.307	0.327	0.519	None detected
D-BKSP	0.190	0.203	0.878	None detected

Sample sets with p-values greater than or equal to $\alpha = 0.05$ are said to be normally distributed. With the exception of sample sets D-BASP and D-BBSP, all the samples sets conclusively exhibit normality.

D-BASP is marginally normal (p-value = 0.050) and D-BBSP is questionably normal (p-value = 0.014). As postulated in Section 4.4, total material loss in the E_1 to E_2 areas may be minimal or even negligible. This is due to the light corrosive environments

inherit with these environments. The fact that a majority of the measurements are negative supports this claim (Figure 13). A nonparametric curve fitting technique (i.e. LOWESS[5]) is employed to validate parametric curve fitting.

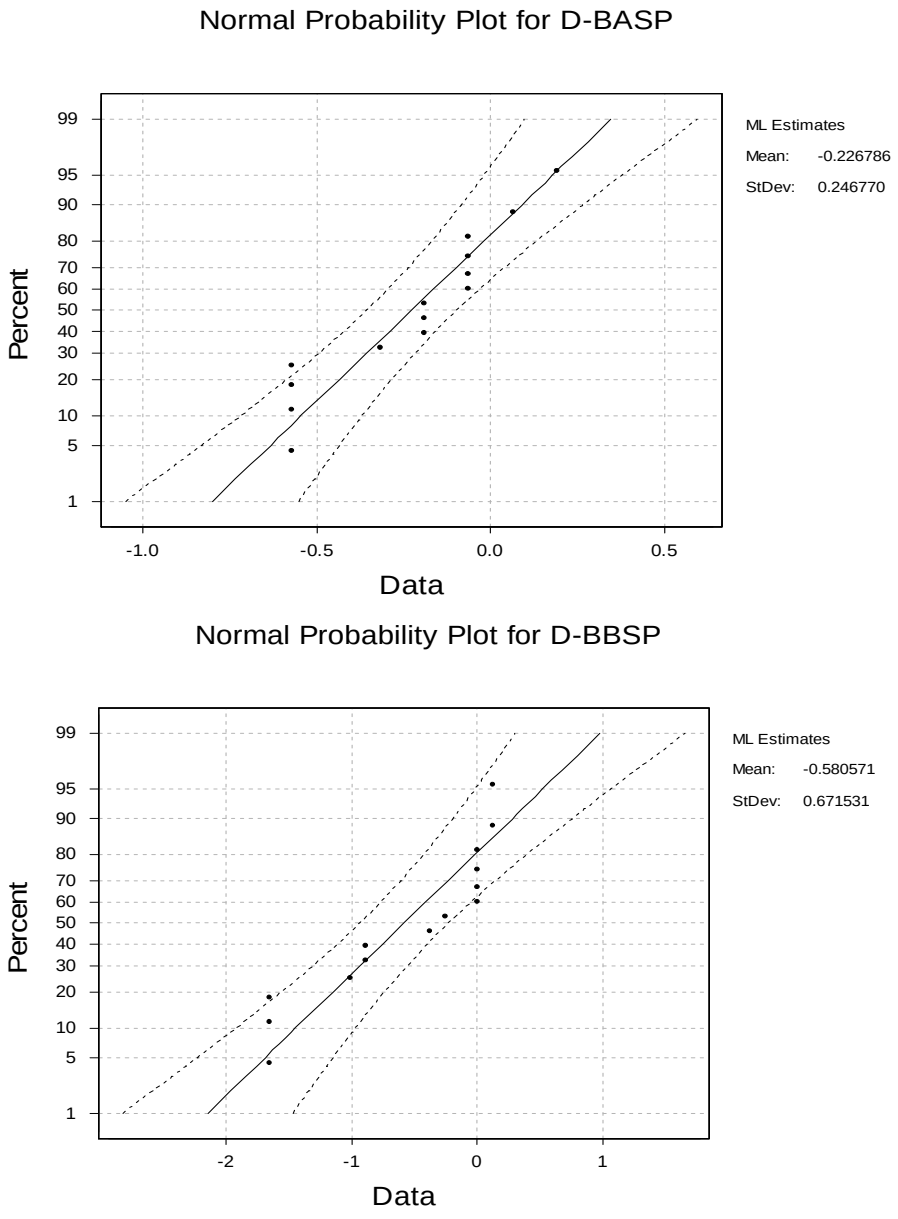

Figure 13. Normal Probability Plots for D-BASP & D-BBSP

[5] Locally Weighted Estimated Scatter Smoother

4.8 Robust Locally Weighted Regression (LOWESS)

To provide a nonparametric picture of the overall material loss profile across the caisson gate shell plating, a robust locally weighted regression (LOWESS) is performed on each of the ten sample sets. LOWESS provides a nonparametric technique for smoothing 2D scatter plots. LOWESS is conducted by performing local polynomial regression at each data point and the points in close vicinity [16, 17].

An iterative technique using Minitab© LOWESS module is conducted where the STEP value is held constant at 2 and FIT is varied from 0.1 to 1.0 in increments of 0.1. For each FIT, an Anderson-Darling normal probability test is performed on the LOWESS residuals. The FIT that produces the maximum Anderson-Darling p-value are selected as best LOWESS fit (Table 3).

Table 3. Step, Fit and Maximum Anderson-Darling p-values on the LOWESS Residuals

Sample Set	LOWESS STEP	LOWESS FIT	Maximum AD p-value
D-AASP	2	0.6	.984
D-ABSP	2	1.0	.821
D-ACSP	2	0.9	.558
D-ADSP	2	0.4	.625
D-AKSP	2	0.8	.705
D-BASP	2	0.8	.571
D-BBSP	2	0.4	.508
D-BCSP	2	0.9	.654
D-BDSP	2	0.4	.717
D-BKSP	2	0.3	.940

Source: MINITAB Release 12.23

Using Minitab© residual model diagnostics module, the goodness-of-fit of each LOWESS curve is validated by checking the residuals:

1. Normal Plot of Residuals – visual check for normality of the residuals
2. I-Chart of Residuals – visual check for autocorrelation of the residuals
3. Histogram of Residuals - visual check for non-normality of the residuals
4. Residuals vs. Fits – visual check for heteroscedasticity of the residuals [21]

The LOWESS curves for each sample set are plotted in Appendix F. However, because LOWESS is nonparametric, the material loss profiles cannot be represented mathematically nor can confidence intervals be easily generated without resorting to manual bootstrapping techniques [84]. To provide a mathematical model of the material loss profiles, polynomial regression modeling (or curve fitting) provide mathematical representations of the LOWESS fits. A careful comparison of the polynomial regression models with each LOWESS fit is performed.

4.9 Polynomial Regression Models (Curve Fitting)

For each sample set, a least squares method is used to create polynomial regression models [2]. The models define the best algebraic expression of material loss as a function of caisson gate frame location for a given elevation. The models are used to (1) extrapolate values in between measured sample points and (2) provide 95% confidence intervals about the point estimates (Appendix F). Normally distributed random error is assumed within the sample sets and supported in Section 4.7.3. Because frame number equal to zero is outside the experimental region, an intercept term was included in all models. Where no relationship between material loss and frame number were detected (i.e. the regression line is horizontal), the sample mean was used [73].

The Minitab© regression analysis module is used to develop the models. The model that produces the maximum adjusted regression coefficient (adj. R^2) and lowest overall p-

value in the regression analysis of variance is selected as best fit. Overlaying the polynomial regression models over the LOWESS models (Section 4.8) provides an independent validation of both models. The details of each polynomial regression and LOWESS model are presented in Appendix F. A summary of the regression coefficients and p-values is provided in Table 4.

Table 4. Polynomial Regression Models - R-squared and p-values

Sample Set	R^2	Adjusted R^2	ANOVA p-value
D-AASP	38.5	20.1	.166
D-ABSP	59.8	56.4	.001
D-ACSP	no correlation, use mean		
D-ADSP	54.7	34.6	.098
D-AKSP	70.8	52.5	.044
D-BASP	89.8	77.8	.013
D-BBSP	57.3	38.7	.076
D-BCSP	46.0	36.2	.034
D-BDSP	56.1	42.9	.035
D-BKSP	77.6	67.6	.005

Source: MINITAB Release 12.23

The adjusted R^2 values range from 20.1% to 77.8% and p-values 0.001 to 0.166. The regression line for D-ACSP is nearly horizontal meaning the arithmetic mean of the sample set is a valid model. The ANOVA p-values for polynomial regression models D-ADSP and D-BBSP exceed the significance test value of $\alpha = 0.05$ but are significant for $\alpha = 0.1$. The ANOVA p-value for polynomial regression model D-AASP exceeds all meaningful levels of significance; possibly for the reasons stated in Section 4.4.

However, validation of polynomial regression model D-AASP (as well as the other nine models) is qualitatively supported due to its close fit to the LOWESS curve and the LOWESS being well within the model's 95% confidence intervals (Appendix F). The polynomial regression models are used to calculate point estimates horizontally along the caisson gate shell plating. The general form of the polynomial regression model is:

$$W_{D-nmSP_x} = f(x) \qquad (4\text{-}1)$$

where W is total material loss (wastage) on caisson gate side n = (A or B) and caisson gate level m = (A, B, C, D or K) for any caisson gate frame location x = (2, 3, 4, …41). *D* and *SP* are designators for caisson gate "D" and "shell plate", respectively.

A composite summary of the polynomial regression models for Sides "A" and "B" indicate high variability in the data (Figure 14).

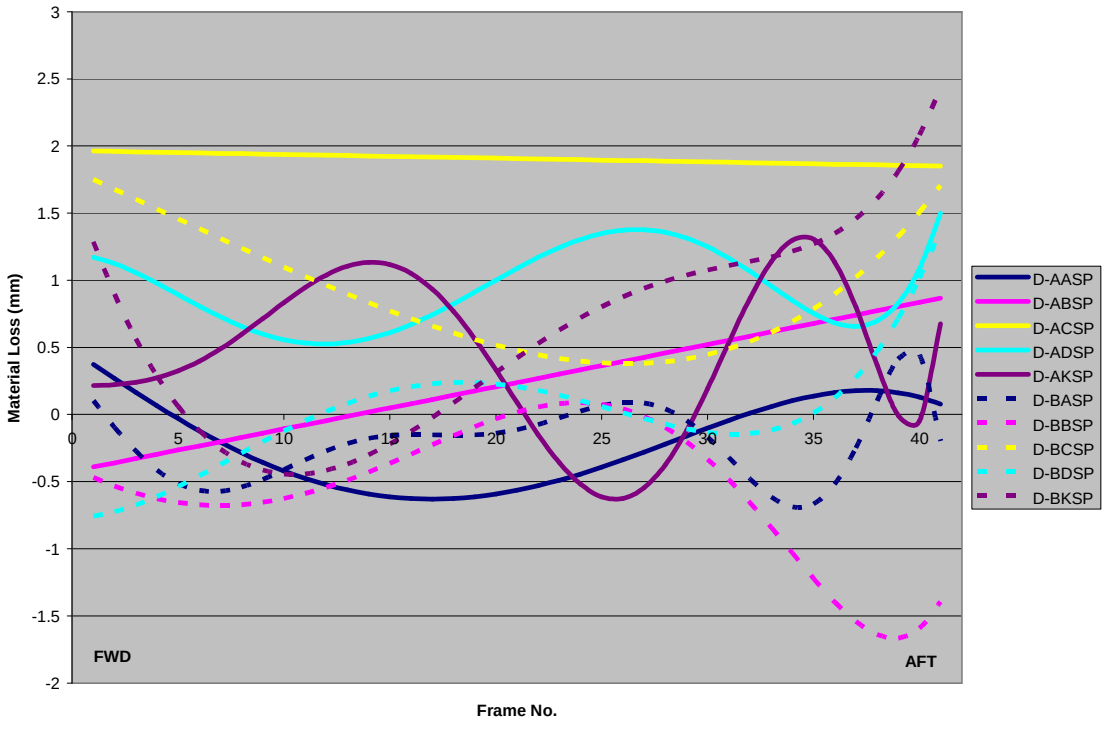

Figure 14. Polynomial Regression Models - Sides "A" and "B"

The solid lines represent the Side “A” profiles and the dashed lines the Side “B” profiles for all five levels.

4.10 Negative Wastage Measurements

The sample sets contain thickness measurements that when subtracted from the original plate thickness yield negative wastage (Figure 14). Plate thickness increase is cited as not an infrequent occurrence and possibly a result of measurement error [51]. However, through comparison of the caisson gate sample sets (Appendix F), negative corrosion is more apparent in shell plating exposed to less (and possibly negligible) corrosive environments (sample sets D-AASP, D-ABSP, D-BASP and D-BBSP); a phenomenon not likely to be caused by measurement error.

An assumption is made that thickness increase in the sample sets is due to plate thickness overage inherit from the manufacturing process. To test this assumption, histograms of all thickness measurements are plotted from shell plating from four caisson gates and a LOWESS curve is fit to define a distribution (Appendix G). The fit of the LOWESS is adjusted until a definable intercept occurs on the negative end (left end) of the distribution. The intercept of each distribution is compared to the ASTM allowable overage tolerance of 1.78 mm [4]. A summary of results is provided in Table 5.

Table 5. Comparisons of shell plating negative wastage measurements

Caisson Gate	Age (Year built)	Negative Intercept
A	1961	-1.05 mm
B	1958	-0.75 mm
C	1978	-1.57 mm
D	1941	-1.75 mm
Allowable Plate Overage: (ASTM A 6/A 6M – 07)		-1.78 mm

A reasonable assumption is made that steel plate manufacturing process has not significantly changed in the last 65 years and negative wastage found in the sample sets is due to plate thickness overage inherit from the manufacturing process. Therefore, for the convenience of keeping the values positive, 1.78mm is added to the polynomial regression models developed in Section 4.9 such that:

$$W_{D-nmSP_x} = f(x) + 1.78 \qquad (4\text{-}2)$$

A sensitivity analysis of the data reveals that this adjustment only shifts the material loss contribution profiles to the right and does not impact overall experimental results.

4.11 Relative Loss Equations

Ten (10) relative loss (RL) equations are defined at Levels A, B, C, D and K and on Sides "A" and "B" for caisson gate "D" (Figure 15).

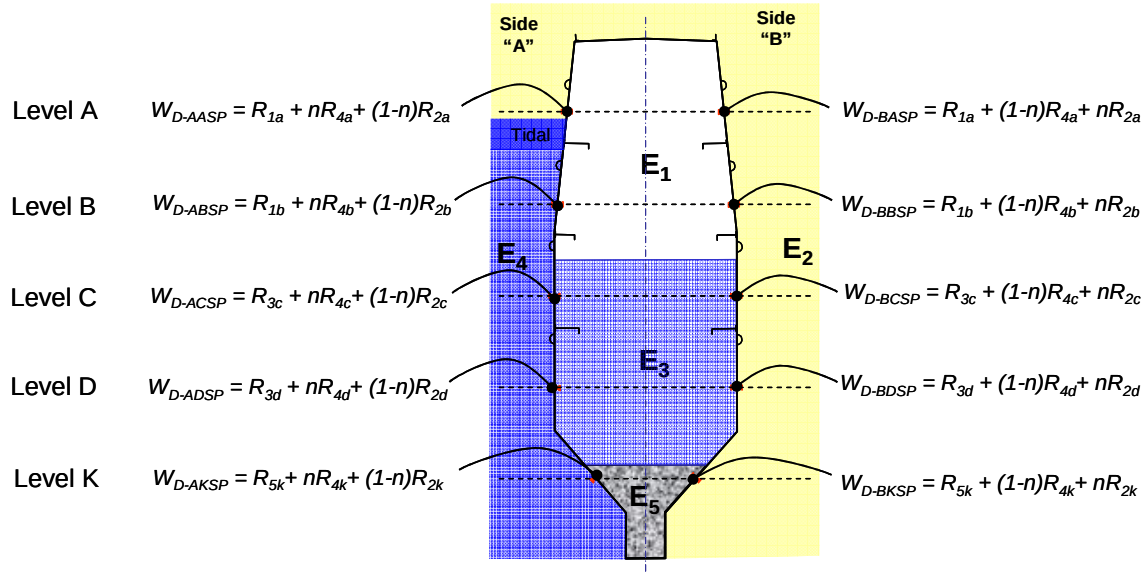

Figure 15. Relative Loss Equations Across Shell Plating on Caisson Gate "D"

where $W_{D\text{-}nmSP}$ is the total wastage measured on side *n*, level *m* and R_{em} is the relative loss contribution influenced by environment *e,* at level *m.* For example, $W_{D\text{-}AASP}$ is the total wastage along Side "A" at Level A. R_{1a} is the relative loss contribution from Environment 1 at Level A. *n* is an operational parameter that describes gate rotation, where *n* is the percentage of time Side "A" has been exposed to $\mathbf{E}_4$ (or conversely, $n - 1$ exposure to $\mathbf{E}_2$). The gate rotation parameter *n* is defined in the next section.

4.12 Gate Rotation Parameter, *n*

Caisson Gate "D" is reversible and can be rotated end for end (180 degrees) at each dock evolution. As a result, the exterior side of the shell plating periodically alternates between river water $\mathbf{E}_4$, and marine atmospheric $\mathbf{E}_2$ (Figure 11). As discussed in Section 4.11, the RL equations take this operational activity into account by including a percentage of Side "A" exposure to river water term, *n*. The calculation of *n* for caisson gate "D" is developed below.

By inspection of the data (Appendix F), Side "A" shell plating exhibits more material loss than Side "B". Quantitatively, paired t-tests are performed on the mean, μ of the sample sets at Levels C and D, on both Sides "A" and "B". In both cases, the null hypothesis is rejected resulting in strong evidence that material loss on Side "A" shell plating is greater than Side "B".

H_0: $\mu_{D\text{-}ACSP} = \mu_{D\text{-}BCSP}$ H_1: $\mu_{D\text{-}ACSP} > \mu_{D\text{-}BCSP}$ (T-value = 3.15, P-value = 0.004)
H_0: $\mu_{D\text{-}ADSP} = \mu_{D\text{-}BDSP}$ H_1: $\mu_{D\text{-}ADSP} > \mu_{D\text{-}BDSP}$ (T-value = 4.75, P-value = 0.000)

In 1985, a revision B to the governing maintenance document MIL-STD-1625 mandated periodic caisson gate rotations as part of routine dock evolutions [6]. This new mandate is confirmed as part of this research with dock operations personnel whom

indicated that routine caisson gate rotations did not occur until approximately the mid 1980s.

Based on the dominate material loss exhibited on Side "A" compared to Side "B", an assumption is made that from years 1940 to 1985, no caisson gate rotation occurred and Side "A" was mainly exposed to river water $\mathbf{E}_4$ during this time period. After the initiation of MIL-STD-1625B(SH), caisson gate "D" gate was routinely rotated at each dock evolution, resulting in Side "A" and "B" shell plating alternating between river water and marine atmospheric environments 50% of the time. The percentage of Side "A" exposure to river water $\mathbf{E}_4$ (and conversely Side "B" exposure to marine atmospheric $\mathbf{E}_2$) is calculated as follows.

$$n = \frac{(1985-1940)+.5(2005-1986)}{2005-1940} = 84\% \qquad \textit{(4-3)}$$

Conversely, the percentage of Side "A" exposure to marine atmospheric $\mathbf{E}_2$ (and Side "B" exposure to river water $\mathbf{E}_4$) is defined:

$$1-n = 16\% \qquad \textit{(4-4)}$$

4.13 Relative Loss Variables, R_{em}

The solution in Figure 15 is indeterminate (10 equations, 15 unknown variables). To solve for the unknown variables, more information is needed. As postulated in Section 4.4 and later supported in Section 4.7.3, marine atmospheric environment, E_2, contribute very little to material loss and may very well be negligible compared to the river and ballast tank water environments. Additionally, is it reasonable to assume that the marine atmospheric environment is longitudinally homogeneous, meaning material loss

contribution is equivalent at all caisson gate levels. Therefore, for caisson gate "D", the following assumption is reasonably made:

$$R_{2a} = R_{2b} = R_{2c} = R_{2d} = R_{2k} \approx 0 \qquad (4\text{-}5)$$

The ten RL equations in Figure 15 are combined with the five assumptions made in Eq. (4-5) to produce 15 equations and 15 unknowns. The solutions are solved using a system of linear, simultaneous algebraic equations [41] such that:

$$\mathbf{AR} = \mathbf{W} \qquad (4\text{-}6)$$

where **A** is a 15 x 15 non singular, coefficient matrix of the ten relative loss equations plus the five assumptions in Eq. (4-5), **R** is a 15 x 1 column vector of unknown variables in terms of relative loss R_{em}, and **W** is 15 x 1 column vector of known total plate thickness loss (wastage) measurements, $W_{D\text{-}nmSP}$.

The polynomial regression models developed in Section 4.9 are used to calculate values of $W_{D\text{-}nmSP}$ in **W** at each caisson gate frame location, x. Rewriting Equation (4-6):

$$\mathbf{R}_x = \mathbf{A}^{-1}\mathbf{W}_x \qquad (4\text{-}7)$$

4.14 Relative Material Loss Contributions, *c(t)*

Equation (4-7) in Microsoft© Excel format:

$$\mathbf{R}_x = \mathbf{MMULT(MINVERSE(A), W)}_x \qquad (4\text{-}8)$$

At each caisson gate frame location, x = (2, 3, 4… 41), a Microsoft© Excel matrix is created using Eq. (4-8) and solutions for R_{em} are determined. For example, Table 6 provides the relative loss variable R_{em} solution at caisson gate frame location, x = 10.

Table 6. Relative Loss Variables, Rem (at frame location: x=10)

		A[1]														W[2]	R[3]	
		R1a	R1b	R2a	R2b	R2c	R2d	R2k	R3c	R3d	R4a	R4b	R4c	R4d	R4k	R5k	Loss	
	D-AASP	1	0	0.16	0	0	0	0	0	0	0.84	0	0	0	0	0	1.360525	R1a = 1.3699
	D-ABSP	0	1	0	0.16	0	0	0	0	0	0	0.84	0	0	0	0	1.672352	R1b = 1.0314
Example	D-ACSP	0	0	0	0	0.16	0	0	1	0	0	0	0.84	0	0	0	3.717099	R2a = 0.0000
	D-ADSP	0	0	0	0	0	0.16	0	0	1	0	0	0	0.84	0	0	2.33714	R2b = 0.0000
	D-AKSP	0	0	0	0	0	0	0.16	0	0	0	0	0	0	0.84	1	2.613437	R2c = 0.0000
	D-BASP	1	0	0.84	0	0	0	0	0	0	0.16	0	0	0	0	0	1.368101	R2d = 0.0000
	D-BBSP	0	1	0	0.84	0	0	0	0	0	0	0.16	0	0	0	0	1.153479	R2k = 0.0000
	D-BCSP	0	0	0	0	0.84	0	0	1	0	0	0	0.16	0	0	0	2.87854	R3c = 2.6812
	D-BDSP	0	0	0	0	0	0.84	0	0	1	0	0	0	0.16	0	0	1.657291	R3d = 1.4973
	D-BKSP	0	0	0	0	0	0	0.84	0	0	0	0	0	0	0.16	1	1.337153	R4a = -0.0111
	R2a	0	0	1	0	0	0	0	0	0	0	0	0	0	0	0	0	R4b = 0.7630
	R2b	0	0	0	1	0	0	0	0	0	0	0	0	0	0	0	0	R4c = 1.2332
	R2c	0	0	0	0	1	0	0	0	0	0	0	0	0	0	0	0	R4d = 0.9998
	R2d	0	0	0	0	0	1	0	0	0	0	0	0	0	0	0	0	R4k = 1.8769
	R2k	0	0	0	0	0	0	1	0	0	0	0	0	0	0	0	0	R5k = 1.0369

1. Ten relative loss equations plus five assumptions.
2. $W_{D\text{-}nmSP}$ = $f(x)$ + 1.78, where $f(x)$ is the polynomial regression model for side: n and level: m, *1.78* mm added to correct for negative wastage. In this example, caisson gate frame location: x = 10 is shown.
3. Relative loss variables, R_{em} contained in R, where R = MMULT(MINVERSE(A),W)

Source: Microsoft© Excel

The coefficients for the fifteen relative loss equations are placed in the 15 x 15 matrix, **A**. The total material losses $W_{D\text{-}nmSP}$ are calculated using the polynomial regression models (at x = 10 in the example) and placed in the first ten rows of the 15 x 1 column matrix, **W**. The assumptions from Eq. (4-5) are placed in the remaining five rows in **W**. For the convenience of producing positive values, 1.78mm is added to each $W_{D\text{-}nmSP}$ (Section 4.10). The material loss contributions are calculated using Eq. (4-8) and displayed in a 15 x 1 column matrix, **R**.

From the solutions in **R**, further decomposition of material loss in terms of contribution $c(t)_{em}$ are defined. For example, at level D-ACSP the total material loss, $W_{D\text{-}ACSP}$ is decomposed such that:

$$
\begin{aligned}
W_{D-ACSP} &= c(t)_{3c} + c(t)_{4c} + c(t)_{2c} \\
&= R_{3c} + 0.84R_{4c} + 0.16R_{2c} \\
&= 2.681 + 0.84(1.233) + 0.16(0) \\
&= 2.681 + 1.036 + 0.000 \\
&= 3.717
\end{aligned}
\qquad (4\text{-}9)
$$

Where:

- R_{3c} defines the loss contribution, $c(t)_{3c}$ due to internal ballast tank water conditions
- $0.84R_{4c}$ defines the loss contribution, $c(t)_{4c}$ due to river water conditions on the external shell plating during times of river side exposure (due to gate rotation)
- $0.16R_{2c}$ defines the loss contribution, $c(t)_{2c}$ due to atmospheric conditions on the external shell plating during times of dock side exposure (due to gate rotation). However, $R_{2c} = 0$ due to assumption.

The process above is repeated for all caisson gate levels and on both caisson gate sides for each caisson gate frame location, x. For the example, at frame location $x = 10$, a summary is presented in Table 7.

Table 7. RML Contributions, c(t) (at frame location: x=10)

Thickness add = 1.78 *n* = 0.84	Elev	RML Contributions, *c(t)* : Ballast	River	Atm	Wastage Total	
D-AASP	101.3	**1.370**	**(0.009)**	**0.000**	**1.361**	
D-ABSP	93.3	**1.031**	**0.641**	**0.000**	**1.672**	
D-ACSP	85.3	**2.681**	**1.036**	**0.000**	**3.717**	**Example**
D-ADSP	77.3	**1.497**	**0.840**	**0.000**	**2.337**	
D-AKSP	69.3	**1.037**	**1.577**	**0.000**	**2.613**	
D-BASP	101.3	**1.370**	**(0.002)**	**0.000**	**1.368**	
D-BBSP	93.3	**1.031**	**0.122**	**0.000**	**1.153**	
D-BCSP	85.3	**2.681**	**0.197**	**0.000**	**2.879**	
D-BDSP	77.3	**1.497**	**0.160**	**0.000**	**1.657**	
D-BKSP	69.3	**1.037**	**0.300**	**0.000**	**1.337**	

For the example, Table 7 reads as follows: At caisson gate frame location x = 10, level C, Side "A", the total material loss across the shell plating is 3.717 mm. The loss contribution due to ballast tank water conditions is 2.681 mm (72%) and loss contribution due to river water conditions is 1.036 mm (28%). The loss contribution due to marine atmospheric is assumed to be near zero and therefore, negligible. The relative material loss can be expressed as a ratio such that:

$$RML_{D-ACSP} = \frac{c(t)_{Ballast}}{c(t)_{River}} = \frac{2.681}{1.036} = 2.59 \qquad (4\text{-}10)$$

Meaning the relative material loss on the shell plating inside due to ballast tank water at this location is 2.59 times the outside surface exposed to the river side.

Time, t in the three loss contribution terms in Eq. (4-9) has no mathematical significance since t is a constant (e.g. t = 65 years). The term, t is included with c in Eq. (4-9) only to not lose focus that material loss contribution is a time based function.

Chapter 5 - Results

5.1 RML Profiles

To approximate a point estimate and account for variability, the RML contributions at each caisson gate frame location and all levels are plotted as vertical profiles along the caisson gate section view. Figure 16 is the profile for the Side “A” total shell plating material loss.

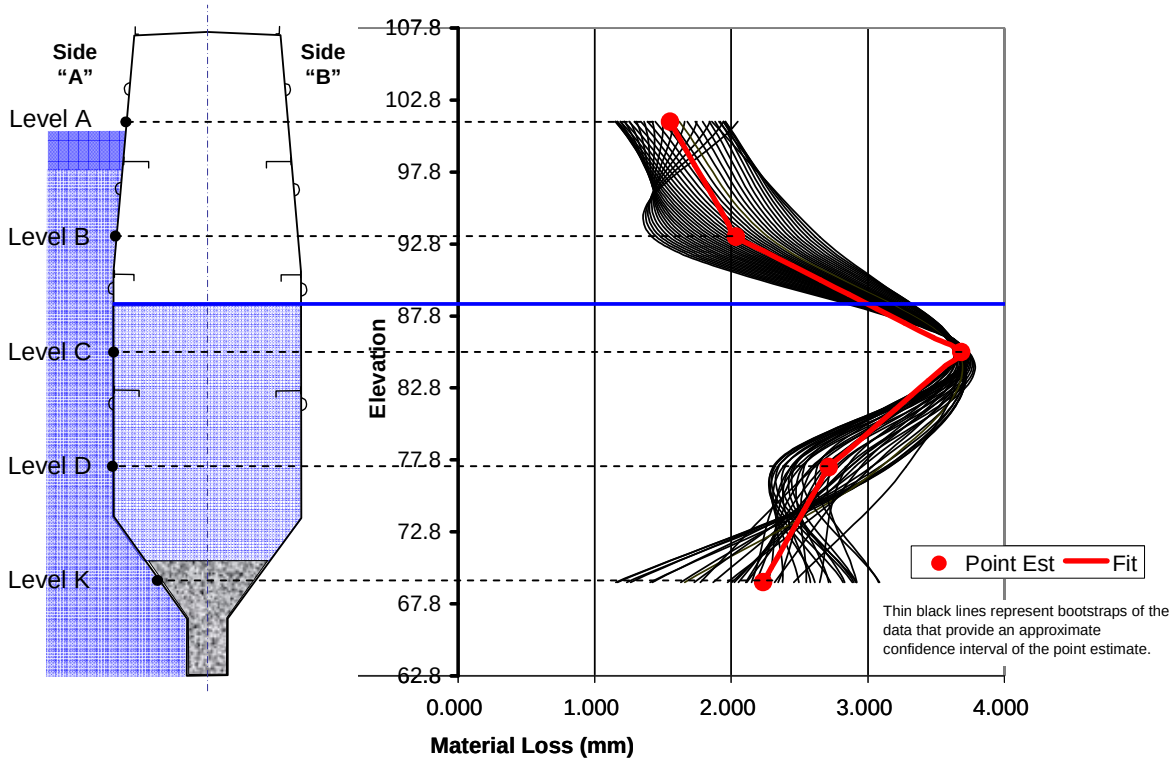

Figure 16. Caisson Gate "D", Side "A", Total Shell Plating Material Loss

The thick red line represents the total loss point estimate and it is calculated by taking the arithmetic mean at all frame locations at a specific level using the polynomial regression models, *f(x)* developed in Section 4.9 such that:

$$\overline{W}_{D-AmSP} = \frac{\sum_{x=i}^{j} f(x)}{j-i+1} \qquad (5\text{-}1)$$

Where $i = 2$, $j = 41$, for all m = (A, B, C, D, K) at D-A*m*SP. The points are connected to produce the profile. The thin black lines are vertical profiles at each caisson gate frame x and provide an approximate confidence interval of the point estimate such that:

$$W_{D-AmSP} = f(x) \qquad (5\text{-}2)$$

Where x = (2, 3, 4, …41) for all m = (A, B, C, D, K) at D-A*m*SP.

Note the inflection points near elevations 73 and 98. These appear to correspond with the changes in environmental conditions due to change in shell plating orientation [38] and tidal splash [51], respectively. Also, note variability remains small at level C which is in close proximity of top of ballast water level verses the variability within the concrete ballast zone (level K) which indicates large swings.

5.2 River Side RML Profile (Side "A")

The procedure outlined in Section 5.1 is repeated for river side contribution producing the river side RML profile in Figure 17. It is not good practice to extrapolate beyond the extents of the known environments [73]. Since transitioning between level A (atmospheric) to level B (marine immersion) involves crossing into dissimilar

environments, it is not assumed that the profiles line between these two points are directly connected. Therefore, the loss contribution point estimate and variability at level A are represented as single points.

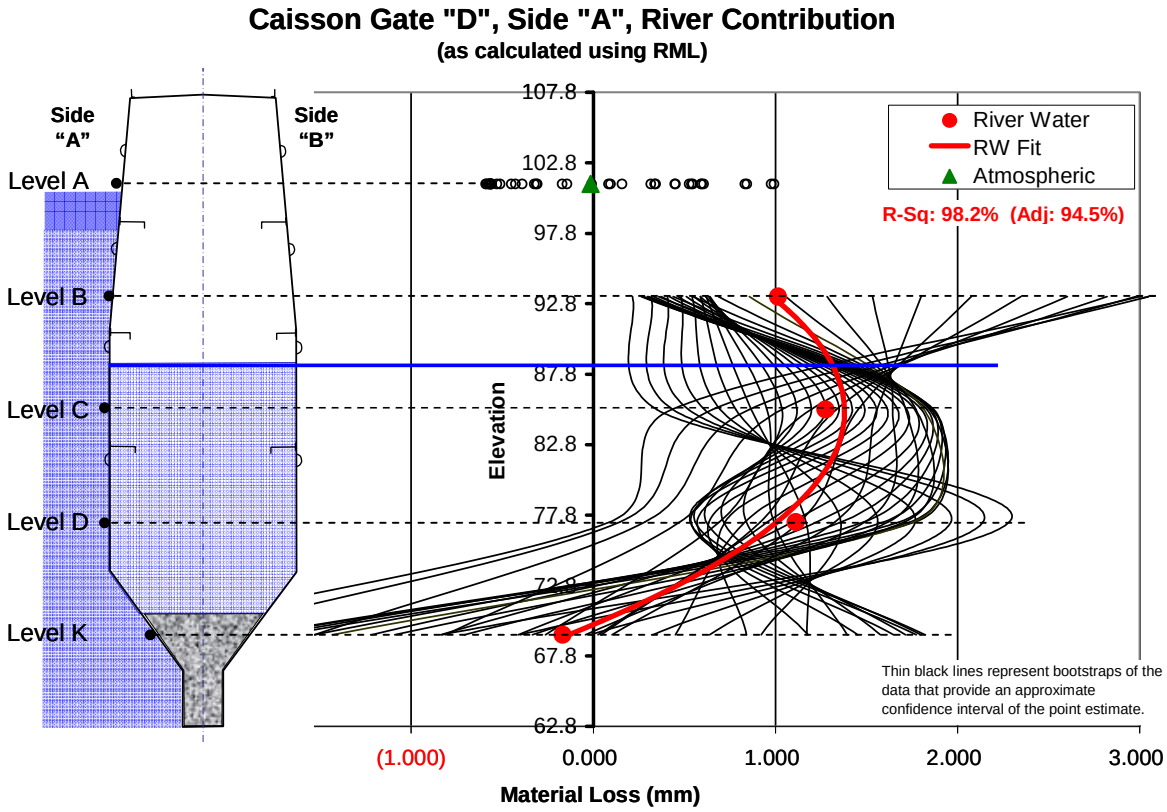

Figure 17. Caisson Gate "D", Side "A", River Side Material Loss Contribution

A least squares fit is performed between the four mean value point estimates at levels B, C, D, and K and profile curve developed (adj. R^2 value = 94.5%). As with Section 5.1, the thin black lines are vertical profiles at each caisson gate frame *x* and provide an approximate confidence interval of the point estimate.

Again, note the inflection points in the confidence interval profiles at elevations 87.8, 82.8 and 73. These inflections appear to correspond to top of ballast water, a horizontal plate stiffener (located between levels C and D) and change in shell plating orientation, respectively.

5.3 Model Validation

Dissolved oxygen content and temperature highly influence corrosion and are used to define the environmental profiles from which model validation will be tested [53, 60]. A single water column sample is taken using a digital multi-meter water quality measuring apparatus. Readings are taken at various depths on the river side adjacent to the caisson gate. The measuring technique and equipment specifications are further detailed in Appendix B.

A least squares fit is performed through the sample points to develop the environmental profiles. Table 8 provides a summary of the adj. R^2 values and p-values of the least squares fits. The environmental profiles are presented in Appendix C.

Table 8. Environmental Profiles (Dissolved Oxygen & Temperature)

Environment	Factor	R^2	Adjusted R^2	p-value
River Water	Temperature	72.6%	63.5%	0.067
River Water	Dissolved O_2	99.1%	98.2%	0.009
Ballast Water	Temperature	98.8%	98.2%	0.006
Ballast Water	Dissolved O_2	93.7%	90.5%	0.032

Source: MINITAB Release 12.23

With the exception of the river water temperature, all the environmental profiles least squares fits are significant (p-value < 0.05). Although the river water temperature fit is marginal (p-value= 0.067), it will be considered adequate for the comparisons.

For quantitative validation, the profiles are assumed to be linear and a Pearson product-moment correlation coefficient [73] is calculated using Minitab© software.

5.3.1 Side "A", Shell Plating Total Loss Validation

The Side "A" shell plating total loss, river water dissolved oxygen and river water temperature profiles are superimposed over top each other in (Figure 18). The dissolved oxygen and temperature profiles have been shifted to coincide with the total loss profile to facilitate visual comparisons.

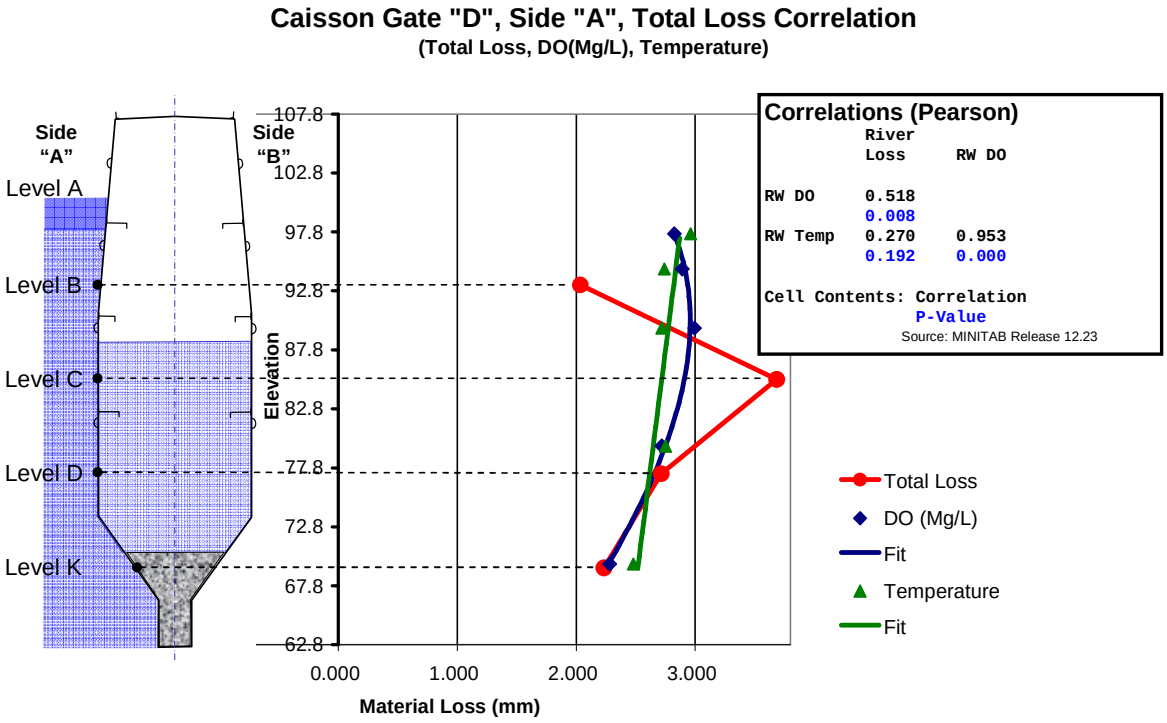

Figure 18. Correlations of Temperature and Dissolved Oxygen to Total Shell Plating Loss

Through visual inspection, there appears to be little correlation between the total loss profile and the other two profiles. This is anticipated for total material loss is a function of all contributing environmental factors. Figure 18 only includes the river side contributing environmental factors and does not account for the ballast tank side contributions.

Note the maximum shell plate total material loss occurs at level C where the plate is exposed to both river water and ballast water conditions. Water quality sampling reveals that dissolved oxygen content is at its maximum at this level for both the river water and ballast tank water environments, contributing to the maximum total loss (Appendix C).

Note the strong correlation between the river water dissolved oxygen profile and the river water temperature profile (Figure 18). Quantitatively, the Pearson correlations support this finding (r-value = 0.953, p-value < 0.001). The strong correlation between dissolved oxygen and temperature is consistent with literature findings [34, 49, 67].

As expected, the correlation between the total loss profile and the dissolved oxygen profile is somewhat weak (r-value = 0.518, p-value = 0.008). A weak correlation between the total loss profile and the temperature profile is also detected (r-value = 0.270, p-value = 0.192) and supported by visual observation.

As shown in the next section, after applying RML theory and isolating each side from the total loss profile, these correlations will tend to strengthen.

5.3.2 Side “A”, Shell Plating River Loss Contribution Validation

The Side “A” shell plating river loss contribution, river water dissolved oxygen and river water temperature profiles are superimposed over top each other in Figure 19. The dissolved oxygen and temperature profiles have been shifted to coincide with the river loss profile to facilitate visual comparisons.

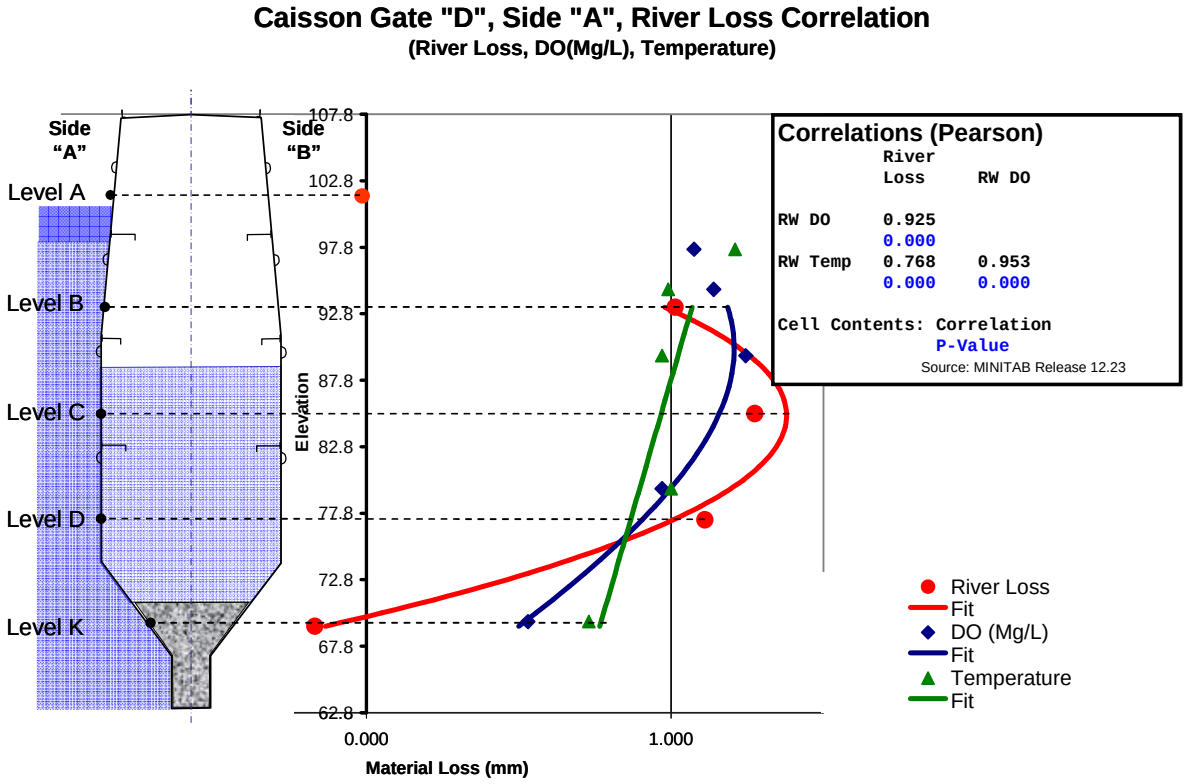

Figure 19. Correlations of Temperature and Dissolved Oxygen to River Side Contribution

By visual inspection, the relationship between the river loss profile and the other two profiles improve and the correlations appear to be stronger. This is quantifiably supported through the improvement of the Pearson correlations (r-value = 0.925, 0.768, 0.953 all with p-values < 0.001). Since Side “A” is exposed to the river water

environment 84% of its life (Section 4.12), strong correlations between river loss contribution and dissolve oxygen content and water temperature is expected.

Note the river side contribution point estimate at level A is near zero. This supports the assumption made in Section 4.13 that marine atmospheric contribution is negligible compared to river and ballast tank water environments.

Another observation is the river loss contribution point estimate at level K is near zero. This suggests material loss at this level is more pronounced inside the concrete ballast tank area rather than on the river side. This is plausible for the river water dissolved oxygen content and water temperature are minimal at this level, causing impedance to the corrosion process. The concrete is aged (65 years old) and it is quite possible that it is deteriorating; allowing salts from the ballast water to wick into cracks and end up adjacent to the shell plating. Being that the inspection of the concrete and the adjacent shell plating is improbable; the study of this phenomenon is important and deserves further research in the near future.

5.3.3 Shell Plating Ballast Tank Loss Contribution Validation

The loss contribution point estimates and approximated confidence intervals for the ballast tank environments are developed similarly (Figure 20). As in Section 5.2, the profile lines are not extended beyond the limits of its environment.

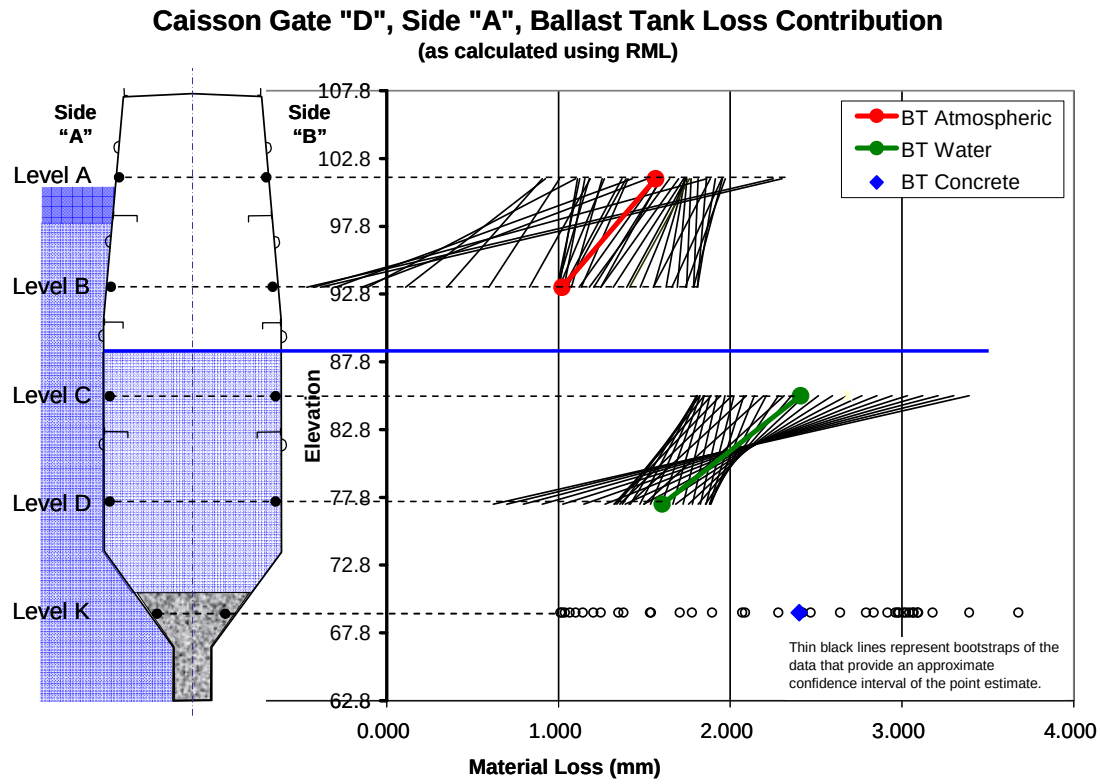

Figure 20. Caisson Gate "D", Side "A", Ballast Tank Side Material Loss Contribution

5.3.3.1 Ballast Tank Atmospheric

The material loss profile between levels A and B inside the caisson gate is due to the ballast tank atmospheric environment. Environmental factors known to cause corrosion in this area include time of wetness (TOW), surface salt concentration and temperature [27, 31]. The corrosion rate at level A is higher than level B because of the increased TOW in this area.

The upper portion of the caisson gate (level A and above) is exposed to day-night temperature fluctuations, that is known to cause dew to form on the inside shell plating surface. As a result, TOW is greater in this region, allowing moisture to condense on the

shell plating and promoting more active corrosion at the level as compared to level B [14]. At level B, the shell plating temperature does not exhibit the wide temperature fluctuations as seen at level A and the surface temperature is conceivably cooler than level B due to the water temperature in direct contact from the river side. Hence, the material loss over time at level B would expect be less than level C as supported in Figure 20.

5.3.3.2 Ballast Tank Water

Within the ballast tank water environment, the material loss is more pronounced at level C than level D (Figure 20) and visually correlates with the measured dissolved oxygen content and water temperatures (Appendix C). Notice the inflection in the confidence intervals detected at elevation 82.8. Consistent with earlier findings, this inflection appears to coincide with the horizontal plate stiffener between levels C and D. Consistent with the findings in Section 5.3.2, the Level K shell plating in the concrete ballast tank area suggests high material loss.

The ballast tank shell plating loss contribution, ballast tank water dissolved oxygen and ballast tank water temperature profiles are superimposed over top each other in Figure 21. The dissolved oxygen and temperature profiles have been shifted to coincide with the river loss profile to facilitate visual comparisons.

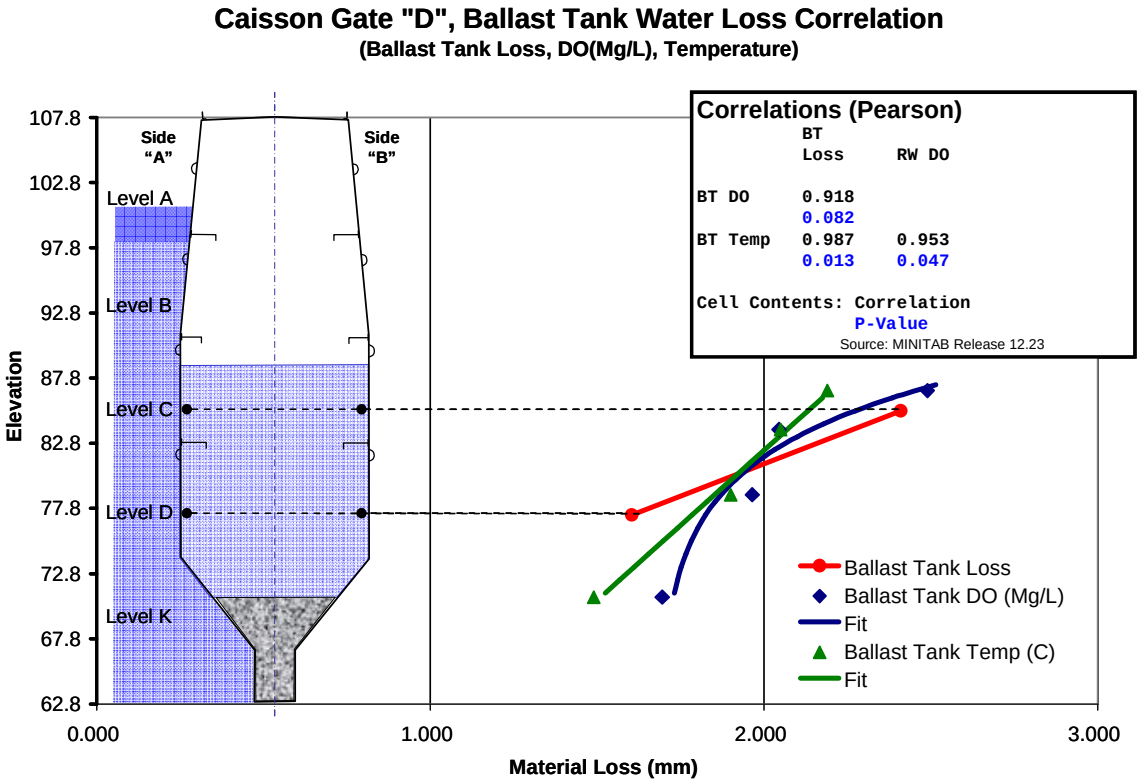

Figure 21. Correlations of Temperature and Dissolved Oxygen to Ballast Tank Contribution

The relationship between the ballast tank loss profile and the ballast tank water dissolved oxygen and ballast tank water temperature profiles provide visual suggestion of high correlation. There is a strong correlation between ballast tank material loss and water temperature (r-value = 0.987, p-value = 0.013). The correlation between ballast tank material loss and dissolve oxygen content is marginally high (r-value = 0.918, p-value = 0.082).

5.3.3.3 Ballast Tank Concrete

At level K, material loss contribution due to the concrete ballast tank environment is the highest compared to other ballast tank levels (Figure 20). The mean value of the

point estimate is 2.4 mm with a wide range of 1.02 to 3.69 mm. As discussed in Section 5.3.2, this high material loss condition is plausible for inspection of the concrete and the adjacent shell plating is impossible and merits future research.

5.4 Atmospheric Side RML Profile (Side "B")

The profile for the Side "B" total shell plating material loss is shown in Figure 22.

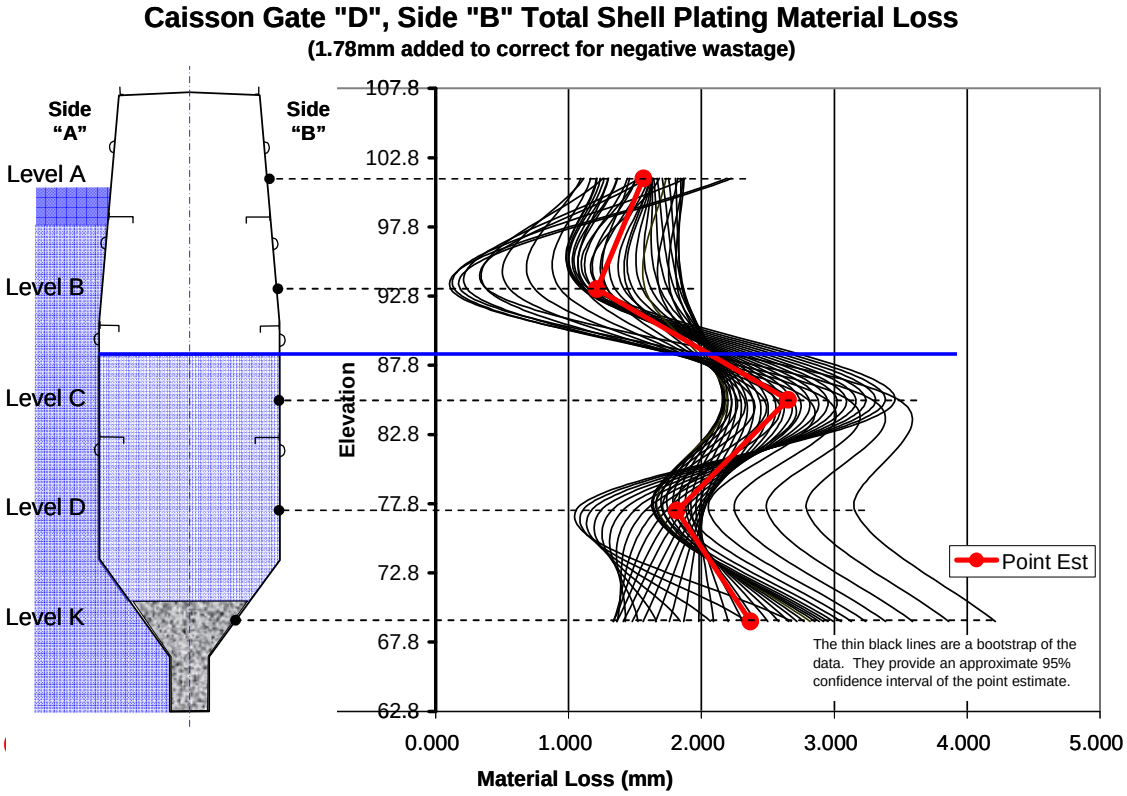

Figure 22. Caisson Gate "D", Side "B", Total Shell Plating Material Loss

Due to the operational condition of gate rotation (Section 4.12), the exterior side "B" shell plating is exposed 84% of the time to marine atmospheric condition and 16% of the time to river water conditions. Since the assumption is marine atmospheric corrosion is

negligible (Section 4.13), it is reasonable to assume the majority of the material loss contribution will be caused by internal ballast tank conditions. Close inspection of the side “B” total shell plate material loss profile (Figure 22) with ballast tank side material loss contribution profile (Figure 20) supports this assumption.

Deducting the interior ballast tank contribution from total Side “B” shell plate material loss, the exterior side “B” river material loss contribution resembles a scaled down profile of the side “A” river side contribution (Figure 23). Inflection points of the bootstrapped confidence intervals suggest locations of structural anomalies such as change in shell plating orientation (elevation 72.8), location of horizontal plate stiffeners (elevation 82.8) and top of ballast tank water level (elevation 88).

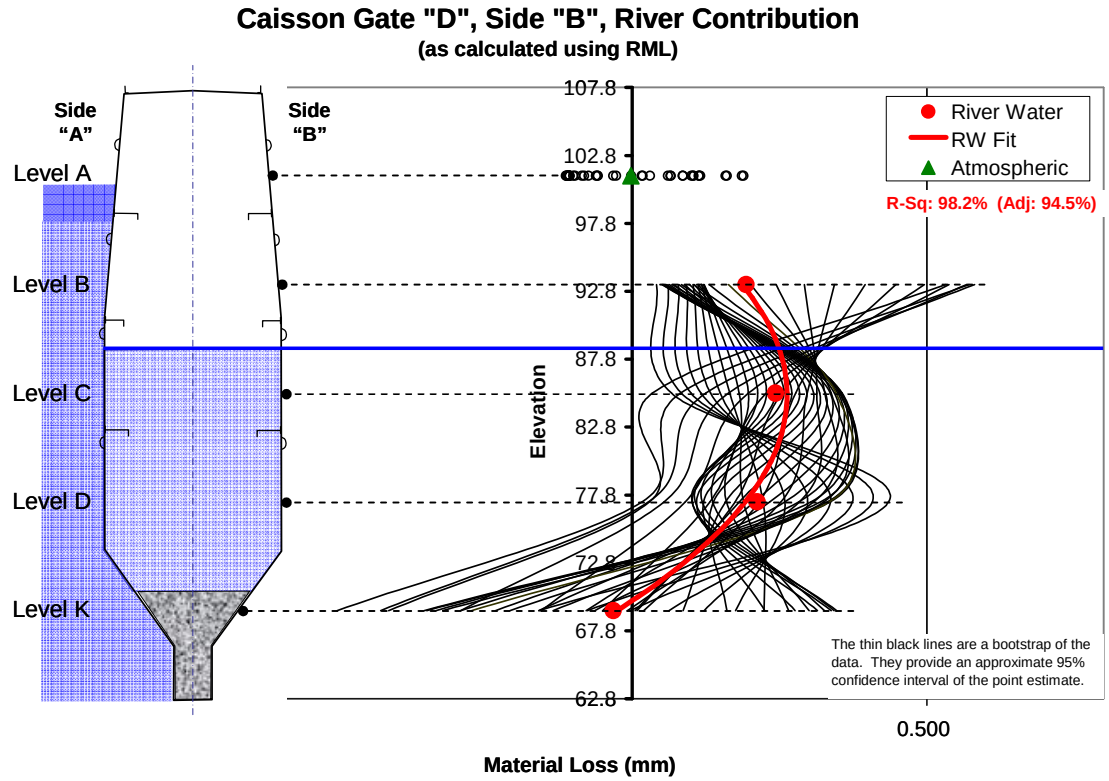

Figure 23. Caisson Gate "D", Side "B", Marine Atmospheric Side Material Loss Contribution

Chapter 6 - Conclusion

The research provides strong evidence that the relative material loss (RML) theory described herein is valid and merits further research.

It has successfully demonstrated the use of relative loss (RL) equations to describe environmental and operational relationships across marine shell plating exposed to dissimilar environments. Solving the RL equations simultaneously, solutions produce effective approximations of material loss contribution on each shell plating side. A unique “at-sea” structure, a sixty-five year old dry dock caisson gate, provides the research platform for which the RML theory is tested.

Qualified technicians use systematic procedures to collect material thickness readings and the normality of the data are verified using standard statistical methods. Polynomial regression models mathematically describe total material loss across the shell plating and nonparametric techniques (LOWESS) verify model correctness. Material loss profiles generated from simultaneously solving RL equations define material loss contribution on each shell plating side.

Strong correlations exist between the material loss profiles on each plate side and the environmental factors known to influence marine corrosion; namely water temperature and dissolved oxygen content. The significance of the correlations is within the standard Type I error of alpha = 0.05. Therefore, the research concludes that there is not enough evidence to reject the null hypothesis; H_0 (Section 4.1) and an effective solution using the RML theory described in Chapter 3 is supported and merits further research.

6.1 Future Research and Spinoffs

The purpose of this experiment is to prove prototypically that RML is plausible. Therefore, the test subject was limited to a single marine structure, a 65-year old dry dock caisson gate. Expansion of the dataset to include additional "at-sea" structures will provide greater confidence in the research findings and is a recommendation for future research. Additional research using more test subjects such as other caisson gates located in different environments (i.e. naval shipyard in Pearl Harbor) is recommended.

Future research should expand to include more variables in the relative loss (RL) equations in order to reduce the assumptions needed to produce a deterministic solution. As an example, it is expected that a relationship between the material loss of the vertical plate stiffener flanges and webs and internal shell plating loss exists and could potentially be included in the RL equations[6].

Additionally, three spinoff discoveries provide promising future research opportunities.

6.1.1 Negative "Wastage"

Negative wastage measurements are evident throughout all the sample sets. The research presents a convincing case that this phenomenon relates to standard mill tolerance overage not taken into account during the wastage calculation. With current literature interests focused on knowing the *remaining* shell plate thickness from a limit state or structural adequacy perspective, negative wastage measurements is of no concern or interest. However, with a paradigmatic shift to relative material loss theory,

[6] Note: preliminary research has revealed that material loss relationships using vertical plate stiffeners do not directly coincide with the internal ballast tank shell plating material loss. However, a relationship may be possible by thorough regression analysis.

accounting for negative wastage becomes paramount. The *original* shell plate thickness becomes the baseline for the relative loss equations used in the methodology and new methods for approximating original shell plate thickness is a reservation for future research.

6.1.2 Diminution of Precision Error

Using RML, the reduction in precision error is possible and theoretically supported in Section 3.2.2. The reduction occurs though cancelation of the error terms during mathematical substitution of the RL equations. However, the research experiment stops short of providing evidence of this phenomenon. In fact, upon observation of the bootstrap confidence intervals, a counter argument is plausible (Figure 17, Figure 20, Figure 23). Further understanding RML variability is a future research requirement.

6.1.3 Bootstrap Inflections for Detecting Anomalies

Inflection points of the bootstrap confidence intervals appear to correspond with changes in structural orientation of shell plating as well as locations of horizontal structural plate stiffeners (Figure 17, Figure 20, Figure 23). Further research of this phenomenon is a future research recommendation. If confirmed, RML theory can expand to include an x-ray or “see through” capability, where locating a structural anomaly behind hidden structure has a potential future value to maintenance inspectors.

References

[1] [ASCE], 2009, ASCE Report Card for America's Infrastructure, http://www.asce.org/reportcard/2009, site accessed on February 10, 2009

[2] [ASTM], 2004, "Standard Guide for Applying Statistics to Analysis of Corrosion Data," Technical Report No. ASTM G 16, American Society for Testing and Materials, West Conshohocken.

[3] [ASTM], 2007, "Standard Practice for Calculating and Using Basic Statistics," Technical Report No. ASTM E 2586, American Society for Testing and Materials, West Conshohocken.

[4] [ASTM], 2007, "Standard Specification for General Requirements for Rolled Structural Steel Bars, Plates, Shapes, and Sheet Piling," Technical Report No. ASTM A 6/A 6M – 07, American Society for Testing and Materials, West Conshohocken.

[5] [FHWA], 2006, "Price Trends for Federal Aid Highway Construction, First Quarter 2006," Federal Highway Administration, Washington, DC.

[6] [NAVSEA], 1985, "Department of Defense Standard Practices: Safety Certification Program for Drydocking Facilities and Shipbuilding Ways for US Navy Ships," NAVSEA 04XQ2.

[7] [NAVSEA], 1992, "Department of Defense Standard Practices: Safety Certification Program for Drydocking Facilities and Shipbuilding Ways for US Navy Ships," NAVSEA 04XQ2.

[8] [NAVSEA], 2003, "Advance Change Notice 7 to MIL-STD-1625C(1), Safety Certification Program for Drydocking Facilities and Shipbuilding Ways for US Navy Ships," NAVSEA 04XQ2.

[9] Anderson, T. W., and Darling, D. A., 1952, "Asymptotic Theory of Certain" Goodness of Fit" Criteria Based on Stochastic Processes," *Annals of Mathematical Statistics*, **23**(2), pp. 193-212.

[10] Ayyub, B. M., and de Souza, G. F. M., 2000, "Reliability-Based Methodology for Life Prediction of Ship Structures," Proc. SSC/SNAME/ASNE Ship Structure Symposium, Ship Structure Committee, Society of Naval Architects and Marine Engineers, and American Society of Naval Engineers, Washington, pp. 25.

[11] Bea, R. G., Cramer, E., Schulte-Strauthaus, R., Mayoss, R., Gallion, K., Ma, K., Holzman, R., and Demsetz, L., 1995, "Ship's Maintenance Project," *Conducted at University of California, Berkeley for US Coast Guard/Ship Structure Committee (SSC), SSC-386*.

[12] Bengtsson, M., 2004, "Condition Based Maintenance System Technology–Where is Development Heading?," Proc. Euromaintenance 2004 – Proceedings of the 17th European Maintenance Congress, Barcelona, Spain.

[13] Boon, J. D., 2004, Secrets Of The Tide: Tide And Tidal Current Analysis And Applications, Storm Surges And Sea Level Trends, Horwood Publishing.

[14] Brackett, R. L., Nordell, W. J., Rail, R. D., Civil Engineering, L., and Calif.) Naval Construction Battalion, C., 1982, Underwater Inspection of Waterfront Facilities: Inspection Requirements Analysis and Non-destructive Testing Technique Assessment, Naval Civil Engineering Laboratory.

[15] Brennan, F., Carlsen, C. A., Daley, C., Garbatov, Y., Ivanov, L., Rizzo, C. M., Simonsen, B. C., Yamamoto, N., and Zhuang, H. Z., 2006, "ISSC Committee V.6: Condition Assessment Of Aged Ships," Proc. 16th International Ship and Offshore Structures Congress, Southampton, UK, 2, pp. 265-315.

[16] Brown, J. L., 2005, "Wanted: Civil Engineers," *Civil Engineering*, **75**(7), pp. 46-49.

[17] Cleveland, W. S., 1979, "Robust locally weighted regression and smoothing scatterplots," *Journal of the American Statistical Association*, **74**(368), pp. 829-836.

[18] Cleveland, W. S., and Devlin, S. J., 1988, "Locally weighted regression: an approach to regression analysis by local fitting," *Journal of the American Statistical Association*, **83**(403), pp. 596-610.

[19] Cohen, J., 2003, Applied Multiple Regression/Correlation Analysis for the Behavioral Sciences, Lawrence Erlbaum Associates.

[20] David, H. A., 1988, "The Method of Paired Comparison," *London: Griffin*.

[21] Dinovitzer, A., and Pussegoda, N., 2003, "Life Expectancy Assessment of Ship Structures," Ship Structures Committee (SSC-427), Washington, DC.

[22] Doane, D. P., and Seward, L. W., 2007, Applied Statistics in Business and Economics, McGraw-Hill/Irwin, Boston.

[23] Emi, H., Arima, T., and Umino, M., 1994, "A Study on Developing a Rational Corrosion Protection System of Hull Structures," *ClassNK Technical Bulletin*, **12**(1), pp. 65-79.

[24] Ernsting, R. A., Preece, M. C., and Stone, K. F., 2006, "Analysis of the Caisson Gates at Northrop Grumman Newport News," Proc. Dry Dock Conference 2006, Jacksonville, FL.

[25] Figliola, R. S., and Beasley, D. E., 2001, Theory and Design for Mechanical Measurements, Third Edition, John Wiley & Sons.

[26] Frangopol, D. M., Kallen, M. J., and van Noortwijk, J. M., 2004, "Probabilistic models for life-cycle performance of deteriorating structures: review and future directions," *Progress in Structural Engineering and Materials*, **6**(4), pp. 197-212.

[27] Gardiner, C. P., and Melchers, R. E., 1998, "Operational Parameters Affecting Bulk Carrier Corrosion," Proc. Proceedings of AME'98 Meeting the Needs of Industry.

[28] Gardiner, C. P., and Melchers, R. E., 2001, "Enclosed atmospheric corrosion in ship spaces," *British Corrosion Journal*, **36**(4), pp. 272-276.

[29] Gardiner, C. P., and Melchers, R. E., 2003, "Corrosion analysis of bulk carriers, Part I: operational parameters influencing corrosion rates," *Marine Structures*, **16**(8), pp. 547-566.

[30] Grubbs, F. E., 1969, "Procedures for detecting outlying observations in samples, technometrics," *Technometrics*, **11**(1), pp. 1–21.

[31] Grubbs, F. E., 1974, "Procedures for Detecting Outlying Observations in Samples," Storming Media.

[32] Gudze, M., and Melchers, R., 2006, "Prediction of naval ship ballast tank corrosion using operational profiles," *International Journal of Maritime Engineering*, **Part A3**(148), pp. 77-86.

[33] Guedes Soares, C., and Garbatov, Y., 1999, "Reliability of corrosion protected and maintained ship hulls subjected to corrosion and fatigue," **43**(2), pp. 65-78.

[34] Guedes Soares, C., and Garbatov, Y., 1999, "Reliability of maintained, corrosion protected plates subjected to non-linear corrosion and compressive loads-effects of general corrosion on ultimate strength," *Marine Structures*, **12**(6), pp. 425-445.

[35] Guedes Soares, C., Garbatov, Y., Zayed, A., Wang, G., Melchers, R. E., Paik, J. K., and Cui, W., 2005, "Non-linear corrosion model for immersed steel plates accounting for environmental factors," *Transactions SNAME*, **115**(1), pp. 19–21.

[36] Herring Jr, L. C., and Titcomb, A. N., 1981, "Investigation of Internal Corrosion and Corrosion-Control Alternatives in Commercial Tankships," Ship Structures Committee (SSC-312), Washington, DC.

[37] Hobbs, D. W., 2001, "Concrete deterioration: causes, diagnosis, and minimizing risk," *International Materials Reviews*, **46**(3), pp. 117-144.

[38] House, D. J., 2003, Dry Docking and Shipboard Maintenance: A Guide to Industry, Witherby & Co. Ltd, London.

[39] Jeffrey, R., and Melchers, R. E., 2007, "Effect of Orientation and Shielding in the Early Corrosion of Mild Steel in Tidal Marine Conditions," *Corrosion*, **63**(9), pp. 872-879.

[40] Keifer, K. A., 2006, "Development of a Pile Condition Index and a Road Map for the Development of a Structural Section Rating," Doctor of Philosophy University of Illinois, Urbana-Champaign.

[41] Kikuta, M., Shimko, M., and Ciscon, D., 1996, "Corrosion Control of Inter-Hull spaces," Ship Structures Committee (SSC-390), Washington, DC.

[42] Kraus, A. D., 2002, Matrices for Engineers, Oxford University Press, Oxford.

[43] Kreysa, G., and Eckermann, R., 1992, "Dechema Corrosion Handbook, Vol. 11," VCH Publishers, New York.

[44] Loseth, R., Sekkesaeter, G., and Valsgaard, S., 1994, "Economics of high-tensile steel in ship hulls," *Marine Structures*, **7**(1), pp. 31-50.

[45] Louis Berger, 2004, "Transfer of National Defense Reserve Fleet Vessels from the James River Reserve Fleet for Disposal at Able UK Facilities, Teesside, UK: Environmental Assessment," US Dept. of Transportation, Maritime Administration.

[46] Melchers, R. E., 1995, "Probabilistic modelling of marine corrosion of steel specimens," Proc. ISOPE 95: 5th International Offshore & Polar Engineering Conference, The Hague, 4, pp. 204-210.

[47] Melchers, R. E., 1997, "Probabilistic modelling of immersion marine corrosion," Proc. Structural Safety and Reliability: Proceedings of ICOSSAR'97, the 7th International Conference on Structural Safety and Reliability, Kyoto, 24-28 November 1997.

[48] Melchers, R. E., 1999, "Corrosion uncertainty modelling for steel structures," *Journal of Constructional Steel Research*, **52**(1), pp. 3-19.

[49] Melchers, R. E., 2001, "Assessment of Existing Structures—Approaches and Research Needs," *Journal of Structural Engineering*, **127**(4), pp. 406-411.

[50] Melchers, R. E., 2002, "Effect of temperature on the marine immersion corrosion of carbon steels," *Corrosion(USA)*, **58**(9), pp. 768-782.

[51] Melchers, R. E., 2003, "Probabilistic Model for Marine Corrosion of Steel for Structural Reliability Assessment," *Journal of Structural Engineering*, **129**(11), pp. 1484-1493.

[52] Melchers, R. E., 2003, "Probabilistic Models for Corrosion in Structural Reliability Assessment—Part 1: Empirical Models," *Journal of Offshore Mechanics and Arctic Engineering*, **125**(4), pp. 264-271.

[53] Melchers, R. E., 2003, "Modeling of Marine Immersion Corrosion for Mild and Low-Alloy Steels Part 1: Phenomenological Model," *Corrosion(USA)*, **59**(4), pp. 319-334.

[54] Melchers, R. E., 2005, "Effect of Immersion Depth on Marine Corrosion of Mild Steel," *Corrosion*, **61**(9), pp. 895-906.

[55] Melchers, R. E., 2005, "Effect of Nutrient-Based Water Pollution on the Corrosion of Mild Steel in Marine Immersion Conditions," *Corrosion*, **61**(3), pp. 237-245.

[56] Melchers, R. E., 2006, "Examples of mathematical modelling of long term general corrosion of structural steels in sea water," *Corrosion Engineering, Science and Technology*, **41**(1), pp. 38-44.

[57] Melchers, R. E., 2006, "Recent Progress in the Modeling of Corrosion of Structural Steel Immersed in Seawaters," *Journal of Infrastructure Systems*, **12**(3), pp. 154-162.

[58] Melchers, R. E., 2006, "Pitting corrosion of mild steel under marine anaerobic conditions-Part 1: Experimental Observations," *Corrosion(Houston, Tex.)*, **62**(11), pp. 981-988.

[59] Melchers, R. E., and Jiang, X., 2006, "Estimation of models for durability of epoxy coatings in water ballast tanks," *Ships and Offshore Structures*, **1**(1), pp. 61-70.

[60] Melchers, R. E., and Wells, T., 2006, "Models for the anaerobic phases of marine immersion corrosion," *Corrosion Science*, **48**(7), pp. 1791-1811.

[61] Melchers, R. E., and Jeffrey, R. J., 2008, "Probabilistic models for steel corrosion loss and pitting of marine infrastructure," *Reliability Engineering and System Safety*, **93**(3), pp. 423-432.

[62] Noor, N. M., and Yahaya, N., 2006, "Statistical Analysis of Seawater Ballast Tank Corrosion Data," Proc. 6th Asia-Pacific Structural Engineering and Construction Conference (APSEC 2006), Kuala Lumpur, Malaysia, pp. E25-E33.

[63] Paik, J. K., Kim, S. K., and Lee, S. K., 1998, "Probabilistic corrosion rate estimation model for longitudinal strength members of bulk carriers," *Ocean Engineering*, **25**(10), pp. 837-860.

[64] Paik, J. K., and Thayamballi, A. K., 2002, "Ultimate strength of ageing ships," *Proceedings of the Institution of Mechanical Engineers, Part M: Journal of Engineering for the Maritime Environment*, **216**(1), pp. 57-77.

[65] Paik, J. K., and Thayamballi, A. K., 2003, Ultimate Limit State Design of Steel-Plated Structures, John Wiley and Sons, West Sussex, England.

[66] Paik, J. K., Thayamballi, A. K., Park, Y. I., and Hwang, J. S., 2003, "A time-dependent corrosion wastage model for bulk carrier structures," *International Journal of Maritime Engineering*, **145**(pp. 61–88.

[67] Paik, J. K., Thayamballi, A. K., Park, Y. I., and Hwang, J. S., 2004, "A time-dependent corrosion wastage model for seawater ballast tank structures of ships," *Corrosion Science*, **46**(2), pp. 471-486.

[68] Paik, J. K., Brennan, F., Carlsen, C. A., Daley, C., Garbatov, Y., Ivanov, L., Rizzo, C. M., Simonsen, B. C., Yamamoto, N., and Zhuang, H. Z., 2006, "ISSC Committee V.6: Condition assessment of aged ships," Proc. 16th international ship and offshore structures congress, Southhampton, UK.

[69] Phull, B. S., Pikul, S. J., and Kain, R. M., 1997, "Seawater corrosivity around the world: results from five years of testing," American Society of Testing and Materials.

[70] Pollard, R. R., and Bea, R. G., 1991, "Evaluation of corrosion damage in crude and product carriers," Department of Naval Architecture and Offshore Engineering, UC Berkeley, Berkeley, California.

[71] Prichard, F. E., and Green, J., 2001, Analytical measurement terminology, Royal Society of Chemistry.

[72] Qin, S., and Cui, W., 2003, "Effect of corrosion models on the time-dependent reliability of steel plated elements," *Marine Structures*, **16**(1), pp. 15-34.

[73] Ruina, A. L., and Pratap, R., 2002, Introduction to Statics and Dynamics, Pre-print for Oxford University Press.

[74] Ryan, T. P., 2007, Modern Engineering Statistics, Wiley-Interscience.

[75] Schofield, W., and Breach, M., 2007, Engineering Surveying, Butterworth-Heinemann.

[76] Schumacher, M., 1979, Seawater corrosion handbook, Noyes Data Corp., Park Ridge, NJ.

[77] Southwell, C. R., Bultman, J. D., and Alexander, A. L., 1976, "Corrosion of Metals in Tropical Environments--Final Report of 16-Year Exposures," *Materials Performance*, **15**(7), pp. 9-25.

[78] Southwell, C. R., Bultman, J. D., and Hummer, J. C. W., 1979, Seawater Corrosion Handbook, Noyes Data Corp., Park Ridge, N.J.

[79] Stambaugh, K. A., and Knecht, J. C., 1991, "Corrosion Experience Data Requirements," Ship Structures Committee (SSC-348).

[80] Sun, H. H., and Bai, Y., 2003, "Time-variant reliability of FPSO hulls," *Marine Structures*, **16**(3), pp. 219-253

[81] Tsang, A. H. C., 1995, "Condition-based maintenance: tools and decision making," **1**(3), pp. 3-17.

[82] Tscheliesnig, P., 2006, "Detection of corrosion attack on oil tankers by means of acoustic emission (AE)," Proc. Conference on-Non Destructive Testing, Auckland, New Zealand.

[83] Wang, G., Spencer, J., and Sun, H., 2005, "Assessment of Corrosion Risks to Aging Ships Using an Experience Database," *Journal of Offshore Mechanics and Arctic Engineering*, **127**(2), pp. 167-174.

[84] Winston, W. L., 1991, Operations Research: Applications and Algorithms, Boston.

[85] Yaffee, R. A., 2002, "Robust Regression Analysis: Some Popular Statistical Package Options," *Paper of the Statistics, Social Science, and Mapping Group, New York: New York University*.

[86] Yamamoto, N., 1997, "Probabilistic Corrosion Model of Ship Structural Members," The Institute of Marine Engineers, London, England.

[87] Yamamoto, N., and Ikegami, K., 1998, "A Study on the Degradation of Coating and Corrosion of Ship's Hull Based on the Probabilistic Approach," *Journal of Offshore Mechanics and Arctic Engineering. Transactions of the ASME*, **120**(3), pp. 121-128.

Appendix A – Ultrasonic Test Procedures and Device Specifications

The readings were taken on December 2004 by an experienced marine surveyor hired by the caisson gate owner. The following was obtained from the surveyor, describing the methodology used to obtain the shell plating material thickness measurements.

The ultrasonic test (UT) unit was calibrated using a ½" thick, machined test block, above and below water to verify the accuracy of the unit. UT equipment used in the inspection was calibrated daily, prior to performing readings. For members tested above water, the surface was prepared by scraping loose material (i.e. paint, corrosion, dirt, etc.) from the coated surface of the member. After loose debris was removed from the surface, an ultrasonic coupling gel was applied to the transducer of the UT unit and the transducer was then applied to the surface of the member. Each reading is verified as follows:

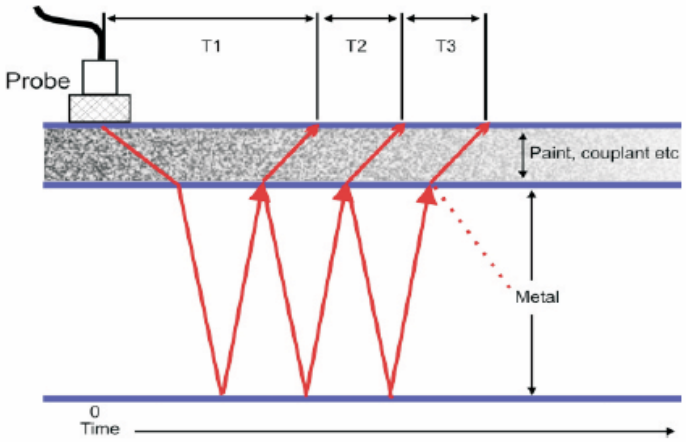

With multiple echo, readings are taken by measuring the time delay between any three consecutive backwall echos. The time of T1(coating thickness) is ignored. The times of T2 and T3 are equal to the time that it takes to travel through the metal. Only by looking at three echoes can the measurements be automatically verified (where T2 = T3).

Source: www.cygnus-instruments.com

Additionally, a minimum of three readings were taken at each specified location to verify the previous reading. Members tested below water (submerged) followed the same protocol as the above water testing. However, the water present was used as the coupling in lieu of the ultrasonic coupling gel. Water provides the same coupling properties as the gel. The device used was a Cygnus 1 Underwater manufactured by Cygnus Instruments.

Specification

Materials	Sound velocities between 2000 m/s and 7000 m/s – covers virtually all common engineering materials
Range in steel	3 mm – 250 mm with 2.25 MHz probe 2 mm – 150 mm with 3.5 MHz probe 1 mm – 50 mm with 5 MHz probe
Accuracy	±0.1 mm or ±0.05 mm (selectable)
Resolution	0.1 mm or 0.05 mm (selectable)
Probes	Remote single crystal soft-faced compression 6 mm – 5 MHz 13 mm – 2.25, 3.5 or 5 MHz 19 mm – 2.25 MHz (Lower frequency probes offer better penetration on heavy corrosion/coatings)
Power	NiMH rechargeable battery pack
Battery Life	30 Hours continuously reading
Display	Large, bright LED display
Size	235 mm x 75 mm
Weight	950 g - with remote probe 860 g - with fixed head probe
Operating Temp	-10°C to +50°C
Environmental Protection	IPX8 Continuous 300 m rating
Compliance	CE, British Standard BS EN 15317:2007 (Specification for the characterisation and verification of ultrasonic thickness measuring equipment)
Environmental	RoHS, WEEE compliant

Source: www.cygnus-instruments.com

Appendix B – Water Quality Measuring Device Specifications and Calibration

YSI 600XL & 600XLM Sensor Specifications

	Range	Resolution	Accuracy
Dissolved Oxygen % Saturation ET✓ 6562 Rapid Pulse™ Sensor*	0 to 500%	0.1%	0 to 200%: ±2% of reading or 2% air saturation, whichever is greater; 200 to 500%: ±6% of reading
Dissolved Oxygen mg/L ET✓ 6562 Rapid Pulse™ Sensor*	0 to 50 mg/L	0.01 mg/L	0 to 20 mg/L: ± 0.2 mg/L or 2% of reading, whichever is greater; 20 to 50 mg/L: ±6% of reading
Conductivity• 6560 Sensor* ET✓	0 to 100 mS/cm	0.001 to 0.1 mS/cm (range dependent)	±0.5% of reading + 0.001 mS/cm
Salinity	0 to 70 ppt	0.01 ppt	±1% of reading or 0.1 ppt, whichever is greater
Temperature 6560 Sensor* ET✓	-5 to +50°C	0.01°C	±0.15°C
pH 6561 Sensor* ET✓	0 to 14 units	0.01 unit	±0.2 unit
ORP	-999 to +999 mV	0.1 mV	±20 mV
Depth & Level Medium	0 to 200 ft, 61 m	0.001 ft, 0.001 m	±0.4 ft, ±0.12 m
Shallow	0 to 30 ft, 9.1 m	0.001 ft, 0.001 m	±0.06 ft, ±0.02 m
Vented Level	0 to 30 ft, 9.1 m	0.001 ft, 0.001 m	±0.01 ft, 0.003 m

• Report outputs of specific conductance (conductivity corrected to 25° C), resistivity, and total dissolved solids are also provided. These values are automatically calculated from conductivity according to algorithms found in *Standard Methods for the Examination of Water and Wastewater* (ed 1989).

Source: www.ysi.com

Certificate of YSI 600 XL Calibration

YSI 600 XL Serial Number 0 was calibrated to the manufacturer's specifications with NIST stands

Model: 600 XL
Pine No: 1782
Serial No: 0

lot Number:pH 4 1712282

Calibration Standard	Instrument Output	Allowable Range	% Difference
PH-Span1: 4PH	4PH	3.8-4.2 PH	0%

lot Number:cond 1.413 2708795

Calibration Standard	Instrument Output	Allowable Range	% Difference
Conductivity-Zero1: 1.413ms/cm	1.413ms/cm	1.34-1.48 ms/cm	0%

lot Number:DO 100% Sat Air

Calibration Standard	Instrument Output	Allowable Range	% Difference
Dissolve Oxygen-Span1: 100%	100%	95-105 %	0%

lot Number:ORP 240mV G2643

Calibration Standard	Instrument Output	Allowable Range	% Difference
Redox: 240mv	240mv	228-252 mv	0%

lot Number:pH 7 4803106

Calibration Standard	Instrument Output	Allowable Range	% Difference
PH-Zero1: 7PH	7PH	6.65-7.35 PH	0%

lot Number:pH 10 1711579

Calibration Standard	Instrument Output	Allowable Range	% Difference
PH-Span1: 10PH	10PH	9.5-10.5 PH	0%

Environmental Conditions of Test Area:

Temperature Degree F: 72.4 %Relative Humidity 47

Date: 7/15/2008 9:14:00 AM

Appendix C – Water Temperature and Dissolved Oxygen Comparisons

Paired T-tests were performed to quantify and confirm environmental dissimilarity.

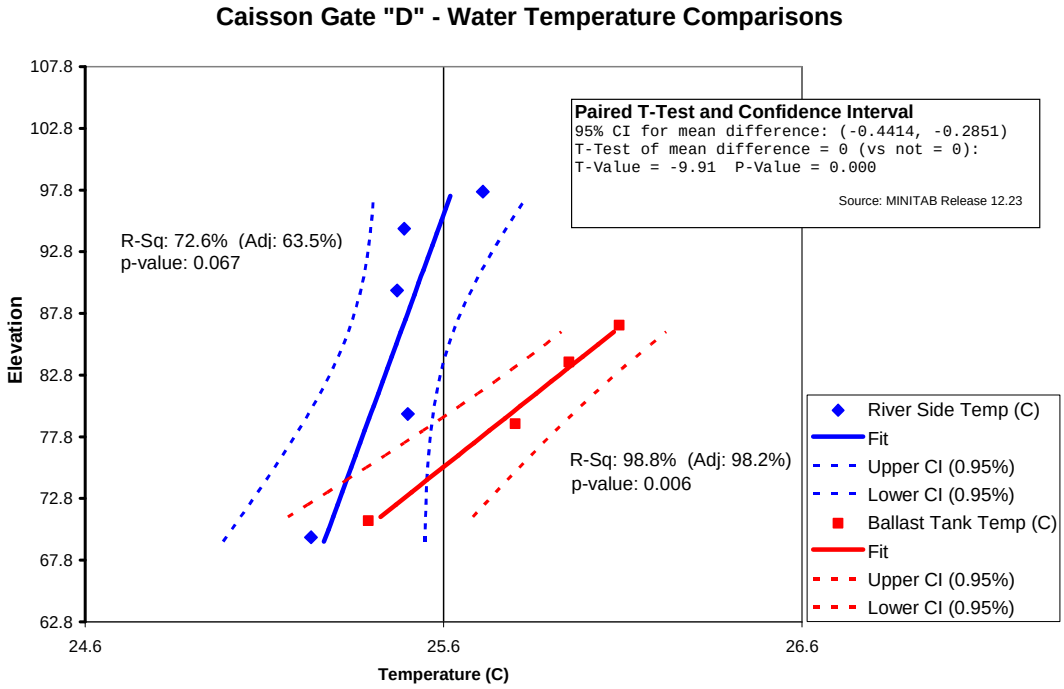

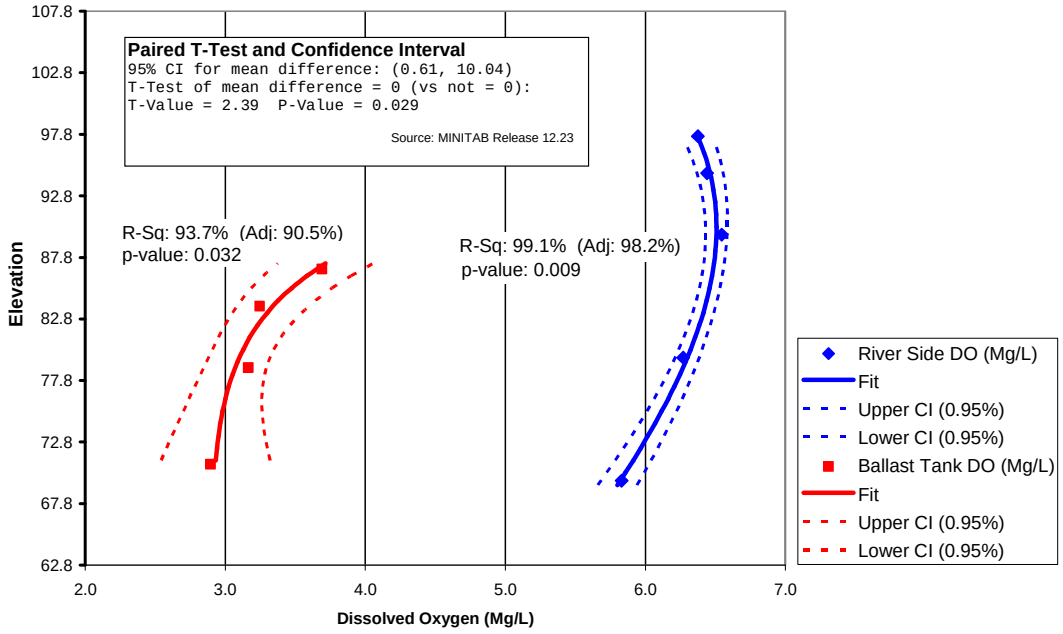

Appendix D - Lateral Homogeneity Test for Sides “A” and “B”

Lateral homogeneity test for Side “A”:

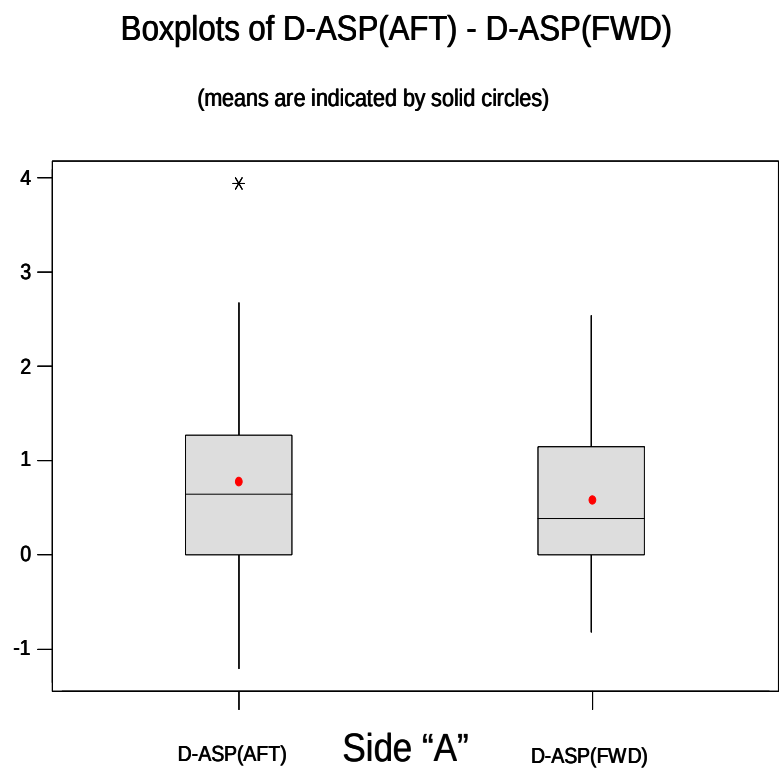

One-way Analysis of Variance

Analysis of Variance

Source	DF	SS	MS	F	P
Factor	1	0.576	0.576	0.66	0.421
Error	68	59.649	0.877		
Total	69	60.225			

Level	N	Mean	StDev
D-ASP(AFT)	35	0.7674	0.9798
D-ASP(FWD)	35	0.5860	0.8913

Pooled StDev = 0.9366

Individual 95% CIs For Mean
Based on Pooled StDev

```
----------+---------+---------+------
        (-----------*-----------)
 (-----------*-----------)
----------+---------+---------+------
       0.50      0.75      1.00
```

Source: Minitab© Release 12.23

Lateral homogeneity test for Side “B”:

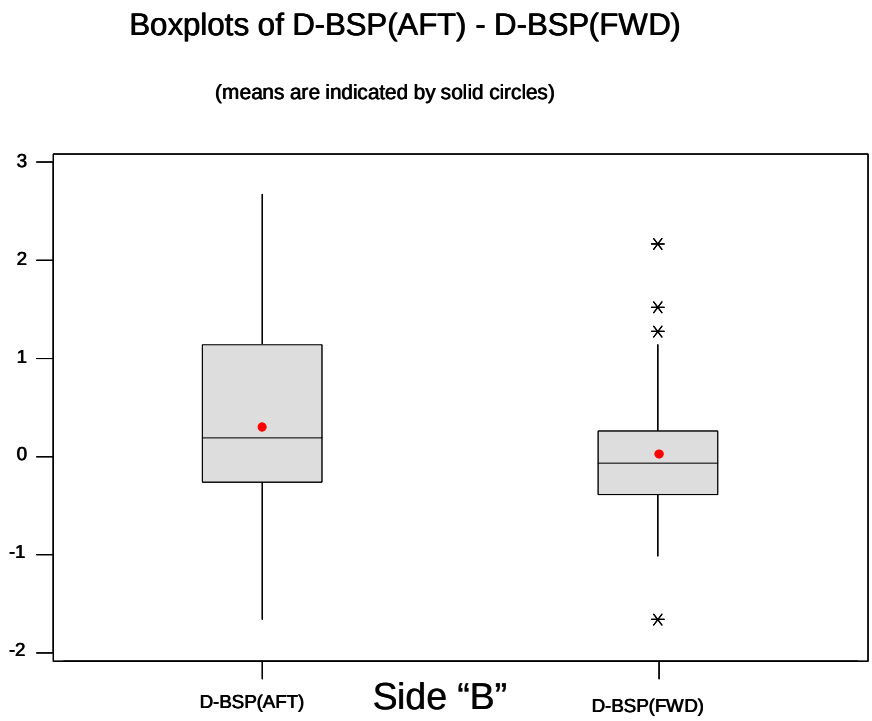

One-way Analysis of Variance

```
Analysis of Variance
Source     DF        SS        MS        F        P
Factor      1     1.366     1.366     1.84    0.180
Error      68    50.550     0.743
Total      69    51.916
                                   Individual 95% CIs For Mean
                                   Based on Pooled StDev
Level       N      Mean     StDev  -+---------+---------+---------+-----
D-BSP(AFT) 35    0.3030    0.9607             (-----------*-----------)
D-BSP(FWD) 35    0.0236    0.7509  (-----------*-----------)
                                   -+---------+---------+---------+-----
Pooled StDev =   0.8622          -0.25      0.00      0.25      0.50
```

Source: Minitab© Release 12.23

Appendix E - Longitudinal Heterogeneity Test for Sides “A” and “B”

Longitudinal heterogeneity test for Side “A”:

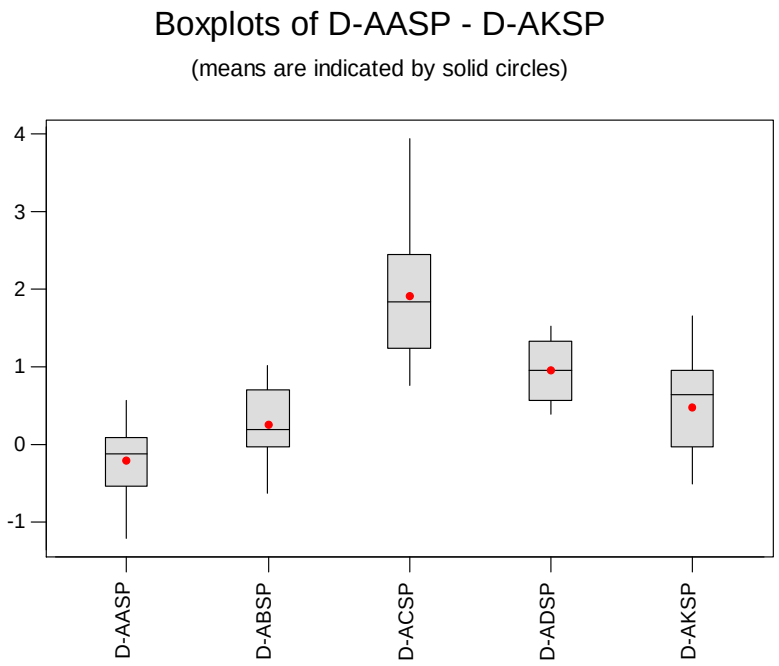

Side “A”

One-way Analysis of Variance

Analysis of Variance

Source	DF	SS	MS	F	P
Factor	4	36.322	9.080	24.69	0.000
Error	65	23.903	0.368		
Total	69	60.225			

Level	N	Mean	StDev
D-AASP	14	-0.2086	0.5101
D-ABSP	14	0.2540	0.5104
D-ACSP	14	1.9050	0.8276
D-ADSP	14	0.9616	0.4277
D-AKSP	14	0.4717	0.6710

Pooled StDev = 0.6064

Individual 95% CIs For Mean
Based on Pooled StDev

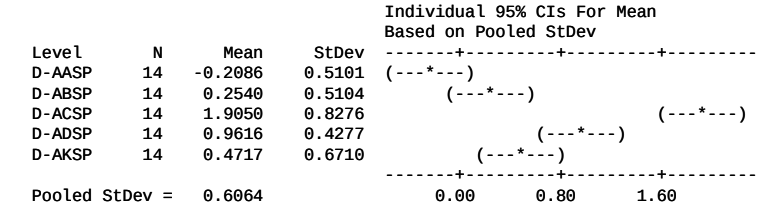

Source: Minitab© Release 12.23

Longitudinal heterogeneity test for Side “B”:

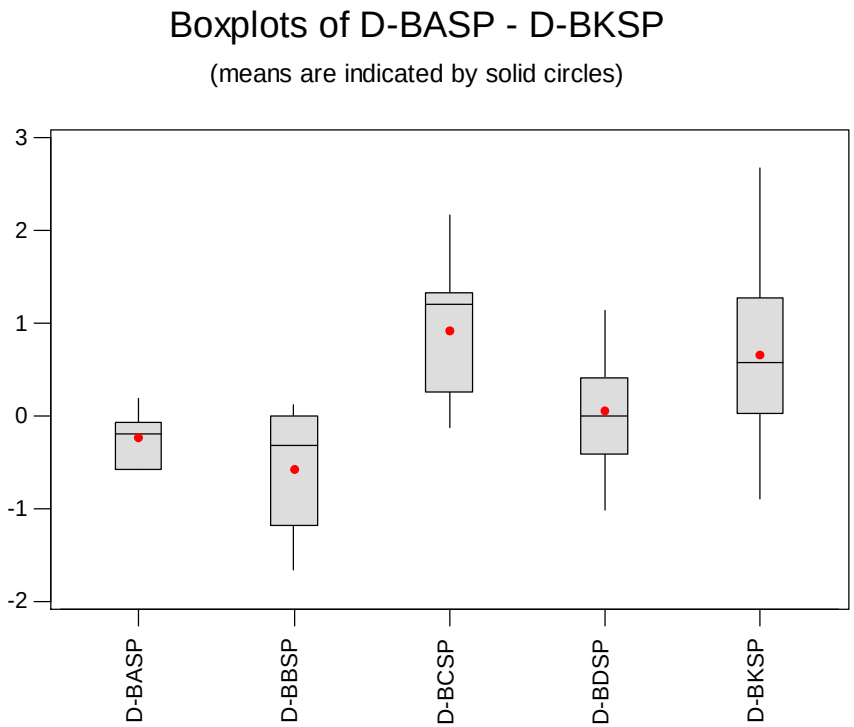

Side “B”

One-way Analysis of Variance

Analysis of Variance

Source	DF	SS	MS	F	P
Factor	4	21.339	5.335	11.34	0.000
Error	65	30.577	0.470		
Total	69	51.916			

Level	N	Mean	StDev
D-BASP	14	-0.2268	0.2561
D-BBSP	14	-0.5806	0.6969
D-BCSP	14	0.9162	0.6906
D-BDSP	14	0.0544	0.6565
D-BKSP	14	0.6531	0.9450

Pooled StDev = 0.6859

Individual 95% CIs For Mean
Based on Pooled StDev

```
----+---------+---------+---------+--
      (----*----)
(-----*----)
                        (----*----)
          (----*----)
                  (----*-----)
----+---------+---------+---------+--
 -0.70      0.00      0.70      1.40
```

Source: Minitab© Release 12.23

Appendix F – LOWESS and Polynomial Regression Models

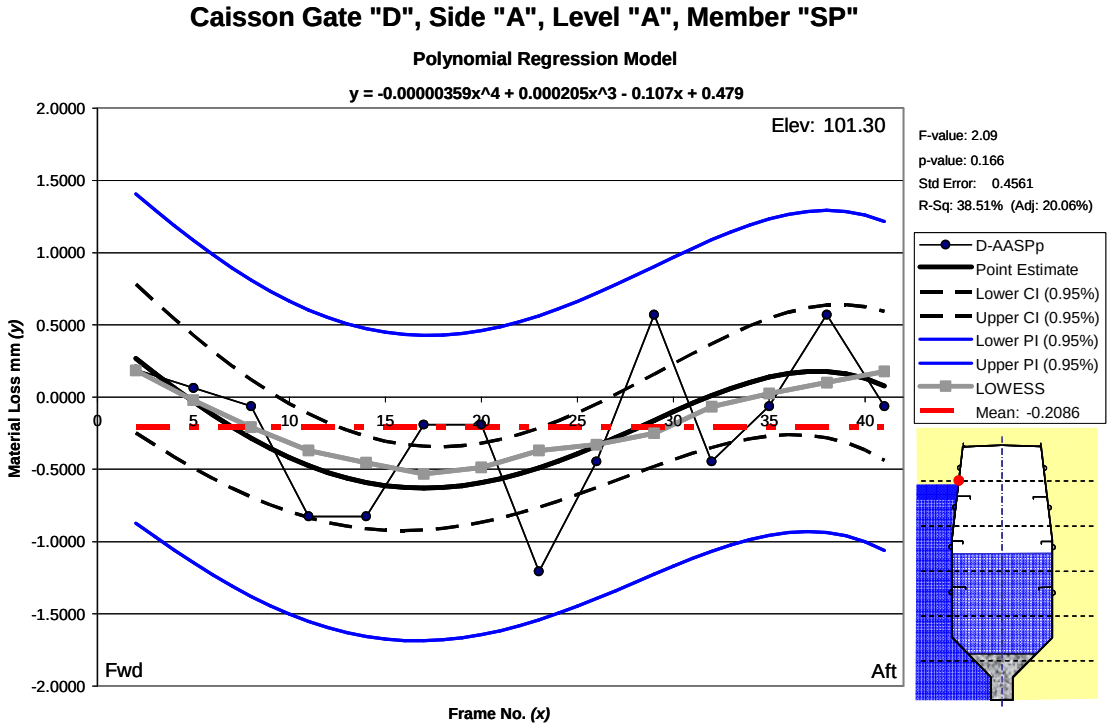

Descriptive Statistics

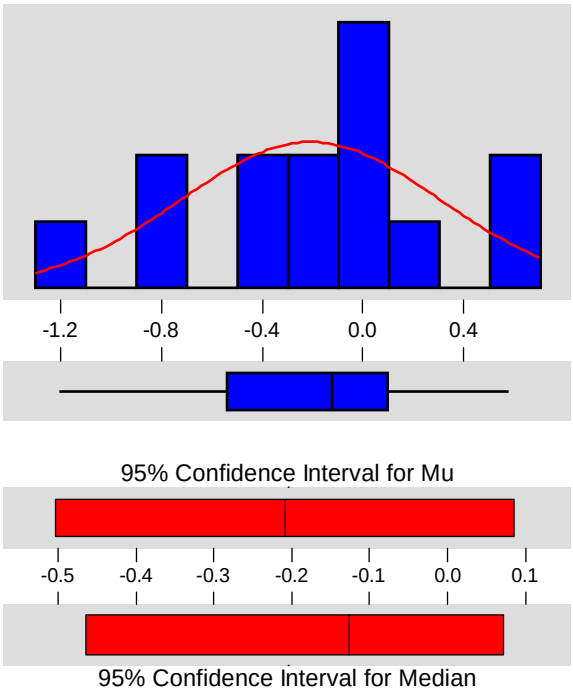

Variable: D-AASP

Anderson-Darling Normality Test

A-Squared:	0.300
P-Value:	0.535
Mean	-2.1E-01
StDev	0.510089
Variance	0.260191
Skewness	-3.0E-01
Kurtosis	-1.2E-01
N	14
Minimum	-1.20650
1st Quartile	-0.53975
Median	-0.12700
3rd Quartile	0.09525
Maximum	0.57150

95% Confidence Interval for Mu

-0.50316 0.08587

95% Confidence Interval for Sigma

0.36979 0.82178

95% Confidence Interval for Median

-0.46411 0.07004

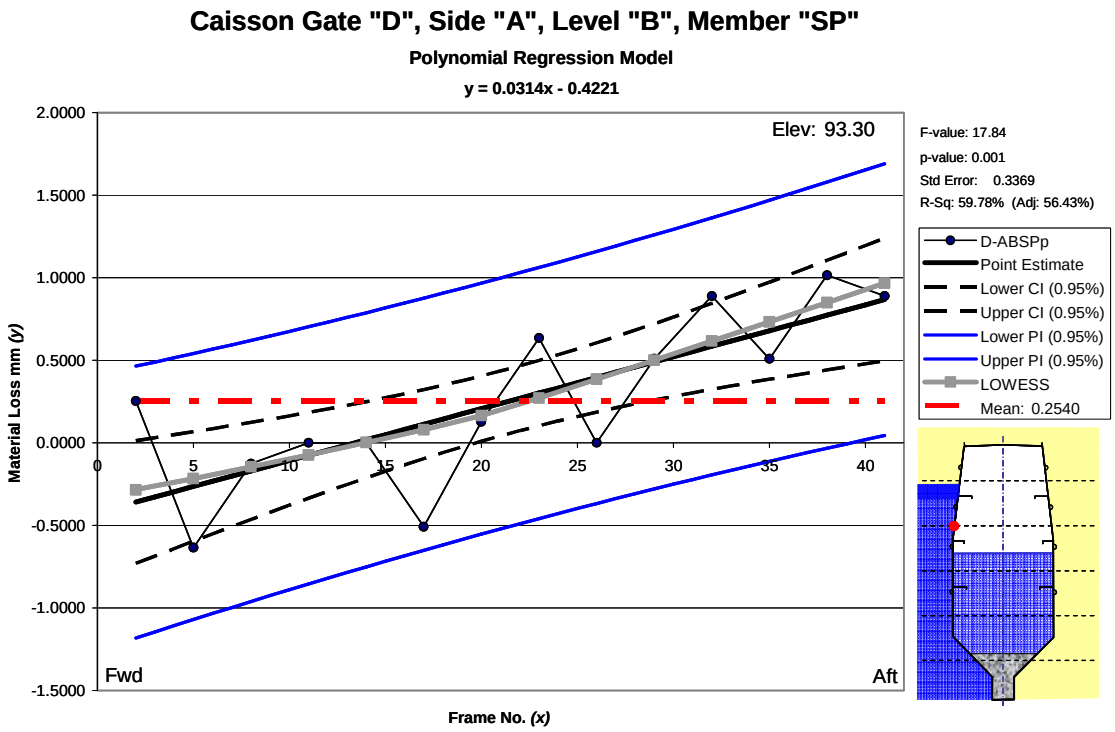

Descriptive Statistics

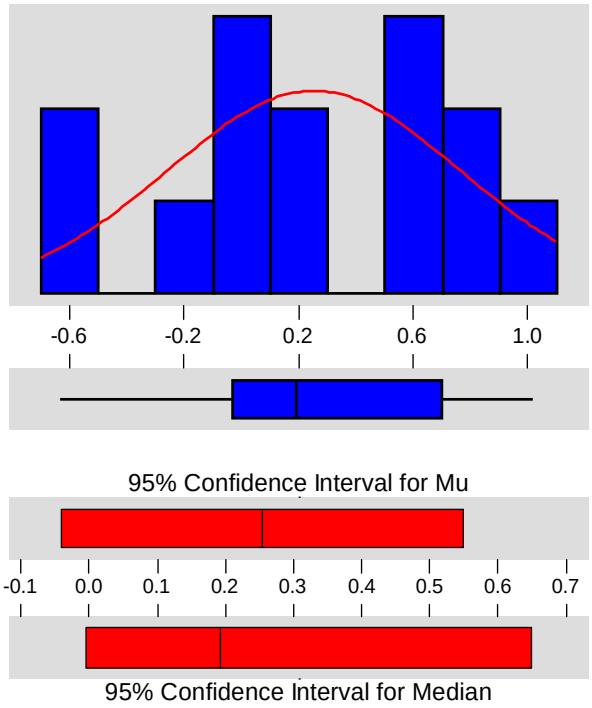

Variable: D-ABSP

Anderson-Darling Normality Test

A-Squared:	0.265
P-Value:	0.636

Mean	0.254000
StDev	0.510436
Variance	0.260545
Skewness	-1.4E-01
Kurtosis	-8.0E-01
N	14

Minimum	-0.63500
1st Quartile	-0.03175
Median	0.19050
3rd Quartile	0.69850
Maximum	1.01600

95% Confidence Interval for Mu

-0.04072	0.54872

95% Confidence Interval for Sigma

0.37004	0.82233

95% Confidence Interval for Median

-0.00654	0.64807

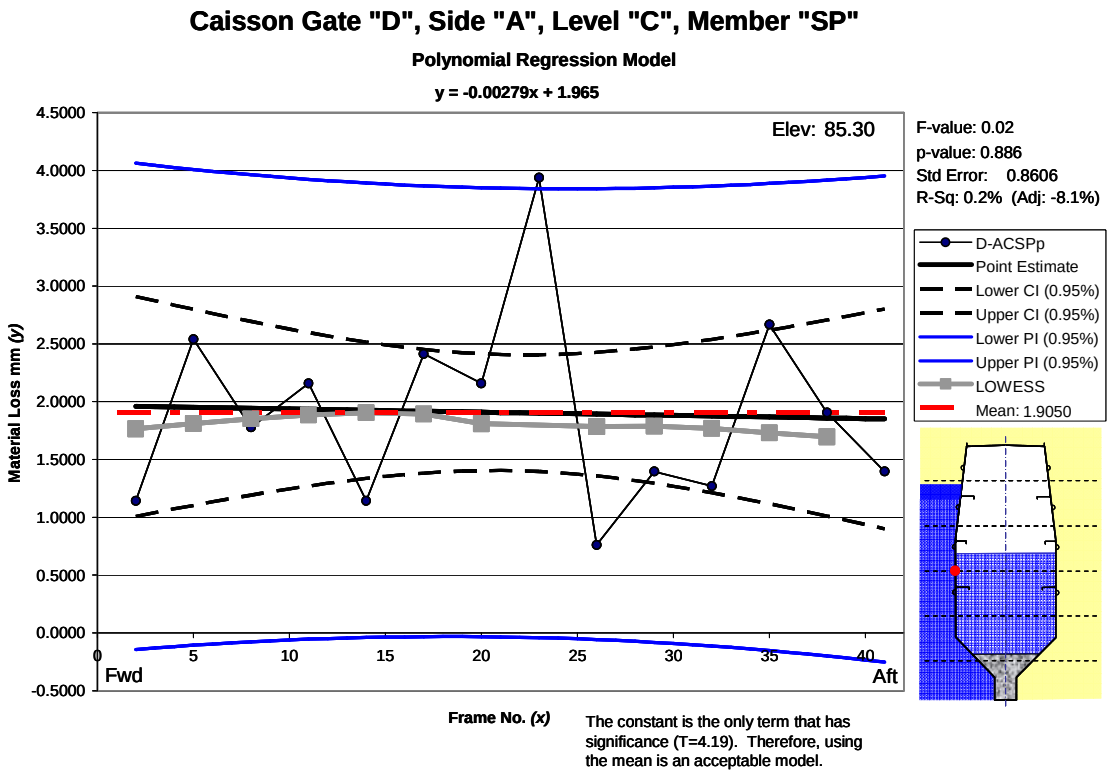

Descriptive Statistics

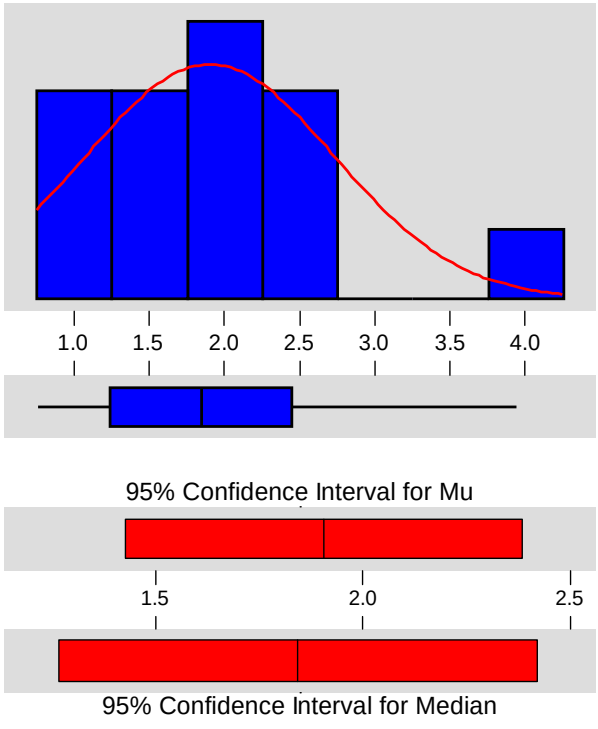

Variable: D-ACSP

Anderson-Darling Normality Test

A-Squared:	0.360
P-Value:	0.396
Mean	1.90500
StDev	0.82756
Variance	0.684862
Skewness	1.00612
Kurtosis	1.45579
N	14
Minimum	0.76200
1st Quartile	1.23825
Median	1.84150
3rd Quartile	2.44475
Maximum	3.93700

95% Confidence Interval for Mu

1.42718	2.38282

95% Confidence Interval for Sigma

0.59995	1.33324

95% Confidence Interval for Median

1.26346	2.41954

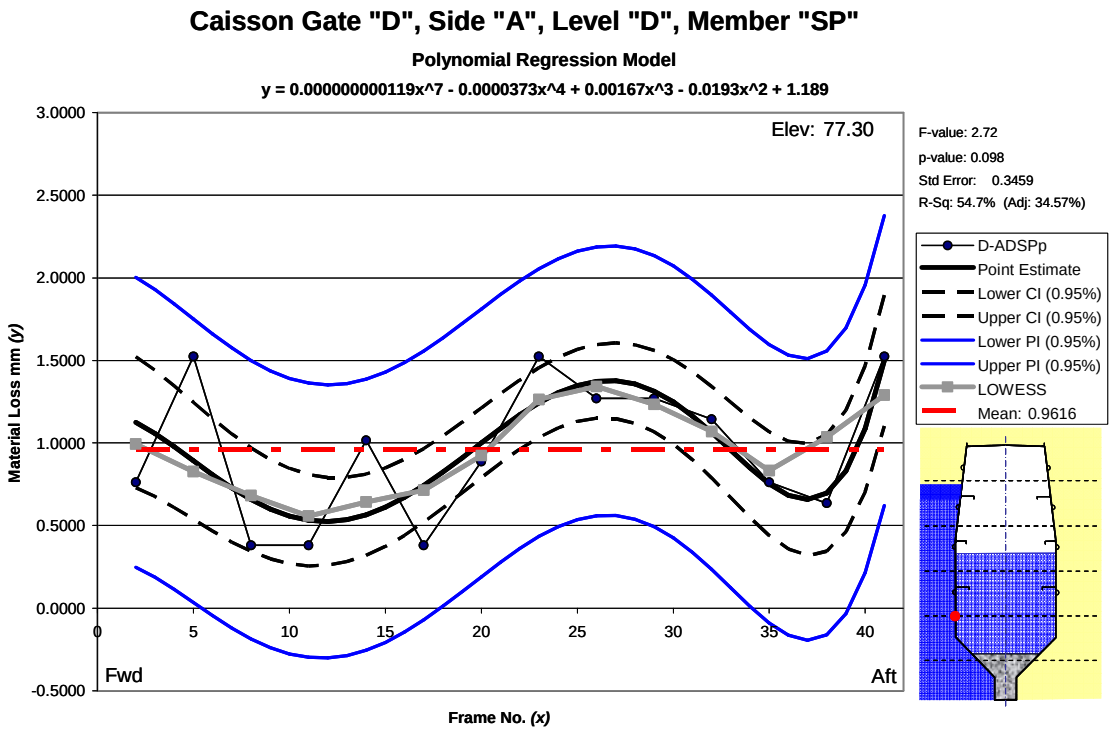

Descriptive Statistics

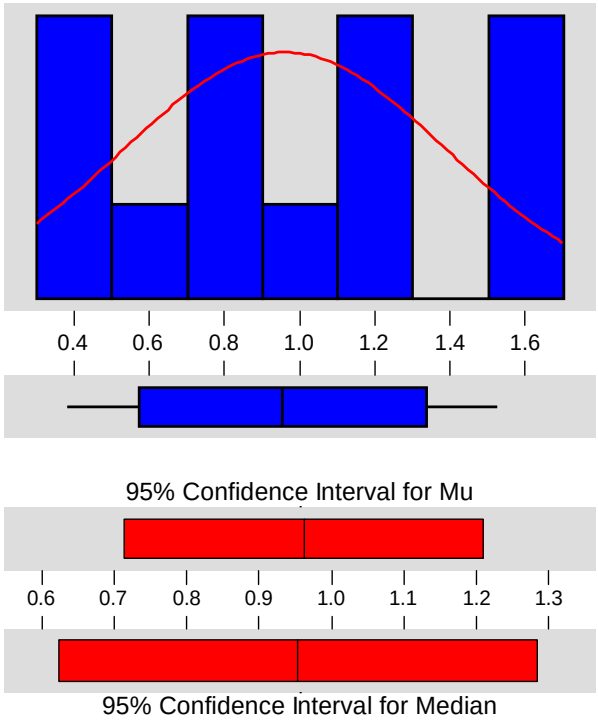

Variable: D-ADSP

Anderson-Darling Normality Test

A-Squared:	0.395
P-Value:	0.324

Mean	0.961571
StDev	0.427684
Variance	0.182913
Skewness	-4.5E-02
Kurtosis	-1.37273
N	14

Minimum	0.38100
1st Quartile	0.57150
Median	0.95250
3rd Quartile	1.33350
Maximum	1.52400

95% Confidence Interval for Mu

0.71463	1.20851

95% Confidence Interval for Sigma

0.31005	0.68902

95% Confidence Interval for Median

0.62193	1.28307

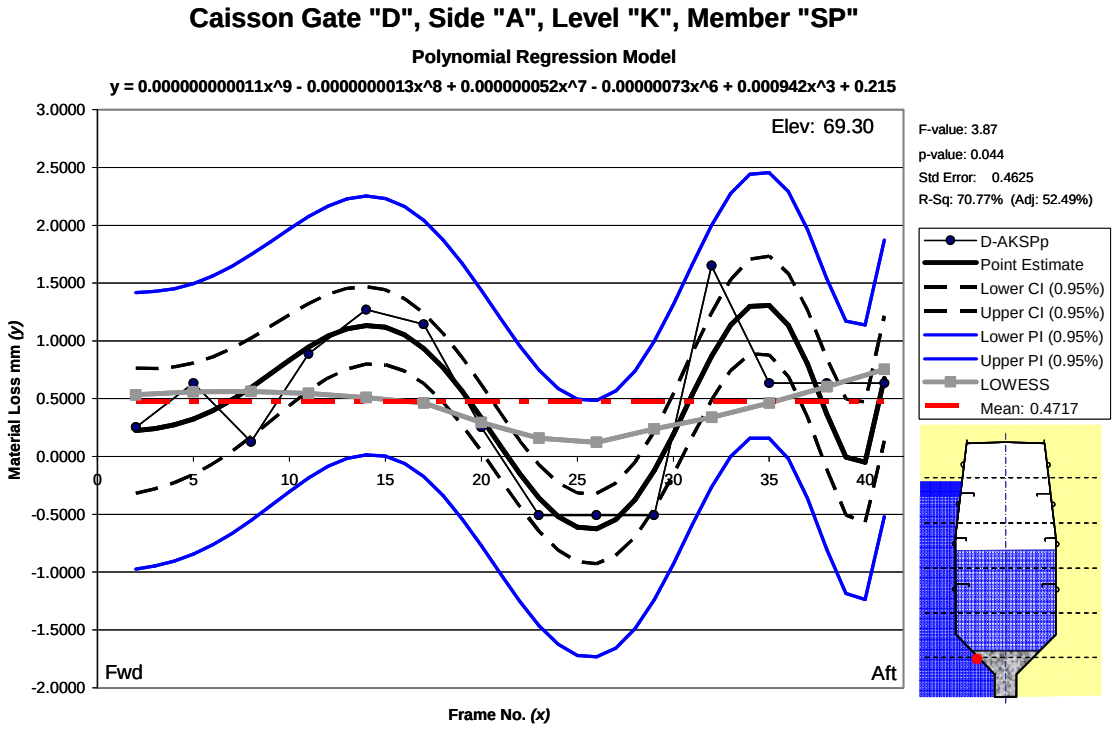

Descriptive Statistics

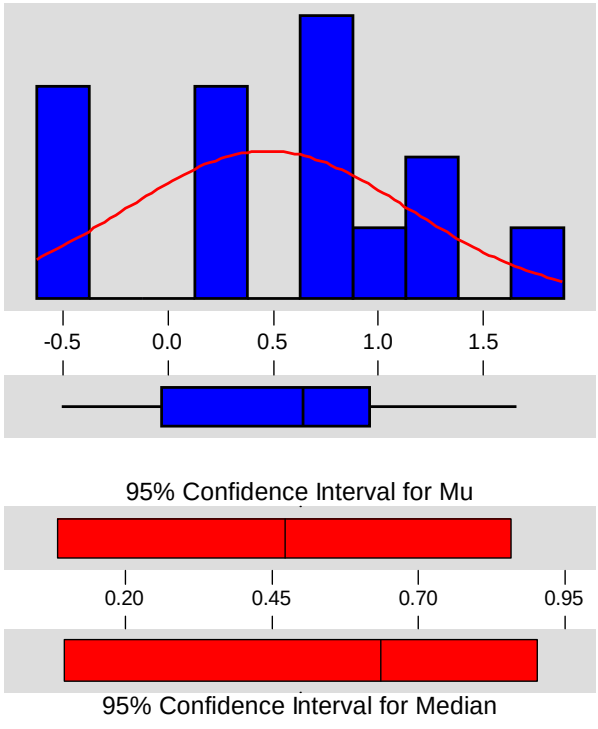

Variable: D-AKSP

Anderson-Darling Normality Test

A-Squared:	0.371
P-Value:	0.373
Mean	0.471714
StDev	0.670965
Variance	0.450194
Skewness	-1.0E-01
Kurtosis	-6.1E-01
N	14
Minimum	-0.50800
1st Quartile	-0.03175
Median	0.63500
3rd Quartile	0.95250
Maximum	1.65100

95% Confidence Interval for Mu

0.08431	0.85912

95% Confidence Interval for Sigma

0.48642	1.08095

95% Confidence Interval for Median

0.09432	0.90207

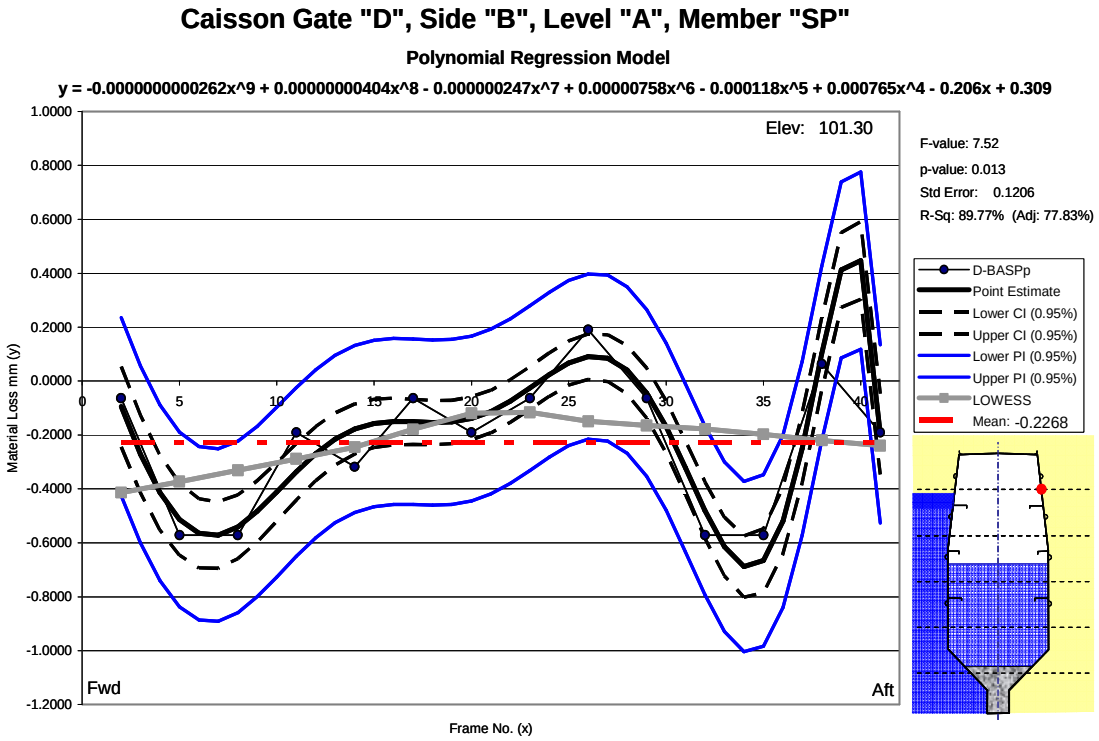

Descriptive Statistics

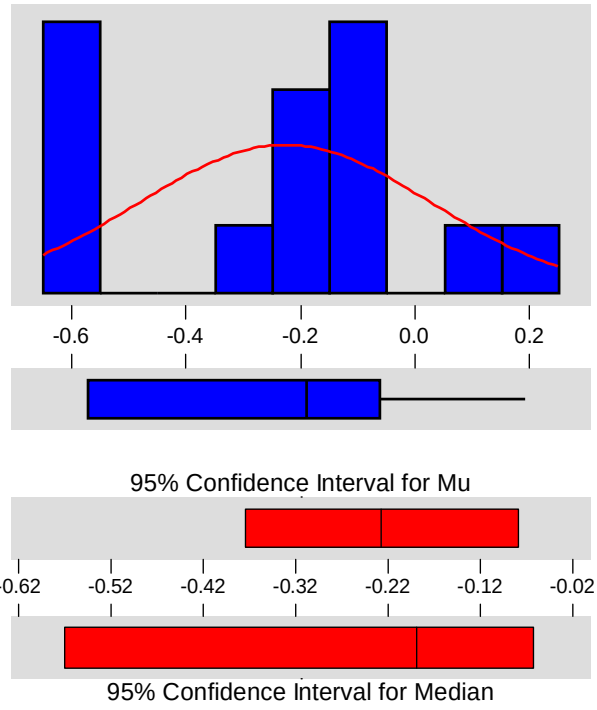

Variable: D-BASP

Anderson-Darling Normality Test

A-Squared:	0.709
P-Value:	0.050
Mean	-2.3E-01
StDev	0.256085
Variance	6.56E-02
Skewness	-2.7E-01
Kurtosis	-1.08591
N	14
Minimum	-5.7E-01
1st Quartile	-5.7E-01
Median	-1.9E-01
3rd Quartile	-6.3E-02
Maximum	0.190500

95% Confidence Interval for Mu

-3.7E-01 -7.9E-02

95% Confidence Interval for Sigma

0.185650 0.412564

95% Confidence Interval for Median

-5.7E-01 -6.3E-02

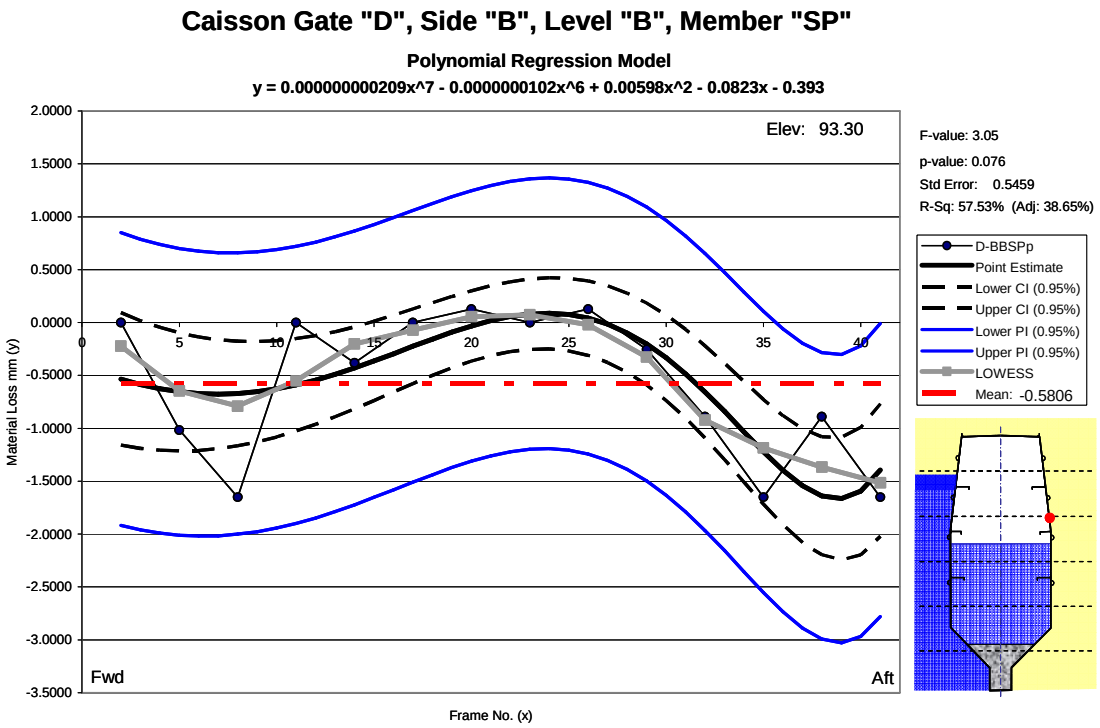

Descriptive Statistics

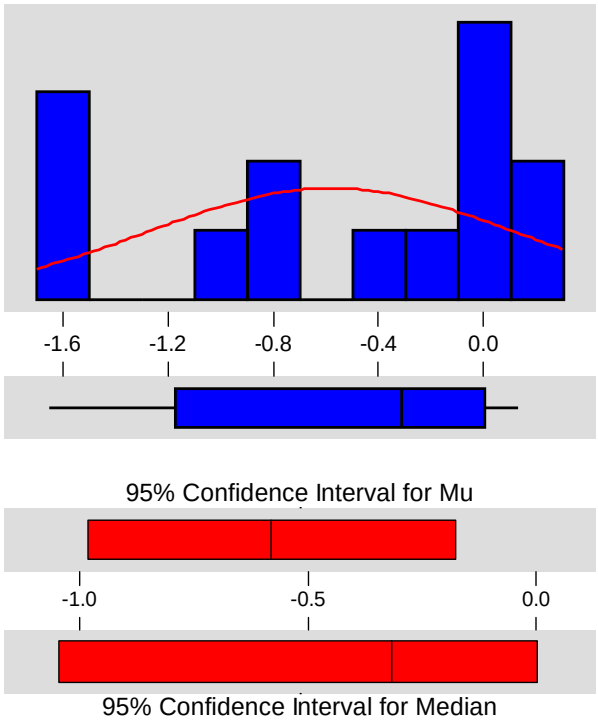

Variable: D-BBSP

Anderson-Darling Normality Test

A-Squared:	0.914
P-Value:	0.014

Mean	-5.8E-01
StDev	0.696880
Variance	0.485642
Skewness	-6.1E-01
Kurtosis	-1.26650
N	14

Minimum	-1.65100
1st Quartile	-1.17475
Median	-0.31750
3rd Quartile	0.00000
Maximum	0.12700

95% Confidence Interval for Mu

-0.98294	-0.17820

95% Confidence Interval for Sigma

0.50521	1.12270

95% Confidence Interval for Median

-1.04868	0.00000

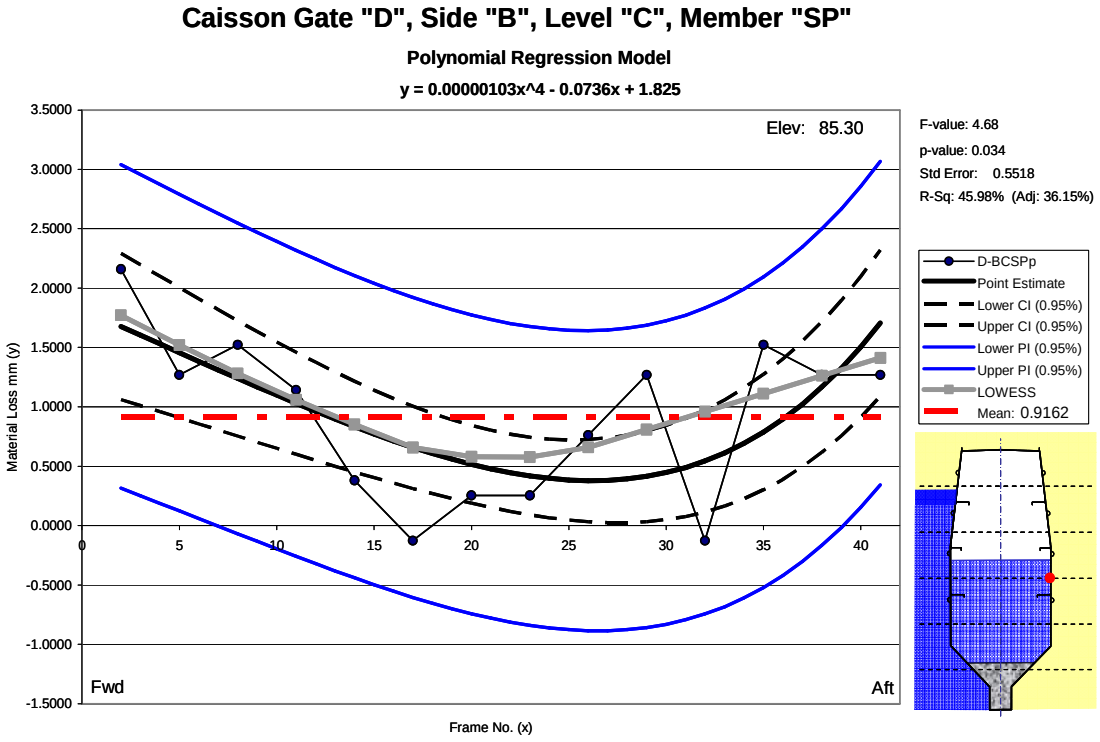

Descriptive Statistics

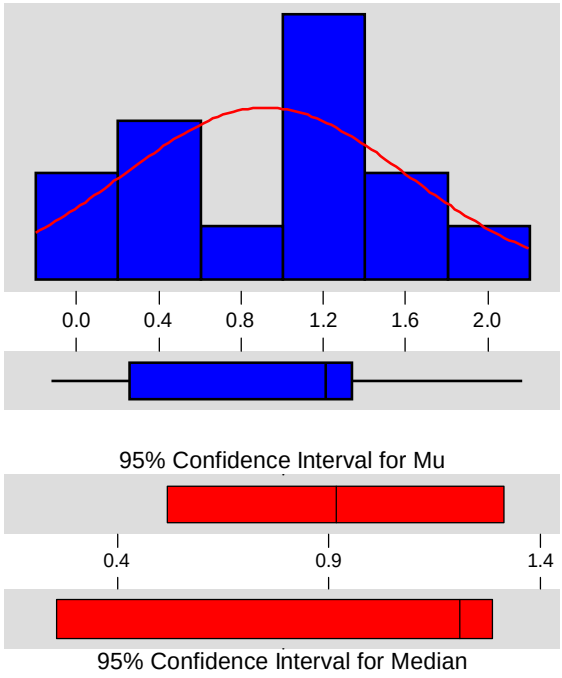

Variable: D-BCSP

Anderson-Darling Normality Test

A-Squared:	0.526
P-Value:	0.147
Mean	0.916214
StDev	0.690557
Variance	0.476869
Skewness	-1.2E-01
Kurtosis	-8.5E-01
N	14
Minimum	-0.12700
1st Quartile	0.25400
Median	1.20650
3rd Quartile	1.33350
Maximum	2.15900

95% Confidence Interval for Mu

0.51750	1.31493

95% Confidence Interval for Sigma

0.50062	1.11252

95% Confidence Interval for Median

0.25400	1.28307

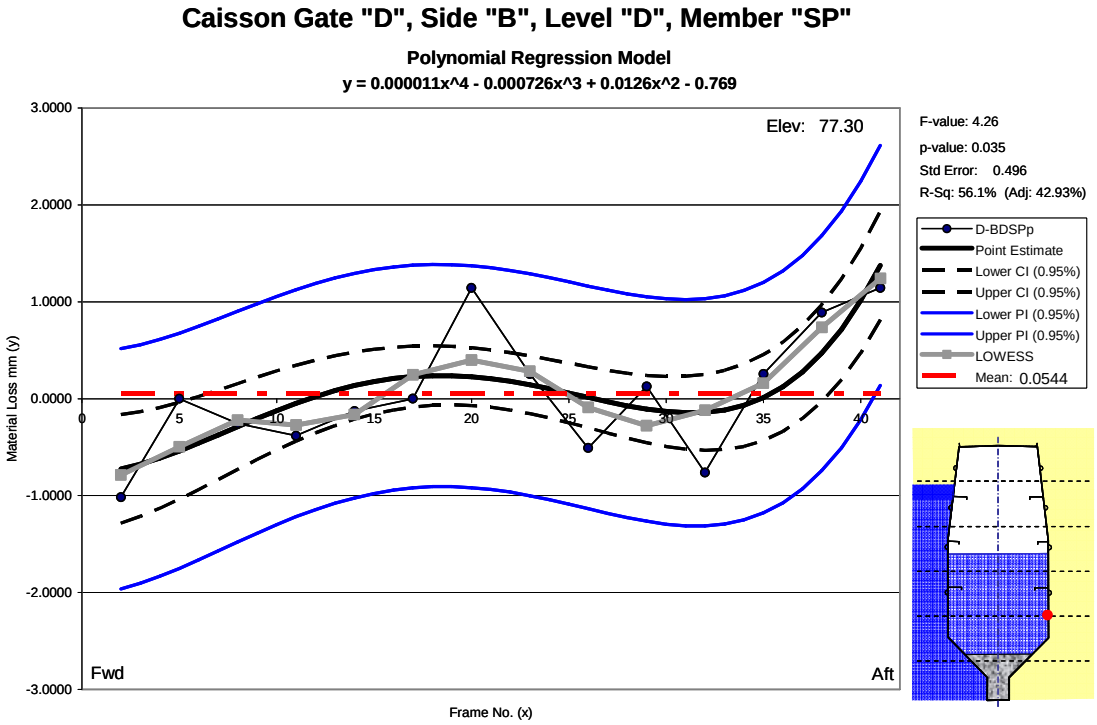

Descriptive Statistics

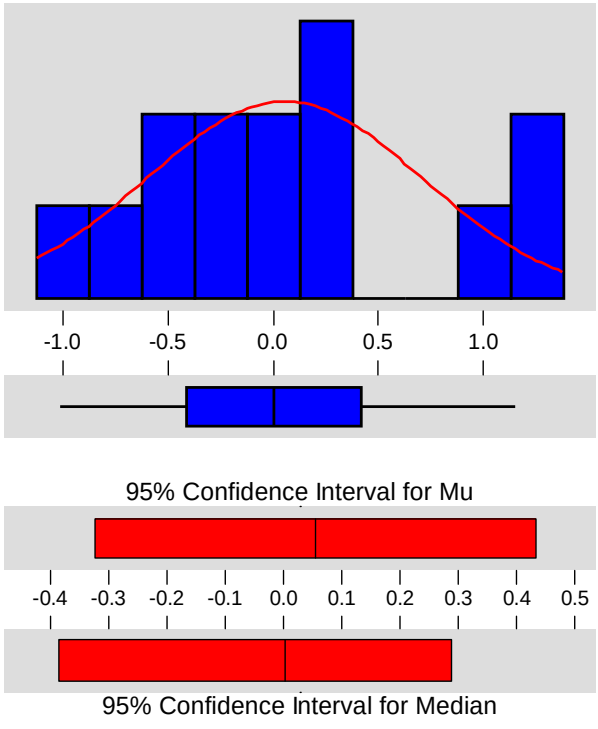

Variable: D-BDSP

Anderson-Darling Normality Test

A-Squared:	0.307
P-Value:	0.519
Mean	0.054429
StDev	0.656545
Variance	0.431052
Skewness	0.352195
Kurtosis	-4.2E-01
N	14
Minimum	-1.01600
1st Quartile	-0.41275
Median	0.00000
3rd Quartile	0.41275
Maximum	1.14300

95% Confidence Interval for Mu

-0.32465 0.43351

95% Confidence Interval for Sigma

0.47597 1.05772

95% Confidence Interval for Median

-0.38754 0.28668

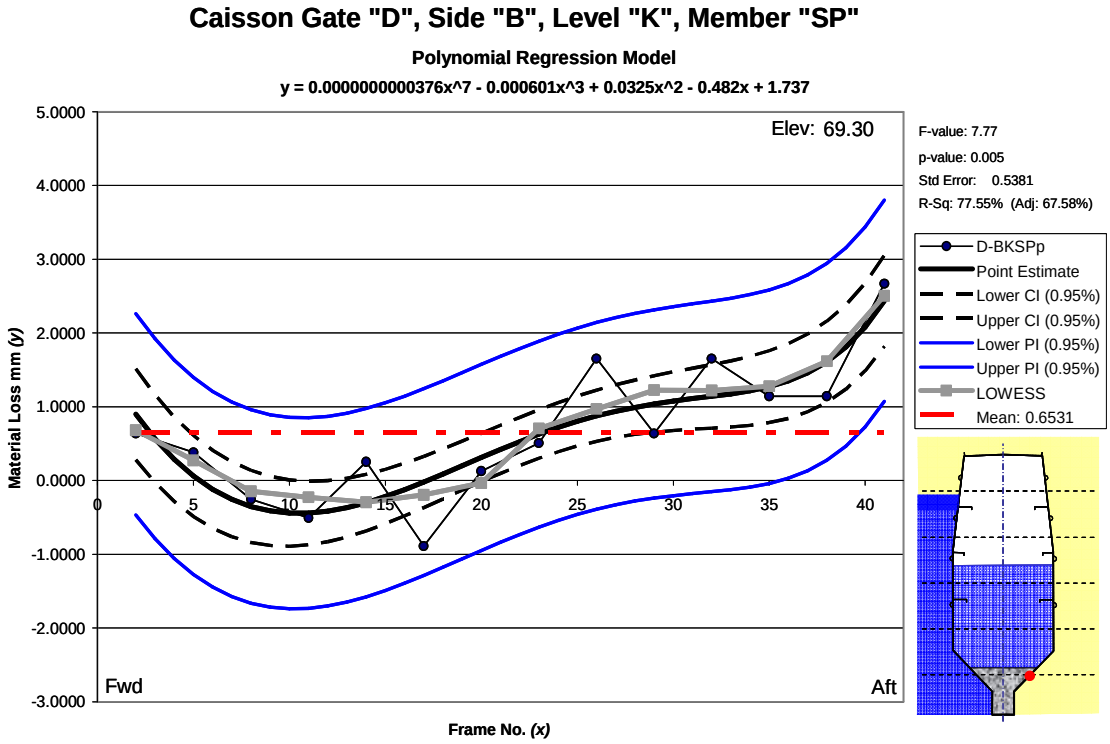

Descriptive Statistics

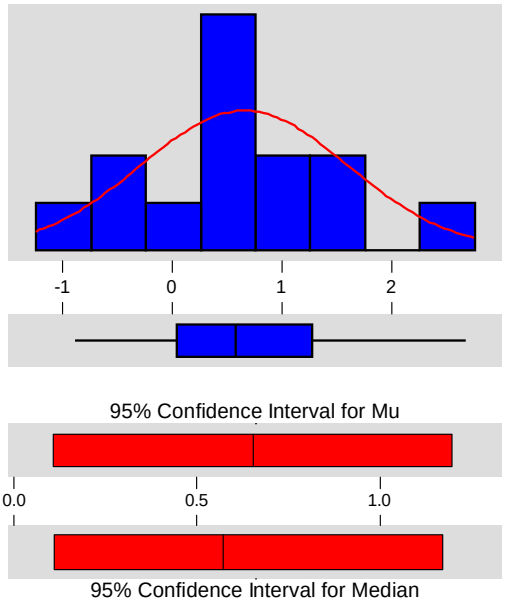

Variable: D-BKSP

Anderson-Darling Normality Test

A-Squared:	0.190
P-Value:	0.878

Mean	0.653143
StDev	0.944957
Variance	0.892944
Skewness	0.444328
Kurtosis	0.273123
N	14

Minimum	-0.88900
1st Quartile	0.03175
Median	0.57150
3rd Quartile	1.27000
Maximum	2.66700

95% Confidence Interval for Mu

0.10754	1.19874

95% Confidence Interval for Sigma

0.68505	1.52237

95% Confidence Interval for Median

0.10739	1.16914

Appendix G – "Negative" Wastage Distributions of Four Caisson Gates

Negative Wastage
Shell Plating, Caisson Gate "A"

Year Built: 1961

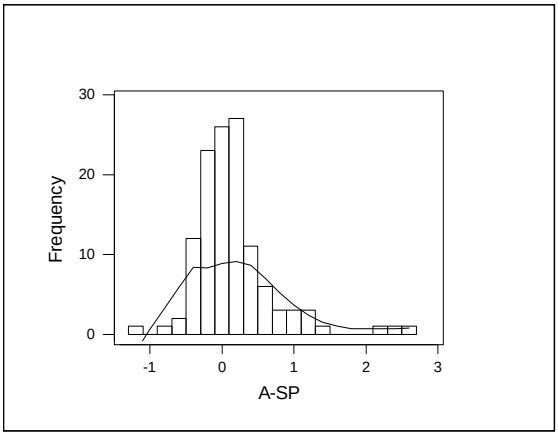

UT data obtained from NGSB 2005 overhaul report

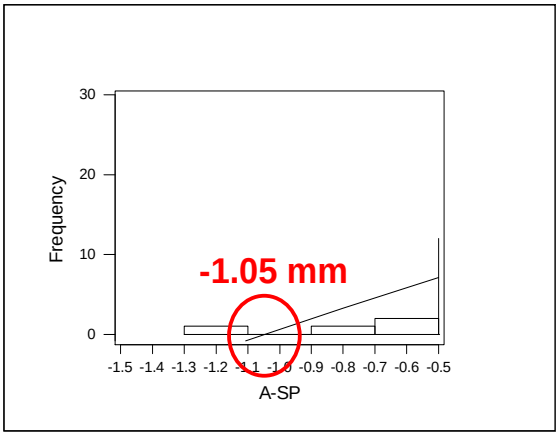

LOWESS
Degree of Smoothing: 0.5
Number of Steps: 2
Source: Minitab© Release 12.23

Negative Wastage
Shell Plating, Caisson Gate "B"

Year Built: 1958

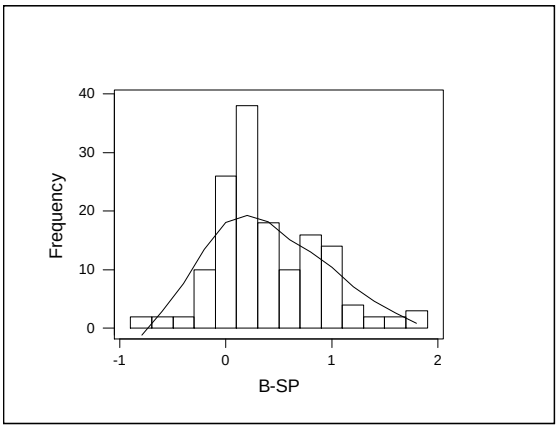

UT data obtained from NGSB 2004 overhaul report

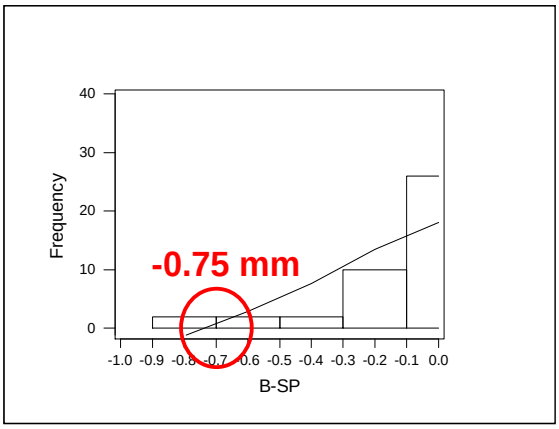

LOWESS
Degree of Smoothing: 0.5
Number of Steps: 2
Source: Minitab© Release 12.23

Negative Wastage
Shell Plating, Caisson Gate “C”

Year Built: 1978

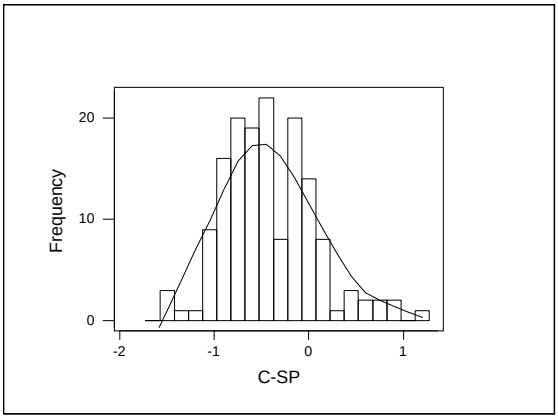

UT data obtained from NGSB 2005 overhaul report

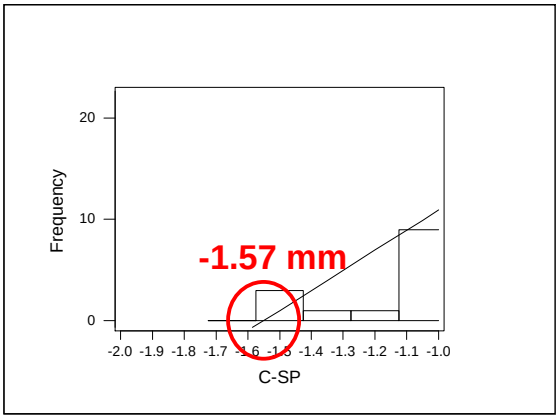

LOWESS
Degree of Smoothing: 0.5
Number of Steps: 2
Source: Minitab© Release 12.23

Negative Wastage
Shell Plating, Caisson Gate “D”

Year Built: 1941

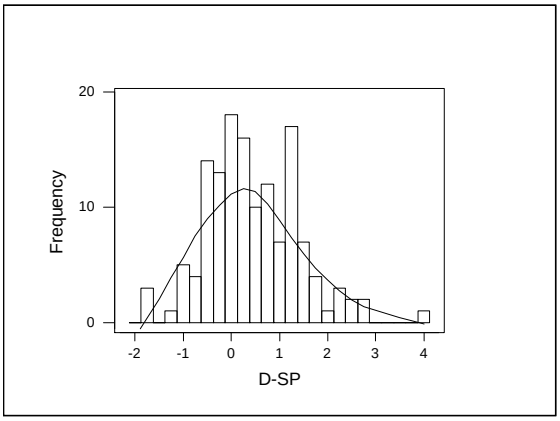

UT data obtained from NGSB 2005 overhaul report

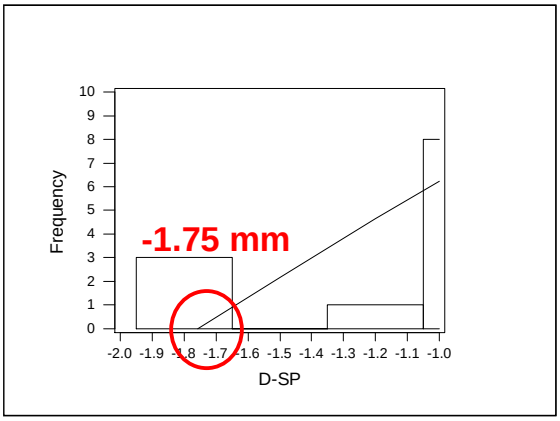

LOWESS
Degree of Smoothing: 0.5
Number of Steps: 2
Source: Minitab© Release 12.23